

Title	多孔質構造の導入によるポリベンズイミダゾールフィルムの性能向上
Author(s)	周, 佳貝
Citation	
Issue Date	2025-03
Type	Thesis or Dissertation
Text version	ETD
URL	<a href="http://hdl.handle.net/10119/19934">http://hdl.handle.net/10119/19934</a>
Rights	
Description	Supervisor: 山口 政之, 先端科学技術研究科, 博士

Doctoral Dissertation

**Performance Enhancement of  
Thermoresistant Polybenzimidazole Film  
by Introducing Porous Structure**

Jiabei Zhou

Supervisor      Masayuki Yamaguchi

Japan Advanced Institute of Science and Technology  
Graduate School of Advanced Science and Technology  
(Materials Science)

March 2025

## Abstract

Polybenzimidazole (PBI) is a high-performance polymer known for its excellent thermal stability, mechanical properties, and chemical resistance, making it a material candidate in demanding environments. In particular, poly(2,5-benzimidazole) (ABPBI) is the simplest chemical structure of PBI, consisting of repeated benzene and imidazole rings. However, several challenges of ABPBI remain such as low sustainability and high-cost availability caused by the commercial time-consuming polycondensation process, heterogeneity and low flexibility of processed film due to the rigid backbones of ABPBI, lack of processability with insolubility in common solvents, and moisture sensitivity which limited their further application as a super engineering plastic.

One of the primary challenges facing the widespread adoption of ABPBI films is the high cost of production. The complex synthesis and processing techniques required to produce ABPBI contribute to its higher price point compared to other polymers. Moreover, scaling up the production of ABPBI films while maintaining their unique properties with crucial uniformity is also required in manufacturing technologies. In Chapter 2, ABPBI was synthesized successfully by using Eaton's reagent, which is a time-saving polycondensation procedure. Notably, the adopted monomer is bio-derivable, which remarkably improves sustainability and reduces the production cost of ABPBI. The fabricated ABPBI film by solution casting method showed heterogeneous and featured branched patterns of thick brown regions, which may have originated from the surface condensation of ABPBI to form sticky fibrous aggregates. Subsequently, a hard-templating method using silica nanoparticle fillers was employed to homogenize the ABPBI film. The composite ABPBI films had reduced heterogeneity and roughness compared with the original ABPBI film. Herein, a formation mechanism could be attributed to the ABPBI aggregate stuck to the surfaces of the silica nanoparticles, which were well dispersed over the film by ultrasonication. The reduced cost of production and improved uniformity suggest the potential of ABPBI as a material for a broader range of industry uses, e.g., fuel cell separators, leakproof films, and filtration membranes.

Although ABPBI is strong and rigid, it can be relatively brittle as well. Its low elongation at break limits its use in applications where flexibility or toughness is required. In Chapter 3, another bio-derivable monomer was incorporated into the ABPBI backbones named poly(BI-*co*-A) to develop flexibility. Poly(BI-*co*-A) was synthesized using viscous poly(phosphoric acid). Moreover, to further enhance the durability, flexibility, and performance of poly(BI-*co*-A) film, porous structures were constructed via a silica-etching method. The prepared porous poly(BI-*co*-A) films showed much higher toughness and mechanical stability, which could be expected to play a crucial role in enabling the next generation of durable and resilient electronic devices, including their potential use in high-performance sensors, smart textiles, and flexible batteries. On the other hand, poly(BI-*co*-A) film has some degree of water absorption, which can affect its mechanical properties over time, especially under humid conditions. This could be problematic in applications where dimensional stability or mechanical strength must be maintained in moist environments. Consequently, dehydration treatment of silica nanocomposite poly(BI-*co*-A) films in an electric furnace was employed to improve the surface wettability of the poly(BI-*co*-A) film by decreasing the hydroxy bonds in the films. The fabricated silica nanocomposite poly(BI-*co*-A) films displayed an enhanced thermal resistance, even comparable to some metals, implying their replacement of heavyweight metal or inorganic materials. Nevertheless, the improved wettability of poly(BI-*co*-A) films further ensures their potential candidate for applications in an extreme environment such as fuel cell membranes, barriers, and anti-fouling film, aircraft, and spacecraft.

Regarding the future scope of this work, the successful PBI films with enhanced performance such as low-cost procedure, sustainable resources, high uniformity, improved flexibility, and enhanced toughness, have significant potential in a variety of industries, from energy and aerospace to electronics and environmental protection. Whether through their role in improving fuel cell performance, protecting advanced electronic devices, or enabling cleaner industrial processes, PBI films are set to play a key role in the future of materials science and engineering. The ongoing advancements in manufacturing, sustainability, and application development will further expand the use of PBI films, making them critical materials for the 21st century and beyond.

**Key words:** Heat-resistant polymers, polybenzimidazole, porous structures, homogenization, high toughness

## Acknowledgments

The author would like to express the special thanks of gratitude to the primary supervisors *Prof. Masayuki Yamaguchi* and *Prof. Tatsuo Kaneko*, second supervisor *Prof. Toshiaki Taniike*, minor research advisor *Prof. Kazuaki Matsumura*, and *Prof. Kenji Takada* for their guidance and support throughout this research. Their constructive suggestions and extensive experience were extremely instrumental in this work.

The author appreciates Prof. Maiko K. Okajima, Prof. Mohammad Asif Ali, Dr. Maninder Singh, Dr. Aniruddha Nag, Dr. Hongrong Yin, Dr. Takumi Noda, Dr. Yasuyoshi Funahashi, Dr. Xianzhu Zhong and Dr. Takuya Kumakura for their excellent help and kind encouragement. The author would also extend his gratitude to the members of Yamaguchi and Kaneko laboratory for their helpful discussion and kind support.

To the staff of the SHIMADZU CORPORATION company, Mr. Koichi Nagano, Mr. Masato Hirade, and Mr. Shogo Onomura, the author thanks for their measurements.

Finally, the author acknowledges the JST SPRING, Japan Grant Number JPMJSP2102 for the financial support in his doctoral life and research grant in this work.

Please note that the responsibility for this work is entirely the author's own.



# Contents

Chapter I General Introduction.....	1
1.1 Bioplastics .....	2
1.2 Heat-resistant polymers .....	4
1.3 Challenges in heat-resistant polymer development.....	8
1.4 Expectable innovations in heat-resistant polymers .....	10
1.5 Porous polymer materials .....	12
1.6 Applications of porous polymers.....	16
1.7 Objectives of this work.....	17
References .....	20
Chapter II Fabrication of silica composite and porous polybenzimidazole film.....	28
2.1 Introduction .....	29
2.2 Experimental.....	32
2.2.1 Materials .....	32
2.2.2 Synthesis.....	32
2.2.3 Fabrication of pure ABPBI film .....	33
2.2.4 Fabrication of silica composite ABPBI film .....	34
2.2.5 Fabrication of porous ABPBI films.....	35

2.3 Measurements .....	36
2.4 Results and Discussion .....	37
2.4.1 Preparation of silica composite and porous polybenzimidazole film.....	37
2.4.2 Porosity calculation .....	40
2.4.3 FT-IR-spectrum .....	42
2.4.4 SEM morphologies .....	44
2.4.5 AFM analysis.....	50
2.4.6 TGA analysis .....	53
2.4.7 Stress-strain (S-S) curves .....	55
2.5 Conclusion.....	58
References .....	60
Chapter III Fabrication of silica composite and porous poly(benzimidazole-aramid) film .....	69
3.1 Introduction .....	70
3.2 Experimental.....	72
3.2.1 Materials .....	72
3.2.2 Syntheses .....	72
3.3 Measurements.....	76
3.4 Results and Discussion .....	78

3.4.1 Fabrication of pure poly(BI-co-A) film.....	78
3.4.2 Fabrication of silica nanocomposite poly(BI-co-A) films.....	79
3.4.3 FT-IR spectra.....	81
3.4.4 SEM morphologies.....	84
3.4.5 TGA analysis.....	87
3.4.6 Contact angle test.....	90
3.4.7 Fabrication of porous poly(BI-co-A) films.....	92
3.4.8 FT-IR spectra of porous film.....	94
3.4.9 Porosities of the prepared porous films.....	96
3.4.10 SEM morphology images.....	97
3.4.11 Mechanical properties.....	99
3.4.12 WAXD patterns.....	101
3.4.13 High-performance SPM.....	103
3.4.14 Hypothesis of mechanism.....	107
3.5 Conclusion.....	109
References.....	110
Chapter IV Conclusions.....	117
Research Achievements.....	123

# *Chapter I*

## *General Introduction*

## 1.1 Bioplastics

Plastics have been an essential production and tremendously benefit our lives because of their high functionality.<sup>1</sup>

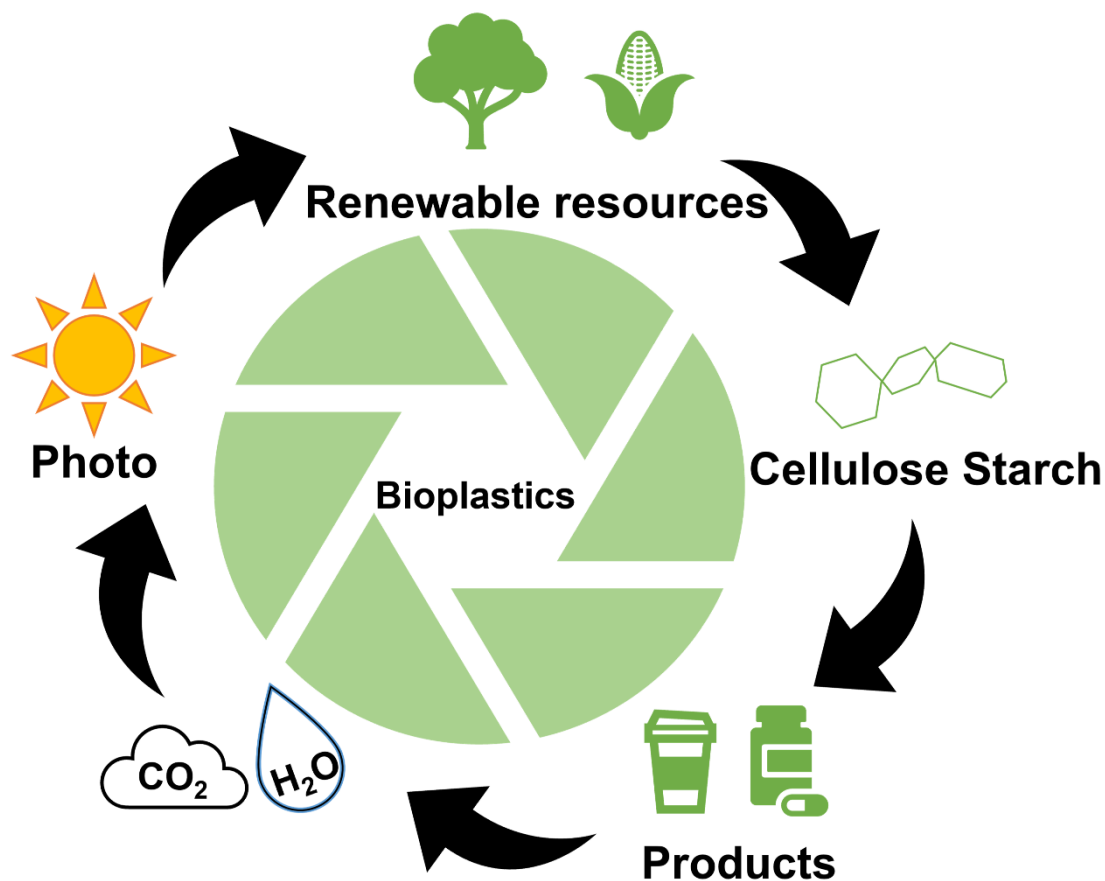


**Figure 1-1.** Image of bioplastic products (<https://www.env.go.jp/recycle/>) and recycling route of the carbon fixation from bioplastics.

However, as reported by European Bioplastics in cooperation with the Nova-Institute,<sup>2</sup> the amount of bioplastics is less than one percent of all plastics produced each year. Most of the commercial plastics are petroleum-derived, which causes numerous

## *Chapter I*

### *General Introduction*

environmental problems, such as the petroleum-sources crisis, marine-microplastics issue, greenhouse-gas emissions, etc.<sup>3-5</sup> Hence, it is necessary to develop bioplastics from renewable biological resources to solve the problems above and achieve the sustainable development goals (SDGs). In addition, the products that result from renewable resources could be recycled through natural powers (water, sunlight, etc.) to the feedstocks of plants, which is more advantageous for establishing a carbon-neutral society (**Figure 1-1**).

Bioplastics could be divided into biodegradable plastics: poly(lactic acid) (Bio-PLA), which is made from fermented plant starch, is widely used in food-packaging; polyhydroxyalkanoates (Bio-PHA), produced by microorganisms, could be applied for medical implants and packaging, and non-biodegradable plastics: polyethylene (Bio-PE), poly(ethylene terephthalate) (Bio-PET), being attractive to numerous researchers for their renewability and comparable physicochemical properties to petroleum-based plastics. Bioplastics contribute to a cleaner environment by reducing carbon emissions and utilizing renewable resources. However, they also face challenges, such as the need for agricultural land to grow the crops for raw materials and hidden environmental costs during production. Additionally, not all bioplastics are easily biodegradable, and the recycling infrastructure for these materials is still developing.

## 1.2 Heat-resistant polymers

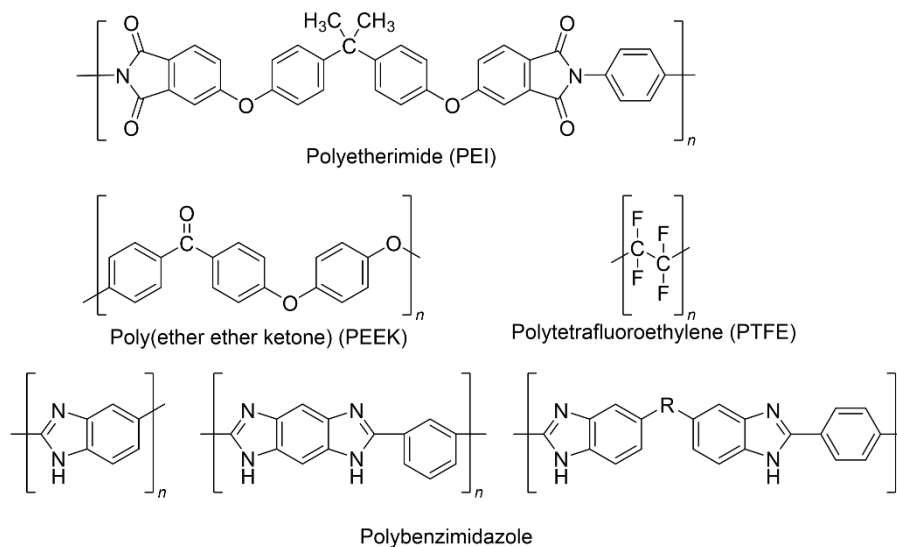


**Figure 1-2.** Molecular structures of various heat-resistant polymers.

Although commercial bioplastics exhibit enough functionality, there is a fatal drawback of their low thermal stability, which limits their application at high temperatures. Heat-resistant polymers are a class of synthetic materials capable of withstanding extreme temperatures without degrading, losing mechanical properties, or breaking down chemically, which are determined by their chemical structure (**Figure 1-2**). Thermal degradation is a process where heat causes the molecular structure of a polymer to break down, leading to a loss of properties such as strength, flexibility, and chemical resistance. Heat-resistant polymers are specifically engineered to delay this process by incorporating aromatic groups, cross-linking, or utilizing inorganic fillers that enhance their stability,

## *Chapter I*

### *General Introduction*

which are also characterized by high glass transition temperatures ( $T_g$ ) and melting points ( $T_m$ ). Nowadays, manufacturers prefer to use stainless steel and nickel alloys for high-performance applications because they are stable and still maintain remarkable performance at high temperatures. However, there are still many incomparable advantages of using thermal-resistant plastics to traditional metal materials, such as lightweight, chemical resistance, dimensional stability, high functionality, etc.<sup>6-9</sup>

Polyetherimide (PEI) (**Figure 1-2**), with a commonly branded name of ULTEM (General Electric), is a kind of amorphous thermoplastics, which is developed in the late 1970s. PEI has become a material of choice in industries due to its high thermal resistance mechanical strength, high chemical resistance, and outstanding dimension stability. Moreover, PEI's unique chemical structure, which consists of aromatic rings and imide groups linked by ether bonds, provides it with a combination of rigidity, toughness, and high thermal resistance with a glass transition temperature ( $T_g$ ) of 217 °C. Therefore, it is usually used for applications where fire safety is critical, such as in aircraft interiors, electrical components, and chemical instruments.

PEEK (**Figure 1-2**), an abbreviation for poly(ether ether ketone), is a semi-crystalline engineering thermoplastic polymer that was first invented by ICI in 1982. PEEK is thermally stable with a glass transition temperature ( $T_g$ ) of around 143 °C and,

## *Chapter I*

### *General Introduction*

a melting temperature ( $T_m$ ) of around 343 °C. Moreover, PEEK has an excellent mechanical property at high temperatures and can withstand for a short period even at 250 °C. Therefore, it can be used as a substitute for metal materials, normally used to fabricate medical implants, electrical cable insulations, spinal fusion devices, etc.

It is well-known that polytetrafluoroethylene (PTFE) (**Figure 1-2**) is a synthetic fluoropolymer, which shows remarkable flexural strength, adequate weathering resistance, and chemical and thermal resistance. PTFE has a high melting point of around 327 °C and can operate continuously at temperatures ranging from -200°C to 260°C without significant degradation. In addition, the tensile strength of about 20 – 30 MPa and excellent ductility, with elongation at break values typically exceeding 200%, and insolubility in most solvents make its broad applications such as wire insulation, lubricants, and chemically-insert liners.

Polybenzimidazole (PBI) (**Figure 1-2**) has the highest heat and wear resistance, exceptional thermomechanical and chemical stability of any engineering thermoplastic, relying on their rigid backbones, strong hydrogen bonds, and  $\pi$ - $\pi$  stacking interactions among their polymer chains, which are first reported by Vogel and Marvel in 1960s. Later, as a result of their unique thermal property with a continuous service temperature of up to 300°C and a short-term exposure limit of 500°C, PBI was commercialized by some

## *Chapter I*

### *General Introduction*

companies (DuPont, Pall Corporation, and BASF fuel cell) as high-performance polymer materials.

Researchers pay attention to PEEK, polyimides, etc., because they can be good substitutes for PBI with some drawbacks, such as water-absorbing nature and high-cost polymerization procedure. The excellent thermal resistance and chemical stability, owing to a great value of applications under harsh environments such as satellites, space shuttles, etc. Recently numerous research on molecular design for low-cost polymerization and hybrid with organic or inorganic components to improve the performance of PBI.<sup>10-13</sup> Several aromatic monomers with different structures such as aromatic diamine-carboxylic acid, aromatic tetraamines, etc., have already been polymerized into PBIs successfully. Poly(2,2'-(*m*-phenylene)-5,5'-bibenzimidazole) (PBI) with a branded name of Celazole<sup>TM</sup> (PBI Advanced Materials Co., Ltd.) has been commercialized because of its high thermal stability and processability. Despite the expensive synthetic procedure, PBI can also be used for the most critical applications like astronaut spacesuits, firefighters' gear, and aircraft wall fabrics. The processed PBI films could also be used for gas separation,<sup>14-16</sup> nanofiltration,<sup>17-19</sup> and high-temperature proton exchange membrane (HTPEM) fuel cell applications.<sup>20-25</sup>

### **1.3 Challenges in heat-resistant polymer development**

Despite their advantages, heat-resistant polymers face several challenges in their development and widespread adoption, such as high cost, processing difficulties, limited availability, and balancing properties.

- High cost

One of the primary challenges of heat-resistant polymers is their cost. High-performance polymers, such as PEEK and polyimides, are significantly more expensive than traditional plastics. This limits their use to high-value applications where performance outweighs the cost.

- Processing difficulties

Heat-resistant polymers often require specialized equipment and processes for manufacturing due to their high melting points and thermal stability. This can increase the complexity and cost of producing parts from these materials.

- Limited availability

Certain heat-resistant polymers, such as PBI, are produced in relatively small

## *Chapter I*

### *General Introduction*

quantities due to their specialized applications. This limited availability can lead to supply chain challenges, especially for industries that require consistent and reliable sources of materials.

- **Balancing properties**

Designing polymers that can withstand high temperatures while maintaining flexibility, chemical resistance, and mechanical strength is a complex task. Engineers and scientists must balance these properties to create materials that are suitable for specific applications, which can be a time-consuming process.

#### **1.4 Expectable innovations in heat-resistant polymers**

The future of heat-resistant polymers is bright, with ongoing research focused on improving their performance and expanding their applications. Innovations in polymer chemistry, nanotechnology, and material science are paving the way for more efficient and durable polymers. Several strategies could be applied to enhance the performance of heat-resistant polymers as shown below.

- Sustainable resources

As sustainability becomes a growing concern, the development of eco-friendly heat-resistant polymers is gaining traction. Researchers are exploring bio-based alternatives to traditional high-temperature polymers, aiming to reduce the environmental impact of manufacturing and disposal, as well as the producing cost. Moreover, advances in biotechnology may lead to heat-resistant polymers that are biodegradable, reducing plastic waste in industries such as automotive and electronics. Furthermore, researchers are working on developing recycling processes for high-temperature polymers, which are traditionally difficult to recycle due to their complex structures and chemical properties.

## *Chapter I*

### *General Introduction*

- Nanocomposites

Nanotechnology is expected to play a significant role in the development of next-generation heat-resistant polymers. By incorporating nanoparticles such as carbon nanotubes, graphene, or ceramic fillers, researchers can enhance the thermal and mechanical properties of polymers without significantly increasing their weight. Generally, nanocomposites can enhance the heat dissipation properties of polymers, making them even more suitable for high-temperature applications. Notably, nanoparticles can increase the strength and durability of polymers, making them resistant to wear and tear in extreme environments.

- Porous structures

One of the most intriguing aspects of heat-resistant polymers is the development and application of porous structures. These materials consist of a polymer matrix embedded with a porous structure, which can vary in size, shape, and interconnectivity. As a result, these structures have unique properties such as lightweight, high surface area, and tunable permeability, making them useful in areas like filtration, catalysis, drug delivery, tissue engineering, and more.

## **1.5 Porous polymer materials**

Porous materials can be viewed in nature such as hollow bamboo, honeycomb with hexagonal cells, sponges, rocks, etc. According to the IUPAC classification, porous materials can be divided into microporous ( $< 2$  nm), mesoporous (2 – 50 nm), and macroporous ( $> 50$  nm), based on the pore sizes.<sup>26,27</sup> On the other hand, it also could be separated into open-celled and closed-celled porous materials, depending on whether the pores are connected or not. Porous materials have absorbed the interest of researchers in recent decades because of their high surface area and well-defined porosity. Especially, porous polymer materials have long been important research subjects due to their advantages over inorganic porous materials, such as lightweight, high processability, and multiple chemical functional abilities, which make their wide applications on gas storage materials,<sup>28–32</sup> catalysts,<sup>33–36</sup> sensors,<sup>37,38</sup> separator membranes,<sup>39,40</sup> etc. Numerous methods to form porous polymers have been developed, such as phase separation, template-assist, emulsion techniques, gas forming, and electrospinning shown below.

- Phase separations

Phase separation is a widely used method for producing porous structures in polymers. It involves separating a polymer-rich phase from a polymer-poor phase,

## *Chapter I*

### *General Introduction*

leading to the formation of a porous network. This technique can be classified into three types: Thermally Induced Phase Separation (TIPS): Here, the polymer is dissolved in a solvent at a high temperature and then cooled, causing phase separation. The resulting structure can be tuned by adjusting the cooling rate and polymer concentration; Solvent-Induced Phase Separation (SIPS): In this process, a polymer solution is exposed to a non-solvent, causing phase separation. This method is often used for producing membranes and filtration materials; Non-Solvent Induced Phase Separation (NIPS): A polymer solution is cast into a mold and then immersed in a non-solvent, which leads to the formation of a porous structure.

- Template-assisted methods

Template-assisted methods involve using a pre-formed template, such as a solid, liquid, or gas, to create pores in the polymer. After the polymer matrix is formed around the template, the template is removed, leaving behind a porous network: Solid Templates: Materials like silica or salt crystals can be used as templates. Once the polymer is formed around the solid template, the template is removed by dissolution or thermal decomposition; Liquid Templates: Emulsions or foams can be used as liquid

## *Chapter I*

### *General Introduction*

templates. The dispersed phase (e.g., oil droplets) is removed after the polymer solidifies, resulting in pores where the liquid phase is located; Gas Templates: Gas bubbles can serve as templates in the production of porous polymers. Foaming agents are introduced into the polymer, creating bubbles that form pores when the gas escapes.

- Emulsion techniques

Emulsion techniques involve dispersing two immiscible liquids to form droplets of one liquid within another. The polymer is dissolved in the continuous phase, and after solidification, the dispersed phase is removed, leaving behind pores. Emulsion techniques are particularly useful for producing microporous and mesoporous structures.

- Gas foaming

Gas foaming involves introducing gas into a polymer matrix, either by physical means (e.g., gas injection or pressure release) or chemical means (e.g., the decomposition of foaming agents). The gas forms bubbles that create pores within the polymer. Gas foaming is commonly used in the production of lightweight materials such as foams for packaging and insulation.

## *Chapter I*

### *General Introduction*

- **Electrospinning**

Electrospinning is a process that involves the use of an electric field to draw a polymer solution into fibers. The fibers can be collected in a random or aligned manner, and the resulting mat has a porous structure. Electrospinning polymers have a wide range of applications, including tissue engineering scaffolds and filtration membranes.

## **1.6 Applications of porous polymers**

Porous polymers are widely used in filtration and separation technologies. Membranes made from porous polymers are capable of selectively allowing certain molecules or ions to pass through while blocking others. This makes them ideal for water purification, gas separation, and chemical processing. Moreover, Porous polymers are crucial in tissue engineering, where they serve as scaffolds to support cell growth and tissue regeneration. Porosity allows for nutrient and oxygen diffusion, while the mechanical properties can be tailored to mimic natural tissue. Polymers such as polycaprolactone (PCL) and poly(lactic acid) (PLA) are commonly used for bone and cartilage scaffolds. Nevertheless, the high surface area of porous polymers makes them excellent candidates for catalytic applications. Functional groups can be attached to the polymer surface to catalyze specific chemical reactions. In sensing applications, porous polymers can detect changes in their environment, such as the presence of gases, by interacting with the target molecules within their pores. As for the biological field, porous polymers can be used to encapsulate drugs and control their release over time in drug delivery systems. The porosity of the material can be tailored to achieve specific release rates, making it possible to deliver drugs in a sustained or targeted manner. This approach has been used in cancer therapy, wound healing, and other medical applications.

## 1.7 Objectives of this work

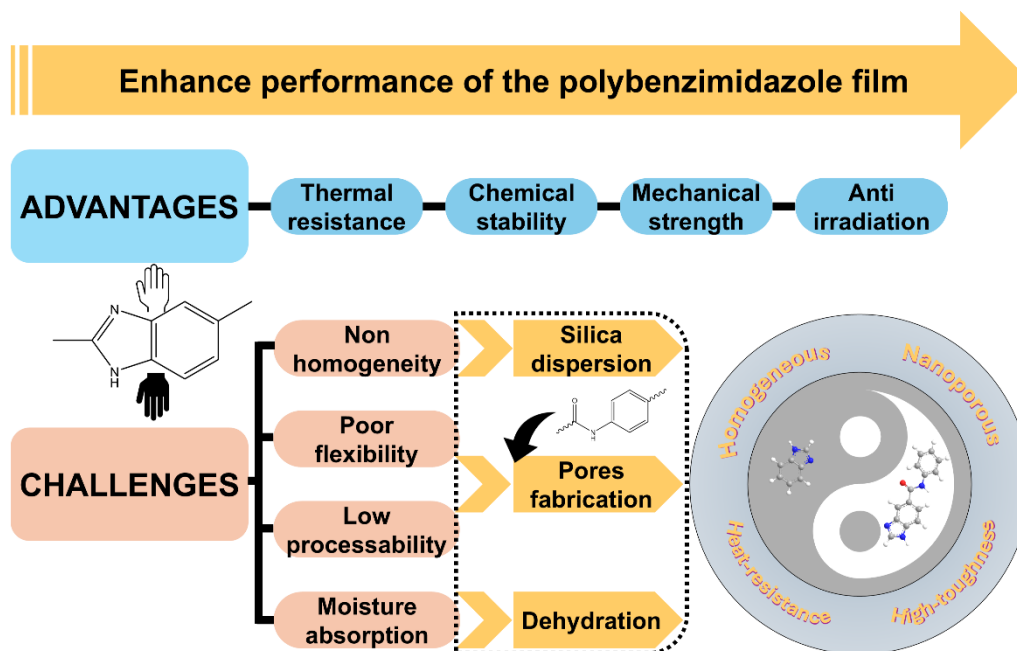


Figure 1-3. Objectives and outlines of this work.

Despite the advantageous properties mentioned above, such as excellent thermal stability, advanced mechanical properties, and chemical resistance, benefiting from the rigid backbones of numerous benzene and imidazole rings, poly(2,5-benzimidazole) (ABPBI) remains a lack of homogeneity, processability, low-cost availability, and flexibility meanwhile, which limited their further application as a super engineering plastic. Hence, it is essential to improve the flexibility of ABPBI film, achieving a stiff and stretchable i.e., high toughness film. In this work, porous structure introduction by

## *Chapter I*

### *General Introduction*

silica-etching method was adopted to improve the shortcomings and enhance the thermal and mechanical properties of ABPBI film (**Figure 1-3**). Introducing porous structures in the film has the merits of a simple procedure, distinguished flexibility increase, no or fewer defects to the original polymer, and so forth. Notably, the monomers used to synthesize polymers in this work are bio-derivable, which reduced the producing cost of PBI remarkably and expanded the adoption in large-scale industrial applications.

Chapter I describes the introduction of the background and objectives of this work.

In Chapter II, a silica nanospheres dispersion method was adopted to refine the branched texture of ABPBI to achieve homogeneous films. Silica with a nanoscale size was sonicated in the polymer solution to disperse the molecular chains. Furthermore, an etching method was adopted to remove the silica nanospheres to obtain nanoporous films with comparable thermal and mechanical properties.

In Chapter III, an aramid part was incorporated into the PBI backbones to improve the processability and flexibility. Moreover, it ameliorates moisture absorption and water-resistance, which may limit their application in the humid environment. Dehydration at high temperatures was employed on the silica nanocomposite poly(benzimidazole-aramid) film. On the other hand, crater-like structures were clarified from the nanoporous poly(benzimidazole-aramid) film, which has an extremely hard edge. In particular, the

## *Chapter I*

### *General Introduction*

hard craters enhanced the mechanical properties remarkably, accomplishing a high toughness and elastic modulus nanoporous film.

Chapter IV summarized the successful performance improvements of PBI film by introducing porous structures, making them significant potential in a variety of industries, from energy and aerospace to electronics and environmental protection. Moreover, the silica-etching method could also be applied to other commercial high-polarity and water-absorbable polymers to enhance their properties and spread wider applications.

## References

- (1) Ghosh, K.; Jones, B. H. Roadmap to Biodegradable Plastics—Current State and Research Needs. *ACS Sustain Chem Eng* **2021**, *9* (18), 6170–6187. <https://doi.org/10.1021/acssuschemeng.1c00801>.
- (2) *Global Production Capacities of Bioplastics 2023-2028 Global Production Capacities of Bioplastics 2023 by Material Type Global Production Capacities of Bioplastics 2028 by Material Type D E C E M B E R 2 0 2 3*. <http://www.european-bioplastics.org/news/publica->.
- (3) Pathak, S.; Sneha, C.; Mathew, B. B. Bioplastics: Its Timeline Based Scenario & Challenges. *Journal of Polymer and Biopolymer Physics Chemistry* **2014**, *2* (4), 84–90. <https://doi.org/10.12691/jpbpc-2-4-5>.
- (4) Papageorgiou, G. Z. Thinking Green: Sustainable Polymers from Renewable Resources. *Polymers (Basel)* **2018**, *10* (9), 952. <https://doi.org/10.3390/polym10090952>.
- (5) Atiwesh, G.; Mikhael, A.; Parrish, C. C.; Banoub, J.; Le, T.-A. T. Environmental Impact of Bioplastic Use: A Review. *Heliyon* **2021**, *7* (9), e07918. <https://doi.org/10.1016/j.heliyon.2021.e07918>.
- (6) Mochane, M. J.; Magagula, S. I.; Sefadi, J. S.; Sadiku, E. R.; Mokhena, T. C. Morphology, Thermal Stability, and Flammability Properties of Polymer-Layered Double Hydroxide

## Chapter I

### General Introduction

- (LDH) Nanocomposites: A Review. *Crystals (Basel)* **2020**, *10* (7), 612.  
<https://doi.org/10.3390/cryst10070612>.
- (7) Smith, G. N.; Hallett, J. E.; Joseph, P.; Tretsiakova-McNally, S.; Zhang, T.; Blum, F. D.; Eastoe, J. Structural Studies of Thermally Stable, Combustion-Resistant Polymer Composites. *Polym J* **2017**, *49* (10), 711–719. <https://doi.org/10.1038/pj.2017.44>.
- (8) Wiswamitra, K. A.; Dewi, S. M.; Choiron, Moch. A.; Wibowo, A. Heat Resistance of Lightweight Concrete with Plastic Aggregate from PET (Polyethylene Terephthalate)-Mineral Filler. *AIMS Mater Sci* **2021**, *8* (1), 99–118.  
<https://doi.org/10.3934/matensci.2021007>.
- (9) Vásquez-Rendón, M.; Sánchez-Arrieta, N.; Álvarez-Láinez, M. Two-Step Processing Method for Blending High-Performance Polymers with Notable Thermal and Rheological Differences: PEI and PBT. *Polym Plast Technol Eng* **2018**, *57* (14), 1411–1417. <https://doi.org/10.1080/03602559.2017.1381256>.
- (10) Escorihuela, J.; Sahuquillo, Ó.; García-Bernabé, A.; Giménez, E.; Compañ, V. Phosphoric Acid Doped Polybenzimidazole (PBI)/Zeolitic Imidazolate Framework Composite Membranes with Significantly Enhanced Proton Conductivity under Low Humidity Conditions. *Nanomaterials* **2018**, *8* (10), 775. <https://doi.org/10.3390/nano8100775>.
- (11) Konovalova, A.; Kim, H.; Kim, S.; Lim, A.; Park, H. S.; Kraglund, M. R.; Aili, D.; Jang,

## Chapter I

### General Introduction

- J. H.; Kim, H.-J.; Henkensmeier, D. Blend Membranes of Polybenzimidazole and an Anion Exchange Ionomer (FAA3) for Alkaline Water Electrolysis: Improved Alkaline Stability and Conductivity. *J Memb Sci* **2018**, *564*, 653–662. <https://doi.org/10.1016/j.memsci.2018.07.074>.
- (12) Wang, D.; Wang, S.; Tian, X.; Li, J.; Liu, F.; Wang, X.; Chen, H.; Mao, T.; Liu, G. Ethyl Phosphoric Acid Grafted Amino-Modified Polybenzimidazole with Improved Long-Term Stability for High-Temperature Proton Exchange Membrane Applications. *Int J Hydrogen Energy* **2020**, *45* (4), 3176–3185. <https://doi.org/10.1016/j.ijhydene.2019.11.219>.
- (13) Krishnan, N. N.; Duong, N. M. H.; Konovalova, A.; Jang, J. H.; Park, H. S.; Kim, H. J.; Roznowska, A.; Michalak, A.; Henkensmeier, D. Polybenzimidazole / Tetrazole-Modified Poly(Arylene Ether) Blend Membranes for High Temperature Proton Exchange Membrane Fuel Cells. *J Memb Sci* **2020**, *614*, 118494. <https://doi.org/10.1016/j.memsci.2020.118494>.
- (14) Berchtold, K. A.; Singh, R. P.; Young, J. S.; Dudeck, K. W. Polybenzimidazole Composite Membranes for High Temperature Synthesis Gas Separations. *J Memb Sci* **2012**, *415–416*, 265–270. <https://doi.org/10.1016/j.memsci.2012.05.005>.
- (15) Joseph, R. M.; Merrick, M. M.; Liu, R.; Fraser, A. C.; Moon, J. D.; Choudhury, S. R.; Lesko, J.; Freeman, B. D.; Riffle, J. S. Synthesis and Characterization of

## Chapter I

### General Introduction

Polybenzimidazole Membranes for Gas Separation with Improved Gas Permeability: A Grafting and Blending Approach. *J Memb Sci* **2018**, *564*, 587–597. <https://doi.org/10.1016/j.memsci.2018.07.064>.

- (16) Moon, J. D.; Bridge, A. T.; D'Ambra, C.; Freeman, B. D.; Paul, D. R. Gas Separation Properties of Polybenzimidazole/Thermally-Rearranged Polymer Blends. *J Memb Sci* **2019**, *582*, 182–193. <https://doi.org/10.1016/j.memsci.2019.03.067>.
- (17) Valtcheva, I. B.; Marchetti, P.; Livingston, A. G. Crosslinked Polybenzimidazole Membranes for Organic Solvent Nanofiltration (OSN): Analysis of Crosslinking Reaction Mechanism and Effects of Reaction Parameters. *J Memb Sci* **2015**, *493*, 568–579. <https://doi.org/10.1016/j.memsci.2015.06.056>.
- (18) Wang, K. Y.; Xiao, Y.; Chung, T.-S. Chemically Modified Polybenzimidazole Nanofiltration Membrane for the Separation of Electrolytes and Cephalexin. *Chem Eng Sci* **2006**, *61* (17), 5807–5817. <https://doi.org/10.1016/j.ces.2006.04.031>.
- (19) Liu, J.; Kong, X.; Jiang, J. Solvent Nanofiltration through Polybenzimidazole Membranes: Unravelling the Role of Pore Size from Molecular Simulations. *J Memb Sci* **2018**, *564*, 782–787. <https://doi.org/10.1016/j.memsci.2018.07.086>.
- (20) Søndergaard, T.; Cleemann, L. N.; Becker, H.; Aili, D.; Steenberg, T.; Hjuler, H. A.; Seerup, L.; Li, Q.; Jensen, J. O. Long-Term Durability of HT-PEM Fuel Cells Based on

## Chapter I

### General Introduction

Thermally Cross-Linked Polybenzimidazole. *J Power Sources* **2017**, *342*, 570–578.

<https://doi.org/10.1016/j.jpowsour.2016.12.075>.

- (21) Wang, F.; Wang, D.; Zhu, H. Montmorillonite–Polybenzimidazole Inorganic–Organic Composite Membrane with Electric Field-Aligned Proton Transport Channel for High Temperature Proton Exchange Membranes. *Polym Plast Technol Eng* **2018**, *57* (17), 1752–1759. <https://doi.org/10.1080/03602559.2017.1422267>.
- (22) Asensio, J. A.; Borrós, S.; Gómez-Romero, P. Proton-conducting Polymers Based on Benzimidazoles and Sulfonated Benzimidazoles. *J Polym Sci A Polym Chem* **2002**, *40* (21), 3703–3710. <https://doi.org/10.1002/pola.10451>.
- (23) Rao, S. S.; Hande, V. R.; Sawant, S. M.; Praveen, S.; Rath, S. K.; Sudarshan, K.; Ratna, D.; Patri, M.  $\alpha$ -ZrP Nanoreinforcement Overcomes the Trade-Off between Phosphoric Acid Dopability and Thermomechanical Properties: Nanocomposite HTPEM with Stable Fuel Cell Performance. *ACS Appl Mater Interfaces* **2019**, *11* (40), 37013–37025. <https://doi.org/10.1021/acsami.9b09405>.
- (24) Cui, W.; Lv, Y.; Sun, P.; Li, Z.; Pei, H.; Yin, X. SPEEK/CMABPBI Ionic and Self-Covalent Cross-Linked Composite Membrane: A Method to Comprehensively Enhance the Properties of High-Temperature Proton Exchange Membranes. *ACS Appl Energy Mater* **2020**, *3* (12), 12115–12126. <https://doi.org/10.1021/acsam.0c02224>.

## Chapter I

### General Introduction

- (25) Nayak, R.; Dey, T.; Ghosh, P. C.; Bhattacharyya, A. R. Phosphoric Acid Doped Poly(2,5-benzimidazole)-based Proton Exchange Membrane for High Temperature Fuel Cell Application. *Polym Eng Sci* **2016**, *56* (12), 1366–1374. <https://doi.org/10.1002/pen.24370>.
- (26) Mohamed, M. G.; EL-Mahdy, Ahmed. F. M.; Kotp, M. G.; Kuo, S.-W. Advances in Porous Organic Polymers: Syntheses, Structures, and Diverse Applications. *Mater Adv* **2022**, *3* (2), 707–733. <https://doi.org/10.1039/D1MA00771H>.
- (27) Malik, T.; Razzaq, H.; Razzaque, S.; Nawaz, H.; Siddiq, A.; Siddiq, M.; Qaisar, S. Design and Synthesis of Polymeric Membranes Using Water-Soluble Pore Formers: An Overview. *Polymer Bulletin* **2019**, *76* (9), 4879–4901. <https://doi.org/10.1007/s00289-018-2616-3>.
- (28) Wood, C. D.; Tan, B.; Trewin, A.; Su, F.; Rosseinsky, M. J.; Bradshaw, D.; Sun, Y.; Zhou, L.; Cooper, A. I. Microporous Organic Polymers for Methane Storage. *Advanced Materials* **2008**, *20* (10), 1916–1921. <https://doi.org/10.1002/adma.200702397>.
- (29) Ghanem, B. S.; Msayib, K. J.; McKeown, N. B.; Harris, K. D. M.; Pan, Z.; Budd, P. M.; Butler, A.; Selbie, J.; Book, D.; Walton, A. A Triptycene-Based Polymer of Intrinsic Microporosity That Displays Enhanced Surface Area and Hydrogen Adsorption. *Chem. Commun.* **2007**, No. 1, 67–69. <https://doi.org/10.1039/B614214A>.
- (30) Han, S. S.; Furukawa, H.; Yaghi, O. M.; Goddard, W. A. Covalent Organic Frameworks

## Chapter I

### General Introduction

as Exceptional Hydrogen Storage Materials. *J Am Chem Soc* **2008**, *130* (35), 11580–11581. <https://doi.org/10.1021/ja803247y>.

- (31) Yuan, S.; Kirklin, S.; Dorney, B.; Liu, D.-J.; Yu, L. Nanoporous Polymers Containing Stereocontorted Cores for Hydrogen Storage. *Macromolecules* **2009**, *42* (5), 1554–1559. <https://doi.org/10.1021/ma802394x>.
- (32) Rochat, S.; Tian, M.; Atri, R.; Mays, T. J.; Burrows, A. D. Enhancement of Gas Storage and Separation Properties of Microporous Polymers by Simple Chemical Modifications. *Multifunctional Materials* **2021**, *4* (2), 025002. <https://doi.org/10.1088/2399-7532/ac005f>.
- (33) Pulko, I.; Wall, J.; Krajnc, P.; Cameron, N. R. Ultra-High Surface Area Functional Porous Polymers by Emulsion Templating and Hypercrosslinking: Efficient Nucleophilic Catalyst Supports. *Chemistry – A European Journal* **2010**, *16* (8), 2350–2354. <https://doi.org/10.1002/chem.200903043>.
- (34) Lee, J.; Kim, J. G.; Chang, J. Y. Fabrication of a Conjugated Microporous Polymer Membrane and Its Application for Membrane Catalysis. *Sci Rep* **2017**, *7* (1), 13568. <https://doi.org/10.1038/s41598-017-13827-w>.
- (35) Pierre, S. J.; Thies, J. C.; Dureault, A.; Cameron, N. R.; van Hest, J. C. M.; Carette, N.; Michon, T.; Weberskirch, R. Covalent Enzyme Immobilization onto Photopolymerized Highly Porous Monoliths. *Advanced Materials* **2006**, *18* (14), 1822–1826.

## Chapter I

### General Introduction

<https://doi.org/10.1002/adma.200600293>.

- (36) Shi, Z.; Hammond, G. B.; Xu, B. Faster and Greener Chemical Reaction Workup Using Silicone Elastomer-Coated Glass Powders. *ACS Omega* **2018**, *3* (6), 6748–6756. <https://doi.org/10.1021/acsomega.8b00966>.
- (37) Silverstein, M. S.; Tai, H.; Sergienko, A.; Lumelsky, Y.; Pavlovsky, S. PolyHIPE: IPNs, Hybrids, Nanoscale Porosity, Silica Monoliths and ICP-Based Sensors. *Polymer (Guildf)* **2005**, *46* (17), 6682–6694. <https://doi.org/10.1016/j.polymer.2005.05.022>.
- (38) Zhao, C.; Danish, E.; Cameron, N. R.; Katakya, R. Emulsion-Templated Porous Materials (PolyHIPEs) for Selective Ion and Molecular Recognition and Transport: Applications in Electrochemical Sensing. *J Mater Chem* **2007**, *17* (23), 2446. <https://doi.org/10.1039/b700929a>.
- (39) Pan, J.-L.; Zhang, Z.; Zhang, H.; Zhu, P.-P.; Wei, J.-C.; Cai, J.-X.; Yu, J.; Koratkar, N.; Yang, Z.-Y. Ultrathin and Strong Electrospun Porous Fiber Separator. *ACS Appl Energy Mater* **2018**, *1* (9), 4794–4803. <https://doi.org/10.1021/acsaem.8b00855>.
- (40) Vargun, E.; Ozaltin, K.; Fei, H.; Harea, E.; Vilčáková, J.; Kazantseva, N.; Saha, P. Biodegradable Porous Polylactic Acid Film as a Separator for Supercapacitors. *J Appl Polym Sci* **2020**, *137* (42). <https://doi.org/10.1002/app.49270>.

## *Chapter II*

### *Fabrication of silica composite and porous polybenzimidazole film*

## **2.1 Introduction**

Porous materials play a crucial role in modern industry owing to their unique properties. These include low bulk densities, high surface areas, low dielectric constants, the ability to act as molecular nanocontainers, and damping capabilities. Moreover, they are useful in catalysts, packaging, drug delivery, segregation, and absorption/desorption.<sup>1-5</sup> Taking inspiration from natural porous materials such as bamboo and honeycomb, various porous materials with diverse structures have been engineered to serve specific purposes.<sup>6-9</sup> For example, metal-organic frameworks<sup>10-12</sup> and covalent-organic frameworks<sup>13,14</sup> with exceptional performances have been designed with intricate porous architectures for the capture and segregation of nitrogen or carbon dioxide, and they have great potential for various applications.<sup>15,16</sup> However, organic porous materials, by their very nature, tend to be relatively unstable when exposed to high temperatures. This limitation restricts their use in applications requiring high thermo-resistance, such as the segregation of waste gases in high-power engines.<sup>17</sup> Furthermore, many existing porous materials, including metal- and covalent-organic frameworks, are derived from fossil fuel-based resources, raising concerns about their sustainability as petroleum resources become depleted. Therefore, there is a pressing need to develop porous materials with high thermo-resistance using natural renewable resources. This

## *Chapter II*

### *Fabrication of silica composite and porous polybenzimidazole film*

endeavor is important for ensuring the long-term sustainability of porous materials in various industrial applications.<sup>18-23</sup>

Polybenzimidazole (PBI) is known for its exceptional thermal stability, chemical durability, and outstanding mechanical properties. It is therefore an excellent candidate for applications that require heat-resistant materials.<sup>24-29</sup> Conventional PBI is used widely in numerous applications owing to its high thermo-resistance. However, its precursor monomer is only available from petroleum-based resources. This poses a significant challenge to the development of conventional PBI from bio-based sources. After a series of chemical modifications to address this challenge, 3,4-diaminobenzoic acid (3,4-DABA) was obtained from bioresources.<sup>30</sup> This breakthrough made producing a bio-based conventional PBI variant, known as poly(2,5-benzimidazole) (ABPBI), feasible. Owing to its unique structural distribution of highly aromatic conjugation, ABPBI has remarkable thermal stability, with a 10% degradation temperature surpassing 600 °C. This places it ahead of conventional PBI in terms of heat resistance. However, casting ABPBI films remains a challenge owing to their non-homogenous texture caused by ABPBI's tendency to aggregate into irregularly branched islands. This results in unstable mechanical properties and low durability and limits the usefulness of the material.

## *Chapter II*

### *Fabrication of silica composite and porous polybenzimidazole film*

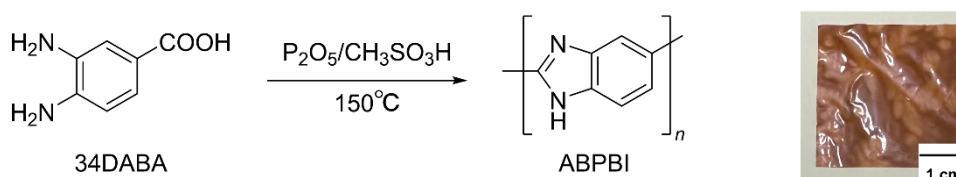
Herein, a porous film was created by mixing ABPBI with a silica porogen and subsequently etching the silica. The process had two results: 1) the surface roughness of the film was reduced by incorporating the silica, and 2) the pore structures were effective in increasing the mechanical toughness of the film compared with the original pure film. Given its high thermal stability and bioavailability, the porous ABPBI film will be useful for industrial applications.

## 2.2 Experimental

### 2.2.1 Materials

3,4-Diaminobenzoic acid (34DABA, 99% purity) and phosphorus pentoxide/methanesulfonic acid ( $P_2O_5/CH_3SO_3H$ ) (Eaton's reagent) were purchased from Tokyo Chemical Industry Co., Ltd. Spherical silica particles (seahostar@KE-P30, diameter: 300 nm) were purchased from Nippon Shokubai Co., Ltd, Osaka, Japan. Hydrofluoric acid (HF, 55% purity) was obtained from Morita Chemical Industries Co. Ltd. Trifluoroacetic acid (TFA), methanesulfonic acid (MSA), sodium bicarbonate, and other chemicals were obtained from Kanto Chemical Co., Inc. All the chemicals and reagents were used as received.

### 2.2.2 Synthesis



**Scheme 2-1** Synthesis of ABPBI from 34DABA using Eaton's reagent. Right picture: photo of ABPBI film. (ABPBI = poly(2,5-benzimidazole); 34DABA = 3,4-

## *Chapter II*

### *Fabrication of silica composite and porous polybenzimidazole film*

Diaminobenzoic acid; Eaton's reagent = phosphorus pentoxide/methanesulfonic acid ( $P_2O_5/CH_3SO_3H$ )).

34DABA (1.521 g, 10 mmol) and 20 mL phosphorus pentoxide/methanesulfonic acid were added to a three-necked flask equipped with a magnetic stirrer at 25 °C under a nitrogen flow. When the 34DABA was dissolved completely, the temperature was increased to 150 °C to initiate polymerization. The viscosity of the solution increased as the polymerization time increased, and the color of the solution changed from yellow to dark brown. After reacting for 24 h, the solution was added to deionized water to precipitate the polymeric fibers. The filtered ABPBI fibers were dried at 100 °C for 24 h in a vacuum and crushed to powder. After neutralizing with a 5 wt% sodium bicarbonate solution, the ABPBI powder was repeatedly washed with deionized water and dried at 60 °C for 12 h.

#### **2.2.3 Fabrication of pure ABPBI film**

ABPBI powder (50 mg) was dissolved in a mixture of TFA with two drops of MSA. After stirring at room temperature for 24 h until a homogeneous solution formed, the TFA

## Chapter II

### Fabrication of silica composite and porous polybenzimidazole film

was evaporated to produce a 1 wt% solution. The ABPBI solution was cast on a silicon wafer substrate to obtain a film. The cast film was immersed in deionized water to remove the residual acid and dried at room temperature for 12 h. After washing repeatedly with deionized water, the ABPBI film was dried at 60 °C for 12 h in a vacuum.

#### 2.2.4 Fabrication of silica composite ABPBI film

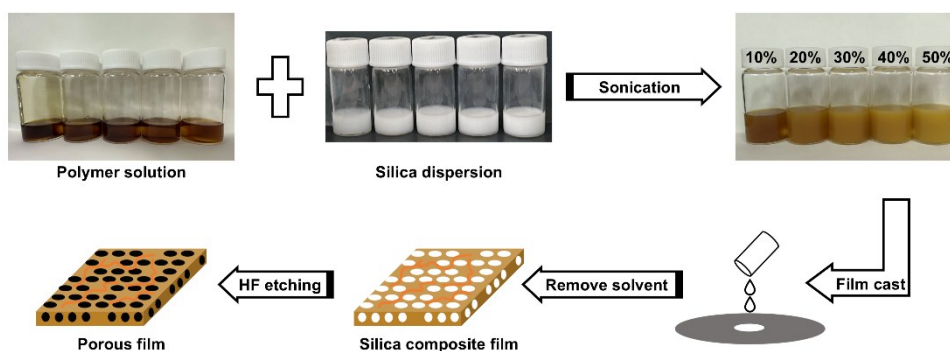


**Figure 2-1.** Fabrication of the porous ABPBI films. (ABPBI = poly(2,5-benzimidazole)).

ABPBI powders (90, 80, 70, 60, and 50 mg) and TFA (3 mL) were added to a screw-capped bottle and magnetically stirred at room temperature for 24 h. After adding 2 drops

## *Chapter II*

### *Fabrication of silica composite and porous polybenzimidazole film*

of MSA and stirring for 24 h at room temperature, the solution became clear. Silica nanoparticles (10, 20, 30, 40, and 50 mg) with an average size of 300 nm were ultrasonicated in TFA at room temperature for 1 h to thoroughly disperse them. The ultrasonicated silica dispersion was immediately mixed with the ABPBI solution and further ultrasonicated at room temperature for 1 h just before casting the film. The ultrasonicated mixture was cast onto a silicon wafer to fabricate ABPBI–silica composite films. After evaporating the TFA at room temperature, the formed ABPBI–silica composite films were washed repeatedly with deionized water and immersed in deionized water for 24 h to completely remove the residual acid. The washed ABPBI–silica composite films were then dried at 60 °C for 12 h in a vacuum.

#### **2.2.5 Fabrication of porous ABPBI films**

The dried ABPBI–silica composite films were immersed in a 40% HF aqueous solution for 24 h to fabricate porous ABPBI films (**Figure 2-1**). After washing repeatedly until the pH reached approximately 7 according to the pH test paper, the porous ABPBI films were soaked in deionized water for 24 h to remove residual acid and dried at 60 °C for 12 h in a vacuum.

### **2.3 Measurements**

Fourier-transform infrared (FT-IR) spectra were obtained to determine the chemical structure of the synthesized ABPBI. The wavenumbers were in the range of 2000 - 400  $\text{cm}^{-1}$ , and the spectra were obtained using a Perkin-Elmer spectrometer with a diamond-attenuated total reflection (ATR) accessory. Thermo-gravimetric analysis (TGA) was performed using a HITACHI STA2700 system. The film specimens were placed in a platinum crucible and heated to a maximum temperature of 800  $^{\circ}\text{C}$  at a rate of 10  $^{\circ}\text{C min}^{-1}$  under a nitrogen atmosphere. The morphology of each fabricated film was determined using a HITACHI TM3030 plus tabletop SEM. Energy-dispersive X-ray spectroscopy (EDS) was used to identify residual elements in the prepared films. The film specimens were pre-coated with Au powder under a vacuum for 30 s (thickness: approximately 15 nm). HITACHI AFM5000 II SPA-400 was used to determine the morphology and roughness of each film. Tensile tests were carried out using an Instron-3365 mechanical tester instrument at an ambient temperature of around 25  $^{\circ}\text{C}$ . The film samples were cut to a rectangular shape (30 mm  $\times$  5 mm) and five specimens with an initial gauge length of 20 mm were measured at a tensile speed of 5  $\text{mm min}^{-1}$ .

## 2.4 Results and Discussion

### 2.4.1 Preparation of silica composite and porous polybenzimidazole film

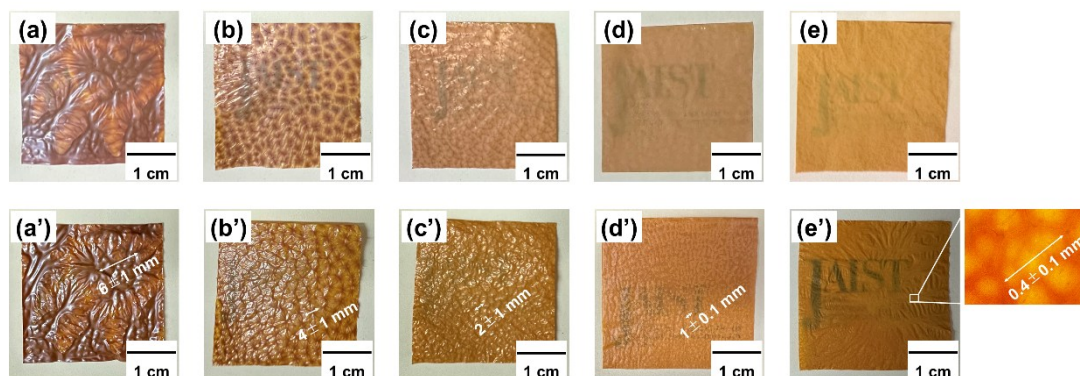


**Figure 2-2.** Photos of ABPBI composite films with silica contents of a) 10, b) 20, c) 30, d) 40, and e) 50 wt% and those with porosities of a') 8, b') 16, c') 24, d') 32, and e') 40 vol%. The porosities were calculated from the silica density. The inset photo of e') is an optical microscope image. (ABPBI = poly(2,5-benzimidazole)).

ABPBI is conventionally synthesized by the polycondensation of DABA using an acidic solvent of very high viscous poly(phosphoric acid). The reaction is time-consuming, and a large amount of water is required to remove the catalyst from the product. Herein, the efficiency of synthesis was attempted to improve by using another reagent, i.e., Eaton's reagent, which is known as a solvent system for polybenzazole syntheses due to the high monomer solubility.<sup>31,32</sup> The polymerization proceeded

## *Chapter II*

### *Fabrication of silica composite and porous polybenzimidazole film*

smoothly, and solvent removal was completed easily. The ABPBI powder was processed into a film by casting method with dissolving in strong acids, e.g., methane sulfonic acid (MSA), trifluoroacetic acid (TFA), sulfuric acid (SA), etc., due to their limited solubility with common organic solvents caused by the rigid molecular structure.<sup>33</sup> TFA with a trace amount of MSA was used as the solvent for casting because ABPBI is readily soluble in it. The film was completely dried within 1 h owing to the low boiling temperatures of MSA (122 °C) and TFA (72.4 °C). The resulting film was mechanically robust and brown in color. The film surface was heterogenous, i.e., featured branched dark brown regions that were a maximum of 30  $\mu\text{m}$  thick separated from the thinner matrix, which was a minimum of 18  $\mu\text{m}$  thick. The statistical difference was calculated as 3.06  $\mu\text{m}$ . During drying, the ABPBI solution condensed and was deposited owing to the strong intermolecular interactions of ABPBI, which is highly polar. When the brown regions began to form, the ABPBI around the solution surface became extremely condensed, inducing interchain self-assembly, which is caused by the interactions from numerous hydrogen bonds and strong  $\pi$ - $\pi$  stacking.<sup>34</sup> Thereupon the assembled matter absorbed the solvent, thereby becoming sticky. The assembled matter grew into a fibrous aggregate following further drying from the solution surface, whereas the ABPBI around the middle and bottom of the solution was still dissolved owing to the increased concentration of

## Chapter II

### *Fabrication of silica composite and porous polybenzimidazole film*

MSA in the mixed solvent. Ultimately, thick brown fibrous branches remained in the cast film. Unfortunately, such heterogeneity limits the usefulness of ABPBI film.

Porous ABPBI was prepared by the silica-etching method,<sup>35,36</sup> using ultrasonication to disperse the silica nanoparticles as uniformly as possible in the ABPBI before casting the films. Consequently, the silica dispersion coexisted stably with the ABPBI for more than 1 h. The aim was to form a homogeneous ABPBI film containing silica nanoparticles. However, the resulting films were firm, but the heterogeneity remained. As shown in **Figure 2-2a'**, the thick brown regions were wrinkled and more branched than in the original ABPBI film without silica. The distance between the wrinkles was  $6 \pm 1$  mm, and the size and distance between them decreased as the amount of silica increased, as shown in **Figure 2-2a'-e'**. The thick brown regions decreased in size from 6 to 0.4 mm when the amount of silica nanoparticles increased from 10 to 50 mg. The branched wrinkles almost disappeared when the weight of the silica nanoparticles matched that of the ABPBI. The silica nanoparticles were mixed with the ABPBI to act as porogens; the results revealed that they acted as homogenizers to produce uniform films of ABPBI. The dispersion mechanism is thought to involve strong interaction between the surfaces of the silica nanoparticle and the ABPBI chains caused by their high polarity and favorable dispersion behavior. When the silica nanoparticles were stably dispersed in the films by

ultrasonication, the ABPBI chains adhered to the particle surfaces were distributed uniformly.

### 2.4.2 Porosity calculation

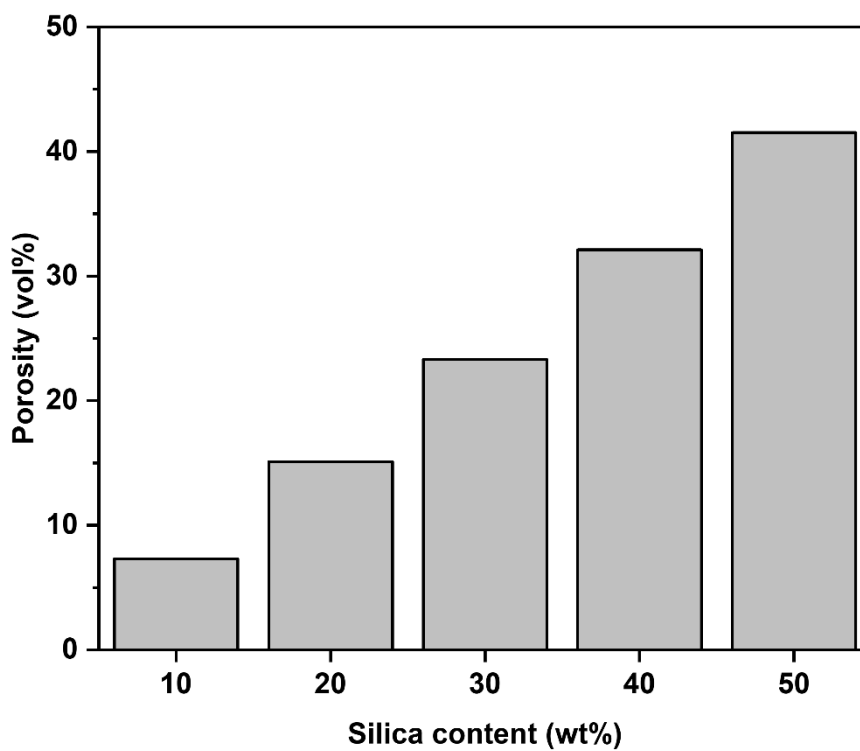


Figure 2-3. Porosity calculation from the added silica nanospheres content.

## *Chapter II*

### *Fabrication of silica composite and porous polybenzimidazole film*

An aqueous solution of HF was used to remove the silica nanoparticles from the silica–ABPBI films to fabricate the porous ABPBI films. The porosities were calculated from the volume fraction to be 8, 16, 24, 32, and 40 vol%, respectively, basing the density ratio of added silica nanosphere contents to polymer, as shown in **Figure 2-3**. Additionally, the volume percentage of the film porosities was also calculated supplementary by the  $3/2$  power of area percentage estimated from SEM images to be 9, 16, 26, 33, and 40%, respectively, using ImageJ processing software. The calculated results of volume porosities by ImageJ showed a good coincidence with that which was calculated from the incorporated silica percentage. Moreover, **Figure 2-2** demonstrates that the patterns of the thick brown regions were almost retained after silica-etching treatment, although the film transparency increased, suggesting that the treatment appropriately dissolved out the silica particles without causing any other film damage.

## 2.4.3 FT-IR-spectrum

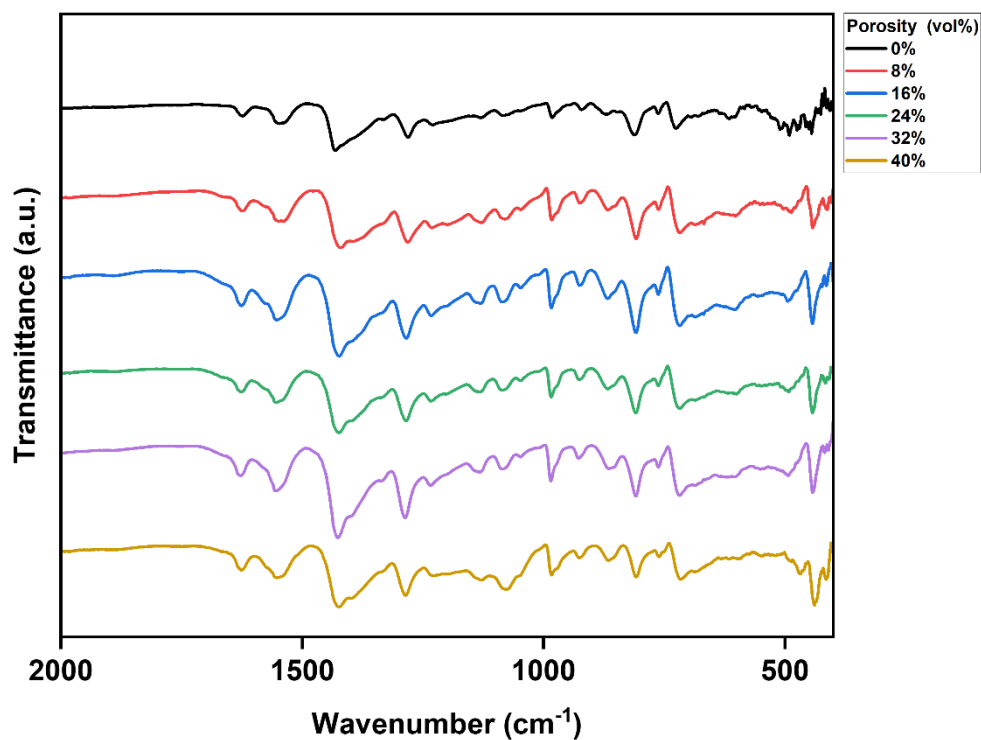


**Figure 2-4.** FT-IR spectra of ABPBI films with various porosities.

The chemical structure of the obtained ABPBI powder was confirmed by FT-IR (ATR mode) and the spectrum is shown in **Figure 2-4**. The signals at 1627, 1551, and 1283 cm<sup>-1</sup> were assigned to the stretching vibrations of the C=N, C=C, and C-N, respectively.<sup>37,38</sup> The FT-IR spectra indicated the successful synthesis of ABPBI using Eaton's reagent. FT-IR/ATR spectroscopy revealed no peak-shifting following the silica-

## *Chapter II*

### *Fabrication of silica composite and porous polybenzimidazole film*

etching treatment of the original ABPBI films to produce the porous films, demonstrating that HF etching did not cause any chemical damage owing to the high chemical resistance and stability of ABPBI. Moreover, no broad absorption peak of Si-O-Si at around 1100  $\text{cm}^{-1}$  was assigned,<sup>39</sup> indicating that the added silica nanospheres in the preparation progress of the porous films were removed by HF completely.

### 2.4.4 SEM morphologies

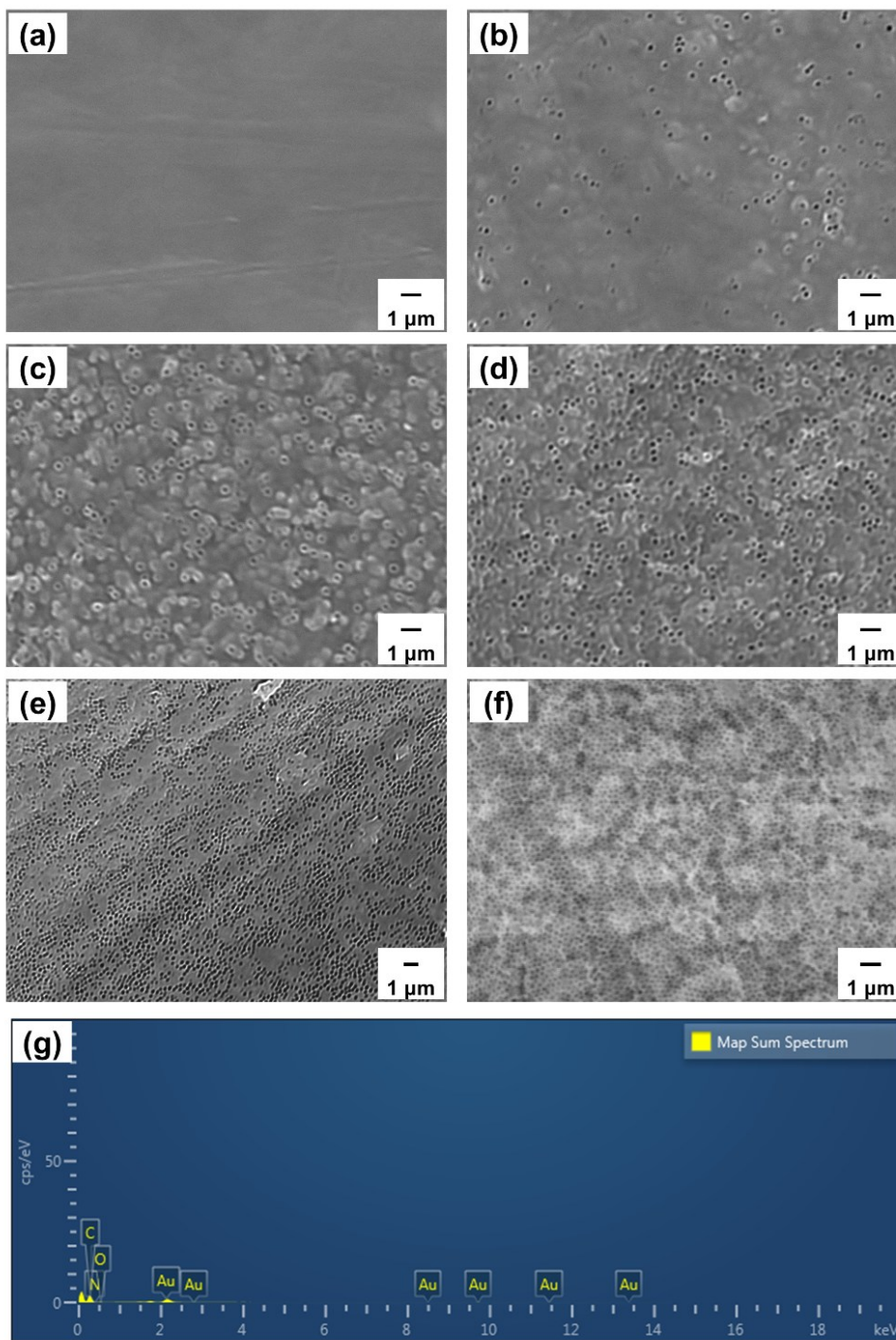


**Figure 2-5.** SEM images of original a) and porous ABPBI films with porosities of b) 8, c) 16, d) 24, e) 32, and f) 40 vol%. g) EDS elemental analysis of f). (SEM = scanning

## Chapter II

### *Fabrication of silica composite and porous polybenzimidazole film*

electron microscopy; ABPBI = poly(2,5-benzimidazole); EDS = energy-dispersive X-ray spectroscopy).

SEM was adopted to investigate the morphologies of the obtained ABPBI films (**Figure 2-5**). The pure ABPBI film had a rather flat surface (**Figure 2-5a**), whereas all the porous ABPBI films had pores on their surfaces. It was confirmed from the SEM images that the increased porosity was caused by increasing the amount of silica in the composition (**Figure 2-5b-f**). Moreover, it indicates the successful preparation of ABPBI films with tailored porosities where the size of the pores was approximately 300 nm, corresponding to that of the added silica nanospheres. Notably, compared with other work,<sup>40-42</sup> the fabricated porous ABPBI films displayed significantly different morphologies with a white rim area surrounding the pores, which could be observed clearly at low porosities especially. The unique phenomenon was extremely attractive and further investigated by other evaluation methods. The EDS mapping results revealed that no elemental silicon or fluorine remained, suggesting that the silica nanoparticles were completely removed by HF and the HF solution was washed out cleanly (**Figure 2-5g and Figures 2-6 – 2-8**).

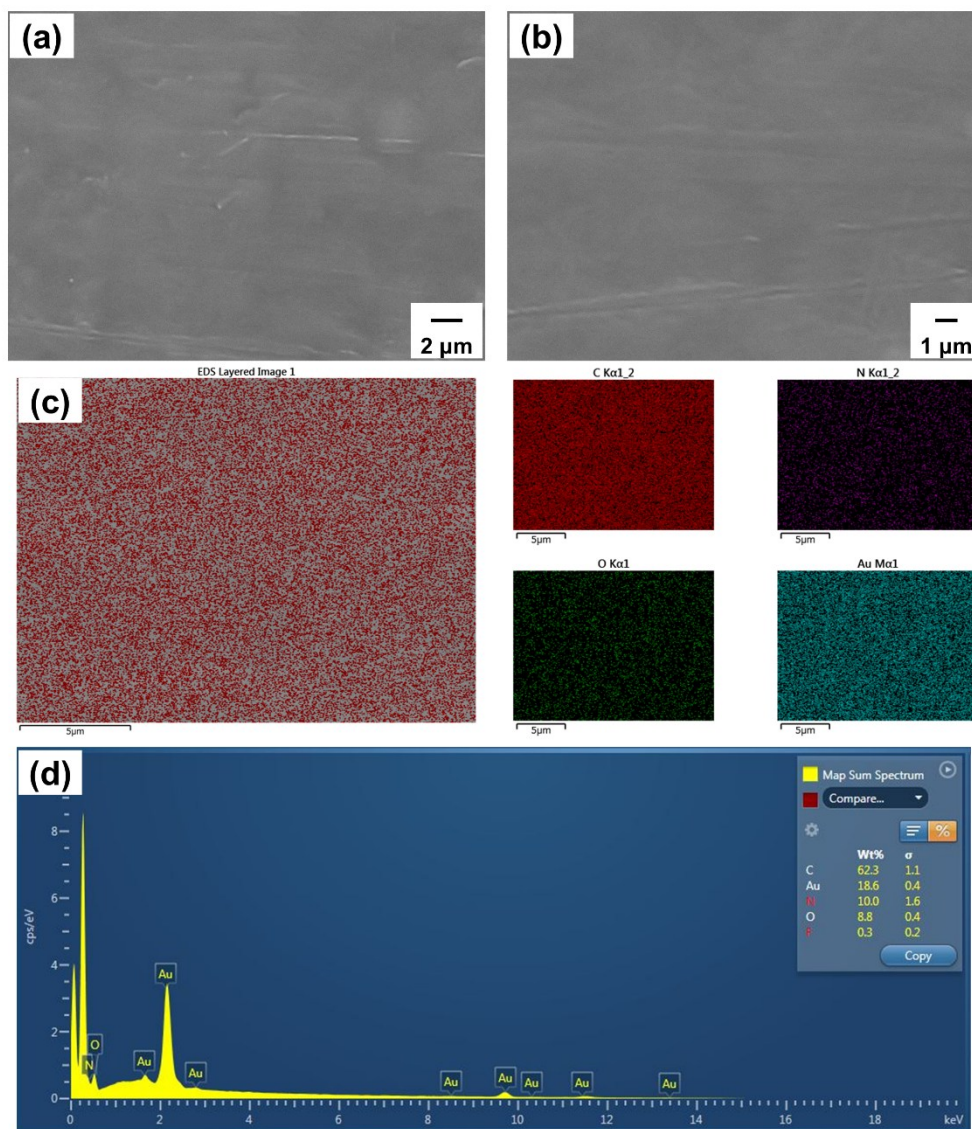


**Figure 2-6.** SEM images at a) 5000 and b) 8000 magnifications, c) EDS mappings, and d) elemental analysis spectrum of original ABPBI film.

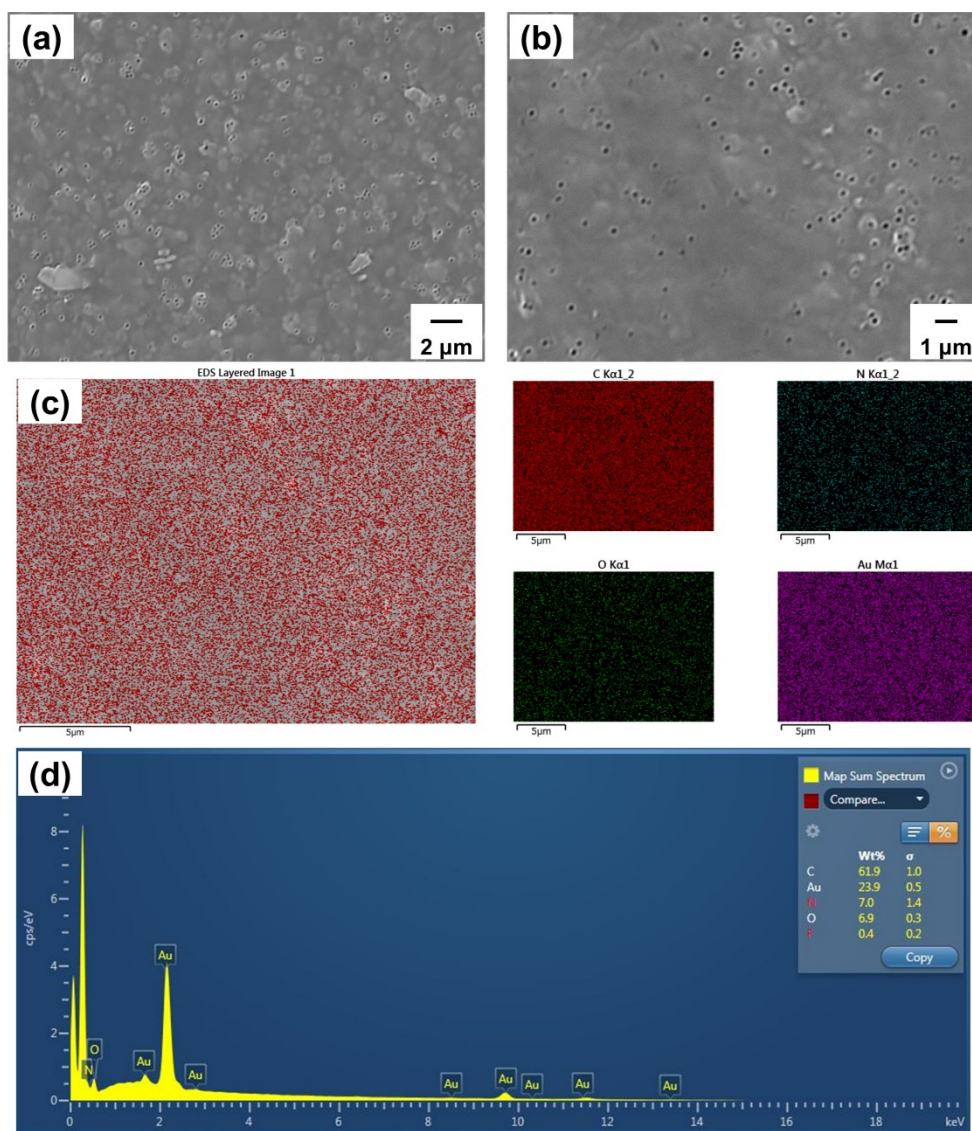


**Figure 2-7.** SEM images at a) 5000 and b) 8000 magnifications, c) EDS mappings, and d) elemental analysis spectrum of porous ABPBI film with 8% porosity (silica content 10 wt%).

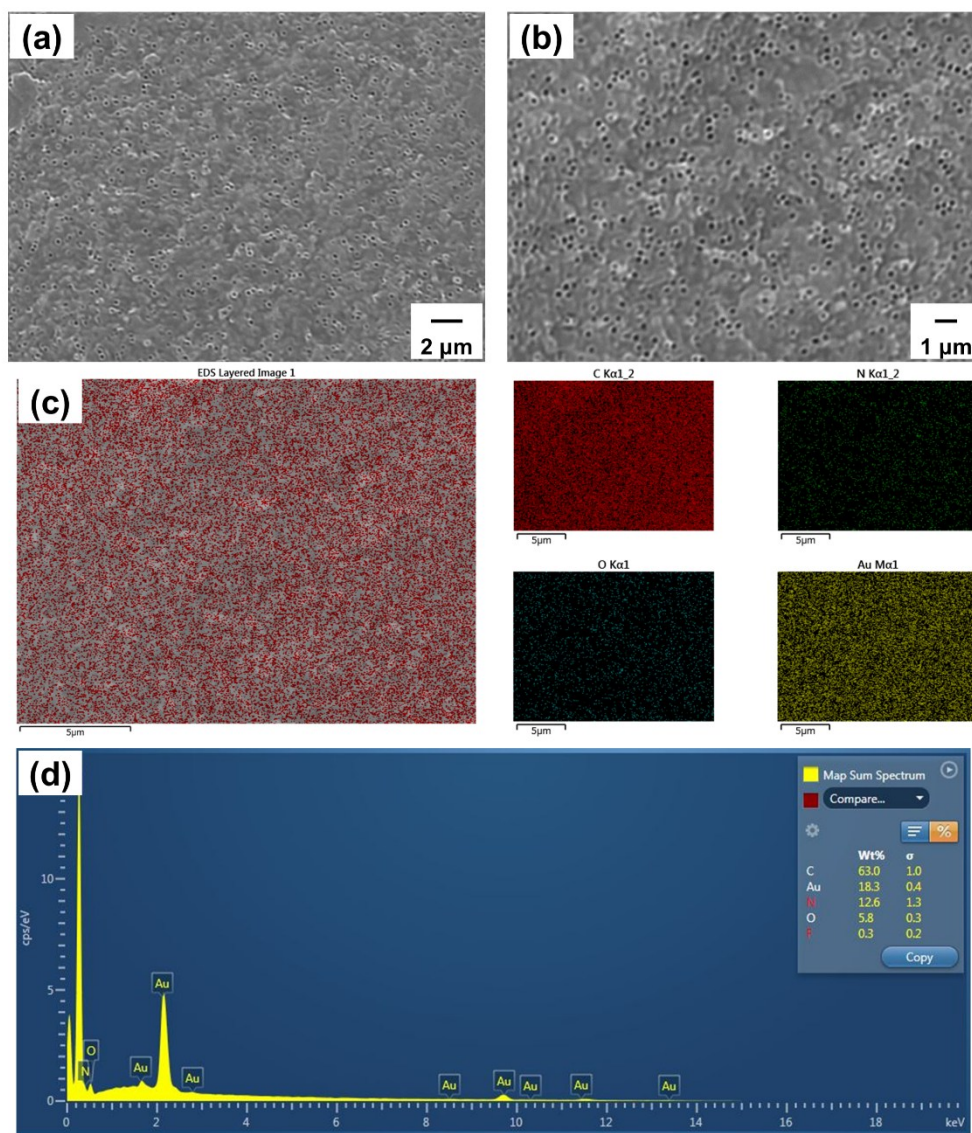


**Figure 2-8.** SEM images at a) 5000 and b) 8000 magnifications, c) EDS mappings, and d) elemental analysis spectrum of porous ABPBI film with 24% porosity (silica content 30 wt%).

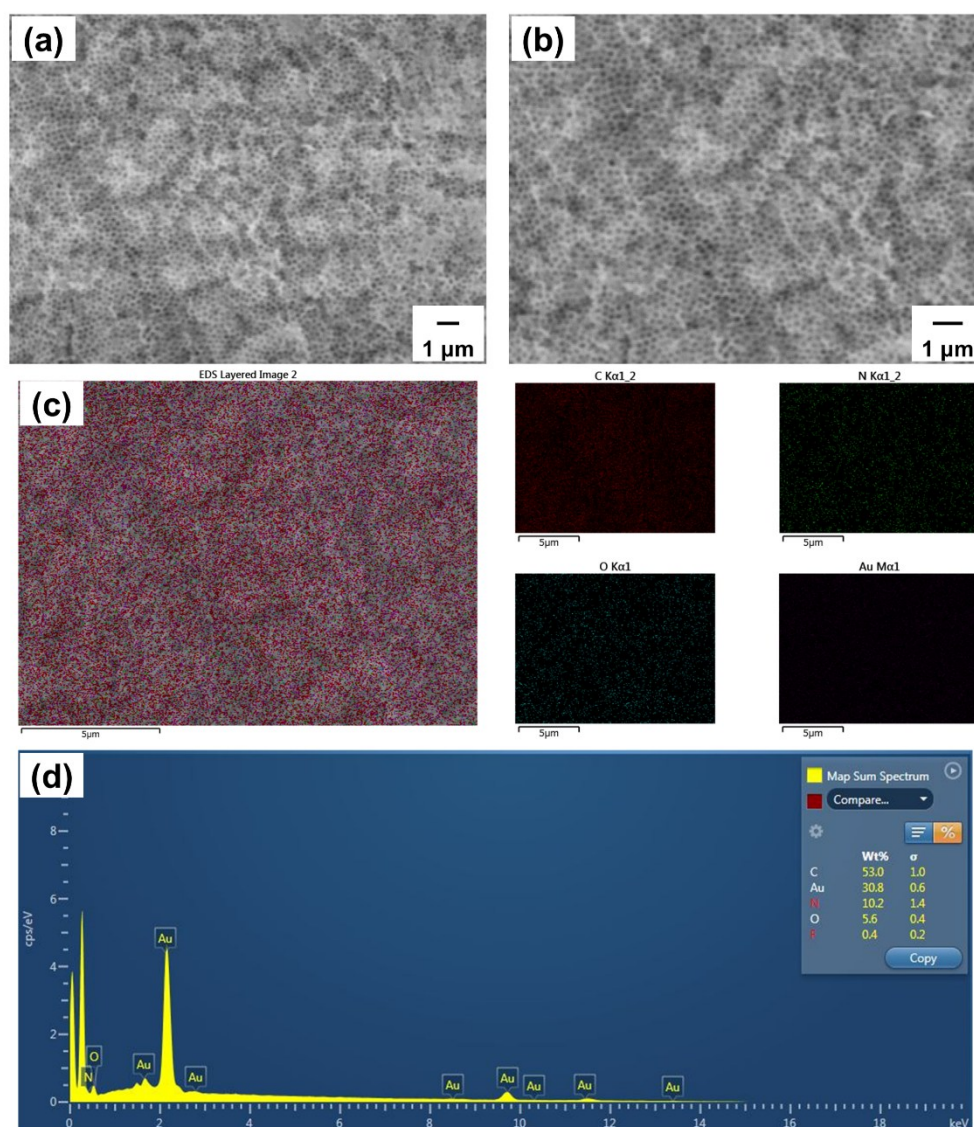


**Figure 2-9.** SEM images at a) 5000 and b) 8000 magnifications, c) EDS mappings, and d) elemental analysis spectrum of porous ABPBI film with 40% porosity (silica content 50 wt%).

## 2.4.5 AFM analysis

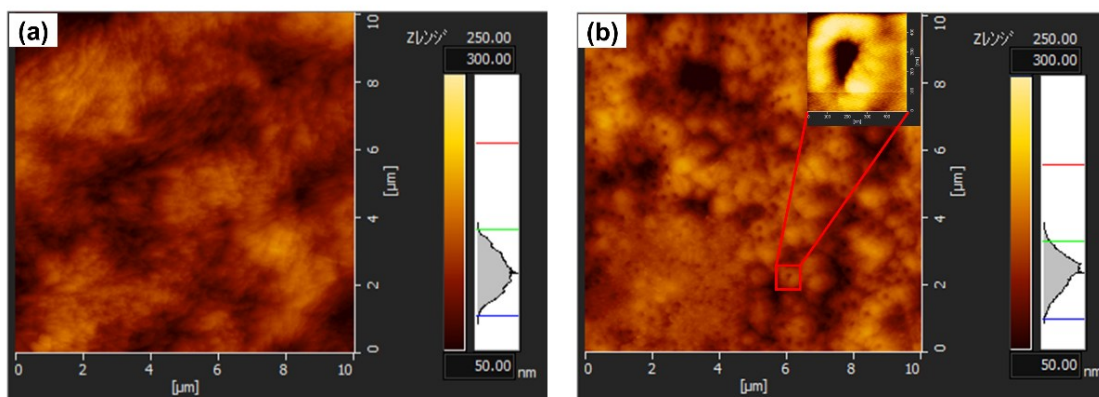


**Figure 2-10.** AFM images of ABPBI films with porosities of a) 0% and b) 16% (insert photo: single pore). (AFM = atomic force microscopy; ABPBI = poly(2,5-benzimidazole).

The SEM images revealed pores with white rim edges, which inspired us to envision the formation of a crater-like morphology. Hence, the pore morphology was subsequently investigated by AFM, using ABPBI films with porosities of 0% and 16% (**Figure 2-10**). The original ABPBI film had a rough surface and produced a broad height distribution curve (**Figure 2-10a**), whereas the ABPBI film with a porosity of 16% had a more homogeneous surface and produced a much narrower height distribution curve (**Figure 2-10b**). It indicated that the roughness was reduced by the silica-etching treatment. The inset of **Figure 2-10b** is the enlarged image of a single pore with a diameter of approximately 300 nm, corresponding with the diameter of the silica nanoparticles.

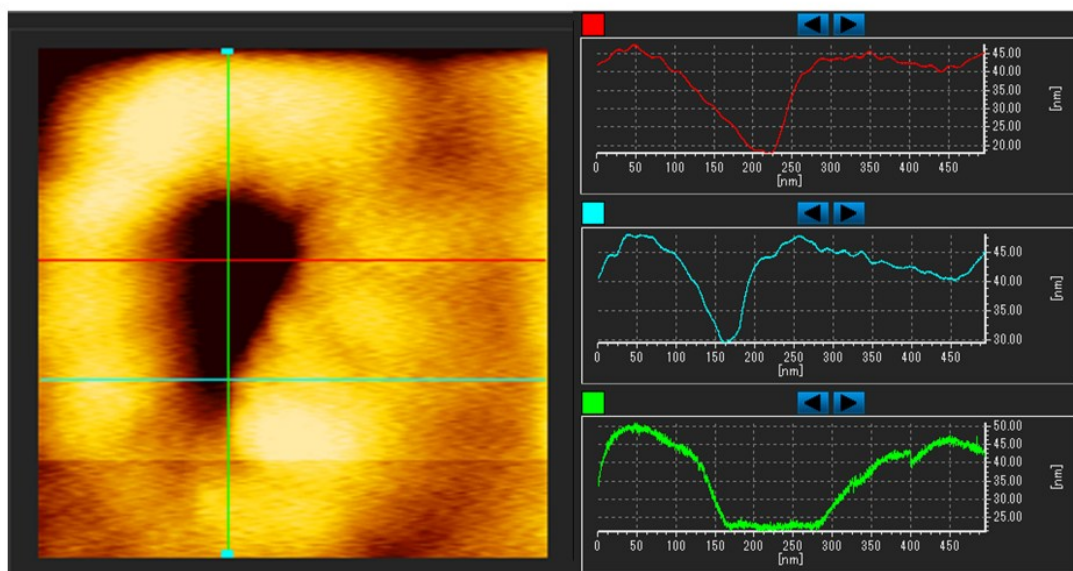


**Figure 2-11.** Linear height analysis of the single pore.

Linear height analysis was used to investigate the height difference between the inner, outer, and rim areas of the single pore (**Figure 2-11**). The highest areas, which were approximately 50 nm high, were located around the pore. Therefore, the circular edges of the pore were swollen, which was named the crater structure. The number of craters increased as the silica nanoparticle content increased. The crater structure formation was also confirmed in films comprising an ABPBI copolymer with 4-aminobenzoic acid.<sup>43</sup> The ABPBI chains aggregated on the silica nanoparticle surfaces, as discussed above, and the aggregated chains remained during the solvent evaporation process.

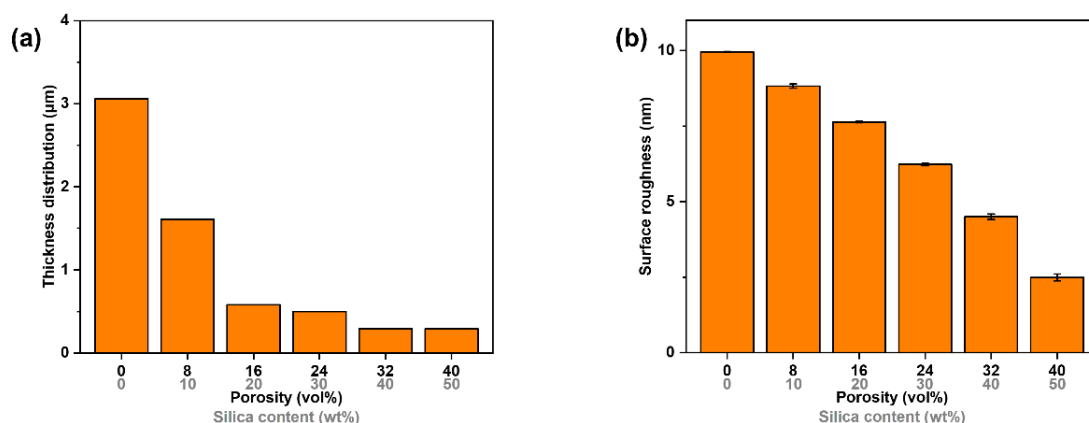


**Figure 2-12.** Thickness distribution a) and surface roughness on the nanoscale b) of ABPBI films with various porosities. (ABPBI = poly(2,5-benzimidazole)).

The thickness distribution, which was calculated from the thickness variations, was quantified as 3.1 to 0.3  $\mu\text{m}$  using a micrometer gauge and decreased as the amount of silica increased from 10 to 50% (**Figure 2-12a**). This confirms that silica-etching treatment reduced the surface roughness of the material by dispersing the assembled polymer chains surrounding the silica nanospheres which contacted each other by the strong interfacial interactions. AFM analysis also revealed a decrease in the roughness of the porous ABPBI films surface on the nanoscale (i.e., 10 to 2.5 nm) (**Figure 2-12b**). The findings indicate that the assembled materials could be readily controlled by adding homogeneously dispersed silica nanoparticles.

### 2.4.6 TGA analysis

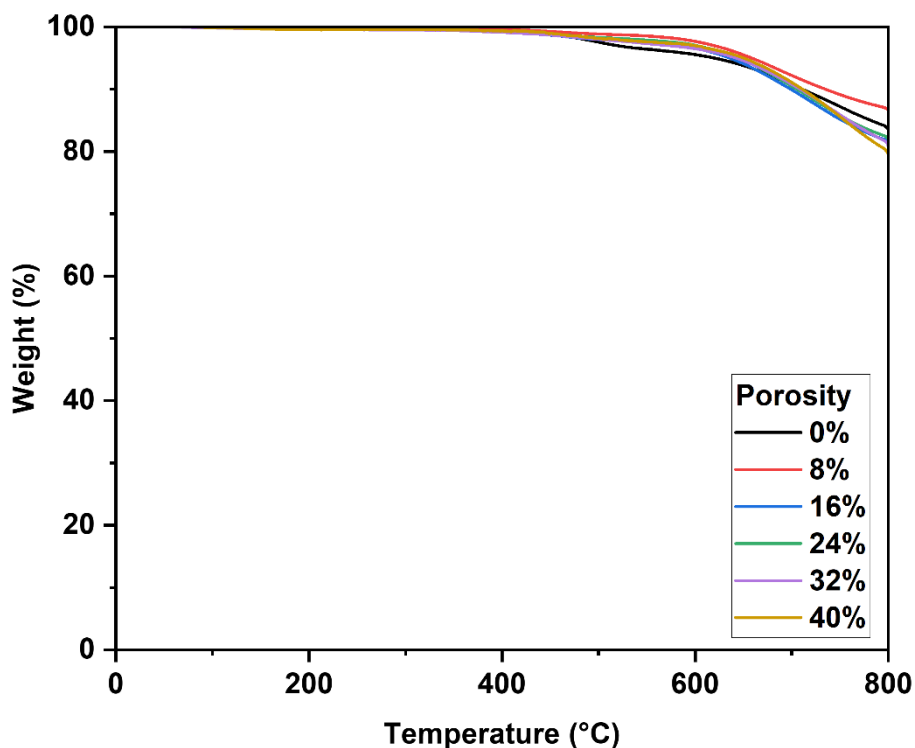


**Figure 2-13.** TGA curves of ABPBI films with various porosities. (TGA = thermogravimetric analysis; ABPBI = poly(2,5-benzimidazole)).

Thermogravimetric analysis (TGA) was used to assess the thermal characteristics of ABPBI films with various porosities (**Figure 2-13**). The TGA results revealed a constant value of approximately 100% mass from 0 to approximately 400 °C, demonstrating the high thermal stability of the original ABPBI film and complete ring-closure to form an

## *Chapter II*

### *Fabrication of silica composite and porous polybenzimidazole film*

imidazole ring during the synthesis process. Furthermore, the resultant ABPBI had an exceptionally high 10 percent mass-loss temperature ( $T_{d10}$ : 710 °C), which was comparable to those of other ABPBI polymers synthesized using the conventional poly(phosphoric acid) method. This suggests that Eaton's reagent is useful for synthesizing ABPBI, including the merits of lower polymerization temperature, less viscosity, and easier handling and removal of the polymerization solvent.<sup>44</sup> Moreover, regardless of their expanded surface areas, the porous ABPBI films had high  $T_{d10}$  values of over 700 °C and high char yields of approximately 80%, as shown in **Table 2.1**. They are therefore potentially useful for many applications such as ultrahigh thermoresistant porous plastics.

## 2.4.7 Stress-strain (S-S) curves

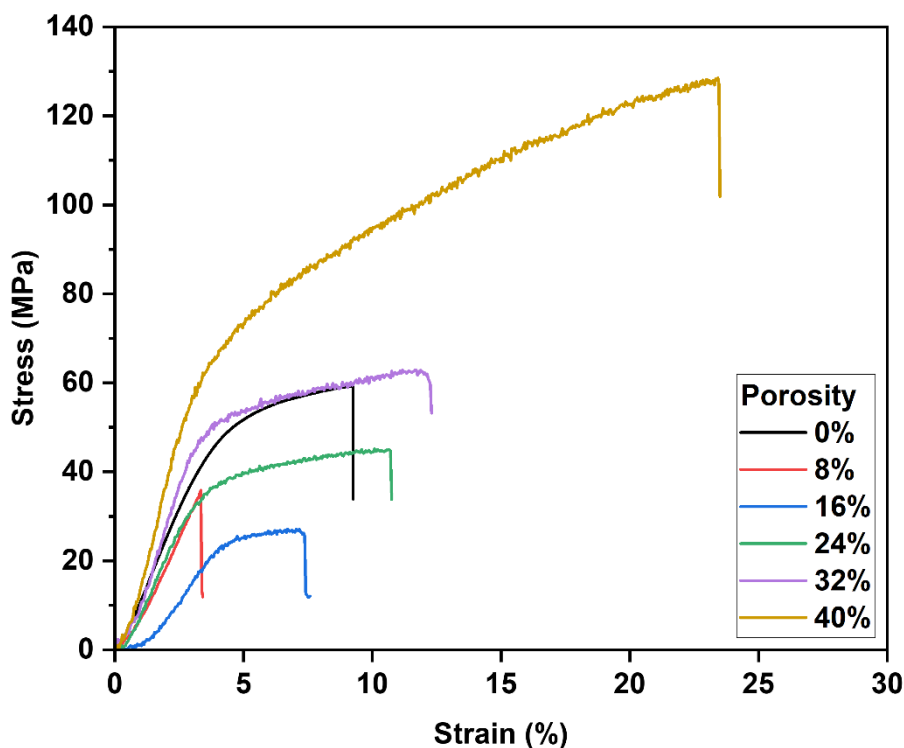


**Figure 2-14.** Stress–strain (S-S) curves of ABPBI films with various porosities. (ABPBI = poly(2,5-benzimidazole)).

The mechanical properties of the ABPBI composite films were assessed by examining their stress-strain curves (**Figure 2-14**). The silica composite films were too brittle for valid investigation, so the porous ABPBI films were focused. When a small number of pores were incorporated, the mechanical properties such as strength at break,

## Chapter II

### *Fabrication of silica composite and porous polybenzimidazole film*

elongation at break, Young's modulus, and strain energy density, showed decreased values, which could be attributed to the low uniformity of the films. However, the mechanical properties were gradually improved as the porosity increased. When the porosity reached 32%, the stress-strain curve became comparable to that of the original ABPBI film. Finally, when the porosity was 40%, the highest value of the strength at break was 128 MPa, and the elongation at break was 23%, both of which values exceeded those of the original non-porous ABPBI film: 59 MPa for the strength at break and 9% for the elongation at break, demonstrating a significant improvement in the mechanical performance. Moreover, the strain energy density increased to  $21.6 \text{ MJ m}^{-3}$ , i.e., almost 5 times as high as that of the original ABPBI film ( $3.9 \text{ MJ m}^{-3}$ ). Despite the presence of pores, Young's moduli of the films with porosities of 32% and 40% exceeded that of the original ABPBI film. The enhanced mechanical properties should be attributed to the fact that the pores effectively improved flexibility, as predicted previously and investigated in other work as well.<sup>45,46</sup> Moreover, the effects of circular aggregates around the crater edges can increase Young's modulus to improve the film's strength and toughness. In addition, it can be noted that the standard deviation values shown by plus/minus values of strength at break and strain energy density (toughness) in **Table 2.1** were decreased with an increase in the porosity and silica nanoparticles. The increased homogeneity,

which was achieved by suppressing the self-aggregation of high-polar ABPBI chains by silica dispersion, is effective in mechanical data accuracy.

**Table 2-1. Thermal and mechanical properties of the porous ABPBI films with various porosities**

Porosity	$T_{d10}^a$ (°C)	Char yield <sup>a</sup> (%)	Young's modulus <sup>b</sup> (GPa)	Strength at break <sup>b</sup> (MPa)	Elongation at break <sup>b</sup> (%)	Strain energy density <sup>b</sup> (MJ/m <sup>3</sup> )
ABPBI-0	710	84	1.34±0.05	59±5	9±1	3.9±0.3
ABPBI-8	735	87	1.09±0.05	36±5	3±1	0.5±0.2
ABPBI-16	700	81	0.71±0.04	27±4	7±1	1.0±0.2
ABPBI-24	705	82	1.30±0.03	45±3	11±1	3.6±0.1
ABPBI-32	710	81	1.92±0.03	62±2	12±1	5.8±0.1
ABPBI-40	710	80	2.48±0.02	128±2	23±2	21.6±0.1

ABPBI = poly(2,5-benzimidazole).

<sup>a</sup> Thermal property obtained by thermo-gravimetric analysis (TGA).

<sup>b</sup> Mechanical properties of the porous ABPBI films obtained from uniaxial tensile tests.

## **2.5 Conclusion**

In this Chapter, an ABPBI film was formed successfully from the bio-based monomer 34DABA and confirmed its structure by FT-IR analysis. ABPBI films were fabricated by solution casting using TFA including a small amount of MSA as a solvent. The surfaces of the films were heterogeneous and featured branched patterns of thick brown regions, which may have originated from the surface condensation of ABPBI to form sticky fibrous aggregates. Subsequently, porous ABPBI films with various porosities were fabricated by a hard-templating method using silica nanoparticle fillers, followed by etching with HF. The successful construction of pores was confirmed by SEM and AFM, which revealed the formation of polymer aggregates like craters around the pore edges. The composite ABPBI films had reduced heterogeneity and roughness compared with the original ABPBI film. Herein, a formation mechanism could be proposed whereby the ABPBI aggregate stuck to the surfaces of the silica nanoparticles, which were well dispersed over the film by ultrasonication. TGA characterization revealed that the porous ABPBI films had a 10% mass loss temperature of 710 °C, indicating that they had ultrahigh thermal stability that surpassed that of most of the available organic materials. Moreover, the porous structure conferred an obvious improvement in mechanical properties owing to the hard aggregates around the pores.

## *Chapter II*

### *Fabrication of silica composite and porous polybenzimidazole film*

This suggests the potential of ABPBI as a porous material for use in, e.g., fuel cell separators, leakproof films, and filtration membranes.

## Chapter II

### *Fabrication of silica composite and porous polybenzimidazole film*

#### References

- (1) Ristić, A.; Logar, N. Z.; Henninger, S. K.; Kaučič, V. The Performance of Small-Pore Microporous Aluminophosphates in Low-Temperature Solar Energy Storage: The Structure–Property Relationship. *Adv Funct Mater* **2012**, *22* (9), 1952–1957. <https://doi.org/10.1002/adfm.201102734>.
- (2) Song, Y.; Phipps, J.; Zhu, C.; Ma, S. Porous Materials for Water Purification. *Angewandte Chemie International Edition* **2023**, *62* (11). <https://doi.org/10.1002/anie.202216724>.
- (3) Fajal, S.; Mandal, W.; Mollick, S.; More, Y. D.; Torris, A.; Saurabh, S.; Shirolkar, M. M.; Ghosh, S. K. Trap Inlaid Cationic Hybrid Composite Material for Efficient Segregation of Toxic Chemicals from Water. *Angewandte Chemie International Edition* **2022**, *61* (32). <https://doi.org/10.1002/anie.202203385>.
- (4) Wang, G.; Wang, L.; Mark, L. H.; Shaayegan, V.; Wang, G.; Li, H.; Zhao, G.; Park, C. B. Ultralow-Threshold and Lightweight Biodegradable Porous PLA/MWCNT with Segregated Conductive Networks for High-Performance Thermal Insulation and Electromagnetic Interference Shielding Applications. *ACS Appl Mater Interfaces* **2018**, *10* (1), 1195–1203. <https://doi.org/10.1021/acsami.7b14111>.
- (5) Zhan, Y.; Cheng, Y.; Yan, N.; Li, Y.; Meng, Y.; Zhang, C.; Chen, Z.; Xia, H. Lightweight and Self-Healing Carbon Nanotube/Acrylic Copolymer Foams: Toward the Simultaneous

## Chapter II

### *Fabrication of silica composite and porous polybenzimidazole film*

Enhancement of Electromagnetic Interference Shielding and Thermal Insulation.

*Chemical Engineering Journal* **2021**, *417*, 129339.

<https://doi.org/10.1016/j.cej.2021.129339>.

- (6) Zhang, Y.; Jiang, M.; Zhao, J.; Ren, X.; Chen, D.; Zhang, G. A Novel Route to Thermosensitive Polymeric Core-Shell Aggregates and Hollow Spheres in Aqueous Media. *Adv Funct Mater* **2005**, *15* (4), 695–699. <https://doi.org/10.1002/adfm.200400378>.
- (7) Wu, Q.; Wang, Z.; Xue, G. Controlling the Structure and Morphology of Monodisperse Polystyrene/Polyaniline Composite Particles. *Adv Funct Mater* **2007**, *17* (11), 1784–1789. <https://doi.org/10.1002/adfm.200700170>.
- (8) Abidian, M. R.; Kim, D. -H.; Martin, D. C. Conducting-Polymer Nanotubes for Controlled Drug Release. *Advanced Materials* **2006**, *18* (4), 405–409. <https://doi.org/10.1002/adma.200501726>.
- (9) Huang, J.; Tao, C.; An, Q.; Zhang, W.; Wu, Y.; Li, X.; Shen, D.; Li, G. 3D-Ordered Macroporous Poly(Ionic Liquid) Films as Multifunctional Materials. *Chem. Commun.* **2010**, *46* (6), 967–969. <https://doi.org/10.1039/B921280A>.
- (10) Wang, X.; Wang, Y.; Lu, K.; Jiang, W.; Dai, F. A 3D Ba-MOF for Selective Adsorption of CO<sub>2</sub>/CH<sub>4</sub> and CO<sub>2</sub>/N<sub>2</sub>. *Chinese Chemical Letters* **2021**, *32* (3), 1169–1172. <https://doi.org/10.1016/j.ccllet.2020.09.036>.

## Chapter II

### *Fabrication of silica composite and porous polybenzimidazole film*

- (11) Adhikari, A. K.; Lin, K.-S. Improving CO<sub>2</sub> Adsorption Capacities and CO<sub>2</sub>/N<sub>2</sub> Separation Efficiencies of MOF-74(Ni, Co) by Doping Palladium-Containing Activated Carbon. *Chemical Engineering Journal* **2016**, *284*, 1348–1360. <https://doi.org/10.1016/j.cej.2015.09.086>.
- (12) Ahmed, I.; Panja, T.; Khan, N. A.; Sarker, M.; Yu, J.-S.; Jung, S. H. Nitrogen-Doped Porous Carbons from Ionic Liquids@MOF: Remarkable Adsorbents for Both Aqueous and Nonaqueous Media. *ACS Appl Mater Interfaces* **2017**, *9* (11), 10276–10285. <https://doi.org/10.1021/acsami.7b00859>.
- (13) Huang, N.; Chen, X.; Krishna, R.; Jiang, D. Two-Dimensional Covalent Organic Frameworks for Carbon Dioxide Capture through Channel-Wall Functionalization. *Angewandte Chemie International Edition* **2015**, *54* (10), 2986–2990. <https://doi.org/10.1002/anie.201411262>.
- (14) Dhankhar, S. S.; Nagaraja, C. M. Porous Nitrogen-Rich Covalent Organic Framework for Capture and Conversion of CO<sub>2</sub> at Atmospheric Pressure Conditions. *Microporous and Mesoporous Materials* **2020**, *308*, 110314. <https://doi.org/10.1016/j.micromeso.2020.110314>.
- (15) Chen, G.; Zhang, Y.; Xu, J.; Liu, X.; Liu, K.; Tong, M.; Long, Z. Imidazolium-Based Ionic Porous Hybrid Polymers with POSS-Derived Silanols for Efficient Heterogeneous

## Chapter II

### *Fabrication of silica composite and porous polybenzimidazole film*

Catalytic CO<sub>2</sub> Conversion under Mild Conditions. *Chemical Engineering Journal* **2020**, *381*, 122765. <https://doi.org/10.1016/j.cej.2019.122765>.

- (16) Lu, W.; Sculley, J. P.; Yuan, D.; Krishna, R.; Wei, Z.; Zhou, H. Polyamine-Tethered Porous Polymer Networks for Carbon Dioxide Capture from Flue Gas. *Angewandte Chemie International Edition* **2012**, *51* (30), 7480–7484. <https://doi.org/10.1002/anie.201202176>.
- (17) Wu, D.; Xu, F.; Sun, B.; Fu, R.; He, H.; Matyjaszewski, K. Design and Preparation of Porous Polymers. *Chem Rev* **2012**, *112* (7), 3959–4015. <https://doi.org/10.1021/cr200440z>.
- (18) Wu, J.; Xu, F.; Li, S.; Ma, P.; Zhang, X.; Liu, Q.; Fu, R.; Wu, D. Porous Polymers as Multifunctional Material Platforms toward Task-Specific Applications. *Advanced Materials* **2019**, *31* (4). <https://doi.org/10.1002/adma.201802922>.
- (19) Wu, D.; Hui, C. M.; Dong, H.; Pietrasik, J.; Ryu, H. J.; Li, Z.; Zhong, M.; He, H.; Kim, E. K.; Jaroniec, M.; Kowalewski, T.; Matyjaszewski, K. Nanoporous Polystyrene and Carbon Materials with Core–Shell Nanosphere-Interconnected Network Structure. *Macromolecules* **2011**, *44* (15), 5846–5849. <https://doi.org/10.1021/ma2013207>.
- (20) Wang, H.; Wang, T.; Yang, S.; Fan, L. Preparation of Thermal Stable Porous Polyimide Membranes by Phase Inversion Process for Lithium-Ion Battery. *Polymer (Guildf)* **2013**,

## Chapter II

### *Fabrication of silica composite and porous polybenzimidazole film*

54 (23), 6339–6348. <https://doi.org/10.1016/j.polymer.2013.09.036>.

- (21) Wang, J.; He, Y.; Wu, Q.; Zhang, Y.; Li, Z.; Liu, Z.; Huo, S.; Dong, J.; Zeng, D.; Cheng, H. A Facile Non-Solvent Induced Phase Separation Process for Preparation of Highly Porous Polybenzimidazole Separator for Lithium Metal Battery Application. *Sci Rep* **2019**, *9* (1), 19320. <https://doi.org/10.1038/s41598-019-55865-6>.
- (22) Escalé, P.; Rubatat, L.; Billon, L.; Save, M. Recent Advances in Honeycomb-Structured Porous Polymer Films Prepared via Breath Figures. *Eur Polym J* **2012**, *48* (6), 1001–1025. <https://doi.org/10.1016/j.eurpolymj.2012.03.001>.
- (23) Tabata, S.; Isshiki, Y.; Watanabe, M. Inverse Opal Carbons Derived from a Polymer Precursor as Electrode Materials for Electric Double-Layer Capacitors. *J Electrochem Soc* **2008**, *155* (3), K42. <https://doi.org/10.1149/1.2826266>.
- (24) Wang, Y.; Chen, L.; Yu, J.; Zhu, J.; Shi, Z.; Hu, Z. Strong and Conductive Polybenzimidazole Composites with High Graphene Contents. *RSC Adv* **2013**, *3* (30), 12255. <https://doi.org/10.1039/c3ra40889b>.
- (25) Tian, X.; Wang, S.; Li, J.; Liu, F.; Wang, X.; Chen, H.; Wang, D.; Ni, H.; Wang, Z. Benzimidazole Grafted Polybenzimidazole Cross-Linked Membranes with Excellent PA Stability for High-Temperature Proton Exchange Membrane Applications. *Appl Surf Sci* **2019**, *465*, 332–339. <https://doi.org/10.1016/j.apsusc.2018.09.170>.

## Chapter II

### *Fabrication of silica composite and porous polybenzimidazole film*

- (26) Geng, K.; Tang, H.; Ju, Q.; Qian, H.; Li, N. Symmetric Sponge-like Porous Polybenzimidazole Membrane for High Temperature Proton Exchange Membrane Fuel Cells. *J Memb Sci* **2021**, *620*, 118981. <https://doi.org/10.1016/j.memsci.2020.118981>.
- (27) Kim, J.; Kim, K.; Ko, T.; Han, J.; Lee, J.-C. Polybenzimidazole Composite Membranes Containing Imidazole Functionalized Graphene Oxide Showing High Proton Conductivity and Improved Physicochemical Properties. *Int J Hydrogen Energy* **2021**, *46* (22), 12254–12262. <https://doi.org/10.1016/j.ijhydene.2020.02.193>.
- (28) Kim, H.; Cho, S. Y.; An, S. J.; Eun, Y. C.; Kim, J.; Yoon, H.; Kweon, H.; Yew, K. H. Synthesis of Poly(2,5-benzimidazole) for Use as a Fuel-Cell Membrane. *Macromol Rapid Commun* **2004**, *25* (8), 894–897. <https://doi.org/10.1002/marc.200300288>.
- (29) Harilal; Shukla, A.; Ghosh, P. C.; Jana, T. Pyridine-Bridged Polybenzimidazole for Use in High-Temperature PEM Fuel Cells. *ACS Appl Energy Mater* **2021**, *4* (2), 1644–1656. <https://doi.org/10.1021/acsaem.0c02821>.
- (30) Nag, A.; Ali, M. A.; Kawaguchi, H.; Saito, S.; Kawasaki, Y.; Miyazaki, S.; Kawamoto, H.; Adi, D. T. N.; Yoshihara, K.; Masuo, S.; Katsuyama, Y.; Kondo, A.; Ogino, C.; Takaya, N.; Kaneko, T.; Ohnishi, Y. Ultrahigh Thermoresistant Lightweight Bioplastics Developed from Fermentation Products of Cellulosic Feedstock. *Adv Sustain Syst* **2021**, *5* (1). <https://doi.org/10.1002/adsu.202000193>.

## Chapter II

### *Fabrication of silica composite and porous polybenzimidazole film*

- (31) Qian, G.; Smith, D. W.; Benicewicz, B. C. Synthesis and Characterization of High Molecular Weight Perfluorocyclobutyl-Containing Polybenzimidazoles (PFCB–PBI) for High Temperature Polymer Electrolyte Membrane Fuel Cells. *Polymer (Guildf)* **2009**, *50* (16), 3911–3916. <https://doi.org/10.1016/j.polymer.2009.06.024>.
- (32) Eaton, P. E.; Carlson, G. R.; Lee, J. T. Phosphorus Pentoxide-Methanesulfonic Acid. Convenient Alternative to Polyphosphoric Acid. *J Org Chem* **1973**, *38* (23), 4071–4073. <https://doi.org/10.1021/jo00987a028>.
- (33) Nayak, R.; Sundarraman, M.; Ghosh, P. C.; Bhattacharyya, A. R. Doped Poly(2, 5-Benzimidazole) Membranes for High Temperature Polymer Electrolyte Fuel Cell: Influence of Various Solvents during Membrane Casting on the Fuel Cell Performance. *Eur Polym J* **2018**, *100*, 111–120. <https://doi.org/10.1016/j.eurpolymj.2017.08.026>.
- (34) Hu, L.; Zhou, S.; Zhang, X.; Shi, C.; Zhang, Y.; Chen, X. Self-Assembly of Polymers and Their Applications in the Fields of Biomedicine and Materials. *Polymers (Basel)* **2024**, *16* (15), 2097. <https://doi.org/10.3390/polym16152097>.
- (35) Kida, T.; Mouri, M.; Akashi, M. Fabrication of Hollow Capsules Composed of Poly(Methyl Methacrylate) Stereocomplex Films. *Angewandte Chemie International Edition* **2006**, *45* (45), 7534–7536. <https://doi.org/10.1002/anie.200602116>.
- (36) Zhang, X.; Yan, W.; Yang, H.; Liu, B.; Li, H. Gaseous Infiltration Method for Preparation

## Chapter II

### *Fabrication of silica composite and porous polybenzimidazole film*

of Three-Dimensionally Ordered Macroporous Polyethylene. *Polymer (Guildf)* **2008**, *49*

(25), 5446–5451. <https://doi.org/10.1016/j.polymer.2008.09.064>.

- (37) Harris, F. W.; Ahn, B. H.; Cheng, S. Z. D. Synthesis of Polybenzimidazoles via Aromatic Nucleophilic Substitution Reactions of Self-Polymerizable (A-B) Monomers. *Polymer (Guildf)* **1993**, *34* (14), 3083–3095. [https://doi.org/10.1016/0032-3861\(93\)90639-R](https://doi.org/10.1016/0032-3861(93)90639-R).
- (38) Kang, J.; Eo, S.; Jeon, I.; Choi, Y. S.; Tan, L.; Baek, J. Multifunctional Poly(2,5-benzimidazole)/Carbon Nanotube Composite Films. *J Polym Sci A Polym Chem* **2010**, *48* (5), 1067–1078. <https://doi.org/10.1002/pola.23862>.
- (39) Yeob, J.; Hong, S. W.; Koh, W.-G.; Park, I. Enhanced Mechanical and Thermal Properties of Polyimide Films Using Hydrophobic Fumed Silica Fillers. *Polymers (Basel)* **2024**, *16* (2), 297. <https://doi.org/10.3390/polym16020297>.
- (40) Das, A.; Ghosh, P.; Ganguly, S.; Banerjee, D.; Kargupta, K. Salt-Leaching Technique for the Synthesis of Porous Poly(2,5-Benzimidazole) (ABPBI) Membranes for Fuel Cell Application. *J Appl Polym Sci* **2018**, *135* (5). <https://doi.org/10.1002/app.45773>.
- (41) Sizov, V. E.; Kondratenko, M. S.; Gallyamov, M. O.; Stevenson, K. J. Advanced Porous Polybenzimidazole Membranes for Vanadium Redox Batteries Synthesized via a Supercritical Phase-Inversion Method. *J Supercrit Fluids* **2018**, *137*, 111–117. <https://doi.org/10.1016/j.supflu.2018.03.018>.

## Chapter II

### *Fabrication of silica composite and porous polybenzimidazole film*

- (42) Luo, T.; Dreusicke, B.; Wessling, M. Tuning the Ion Selectivity of Porous Poly(2,5-Benzimidazole) Membranes by Phase Separation for All Vanadium Redox Flow Batteries. *J Memb Sci* **2018**, *556*, 164–177. <https://doi.org/10.1016/j.memsci.2018.03.086>.
- (43) Zhou, J.; Zhong, X.; Nag, A.; Liu, Y.; Takada, K.; Kaneko, T. Reinforcement of Ultrahigh Thermoresistant Polybenzimidazole Films by Hard Craters. *Polym Chem* **2022**, *13* (28), 4086–4089. <https://doi.org/10.1039/D2PY00548D>.
- (44) Borjigin, H.; Stevens, K. A.; Liu, R.; Moon, J. D.; Shaver, A. T.; Swinnea, S.; Freeman, B. D.; Riffle, J. S.; McGrath, J. E. Synthesis and Characterization of Polybenzimidazoles Derived from Tetraaminodiphenylsulfone for High Temperature Gas Separation Membranes. *Polymer (Guildf)* **2015**, *71*, 135–142. <https://doi.org/10.1016/j.polymer.2015.06.021>.
- (45) Feng, W.; Li, W.; Wang, W.; Chen, Y.; Wang, W.; Yu, D. Facile and Rapid Synthesis of Flexible PEG Porous Polymers as Substrates for Functional Materials by Thiol-Ene Click Chemistry. *Chemical Engineering Journal* **2023**, *470*, 144078. <https://doi.org/10.1016/j.cej.2023.144078>.
- (46) Lv, P.; Dong, Z.; Dai, X.; Qiu, X. Flexible Polydimethylsiloxane-Based Porous Polyimide Films with an Ultralow Dielectric Constant and Remarkable Water Resistance. *ACS Appl Polym Mater* **2019**, *1* (10), 2597–2605. <https://doi.org/10.1021/acsapm.9b00484>.

## *Chapter III*

### *Fabrication of silica composite and porous poly(benzimidazole-aramid) film*

### **3.1 Introduction**

Production of bioplastics from renewable biological resources is imperative for developing a sustainable society and achieving low-carbon technology.<sup>1,2</sup> One of the major research topics in this regard is the synthesis of highly heat-resistant bioplastics because carbon dioxide in the atmosphere can be immobilized in durable materials for a considerable amount of time. For instance, 3-amino-4-hydroxybenzoic acid produced by genetically modified *Escherichia coli* can be converted to polybenzimidazole (PBI) and its copolymers, both of which show extremely high heat resistance. Despite having the highest thermal decomposition temperature on record, poly(benzimidazole-*co*-aramid) (poly(BI-*co*-A) films are found to be brittle in nature due to their rigid chain structure. Numerous studies have been conducted to improve the flexibility of PBI through molecular design,<sup>3,4</sup> inorganic composites,<sup>5,6</sup> and porous structure formation.<sup>7,8</sup> Porous structure formation consists of the merits of lightweight, physical stability, and high resiliency, which have attracted the attention of researchers in the last few decades.<sup>9,10</sup> Luo and coworkers prepared porous PBI films using a phase separation process induced by water vapor. Chaudhari and coworkers prepared these films using the immersion precipitation method.<sup>11,12</sup> The effects of the porous structure on the mechanical properties of the films were rarely discussed in those reports, but the results revealed that the

### *Chapter III*

#### *Fabrication of silica composite and porous poly(benzimidazole-aramid) film*

formation of porous structures improves the elongation rate of the material while degrading their mechanical properties. On the other hand, the silica ( $\text{SiO}_2$ ) hard-template method, which is primarily used for water-absorbable materials such as hydrogels, does not alter the components or chemical structure of the polymer, thus being a promising strategy for the processing of materials.<sup>13,14</sup> In this study, the high-performance polymer films are also water-absorbable plastics due to their polar structures.<sup>15,16</sup>

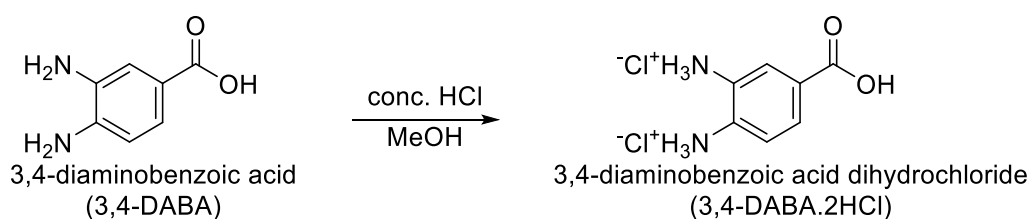
## 3.2 Experimental

### 3.2.1 Materials

3,4-Diaminobenzoic acid (3,4-DABA, 99% purity) and 4-aminobenzoic acid (ABA, 99% purity) were purchased from Tokyo Chemical Industry Co., Ltd. Polyphosphoric acid (PPA, 80% purity) was obtained from FUJIFILM Wako Pure Chemical Corp. Spherical silica particles (seahostar@KE-P30, diameter: 300nm) were purchased from Nippon Shokubai Co., Ltd., Japan. Hydrofluoric acid (HF, 55% purity) was obtained from Morita Chemical Industries Co., Ltd. Trifluoroacetic acid (TFA), Methanesulfonic acid (MSA), Sodium bicarbonate, Hydrochloric acid, methanol, acetone, and other chemicals were obtained from Kanto Chemical Co., Inc. All the chemicals and reagents were used as received.

### 3.2.2 Syntheses

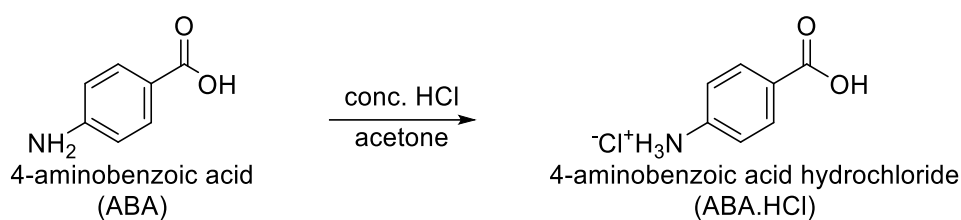
#### Preparation of 3,4-Diaminobenzoic acid dihydrochloride (3,4-DABA·2HCl)



**Scheme 3.1** Synthesis of 3,4-Diaminobenzoic acid dihydrochloride (3,4-DABA·2HCl).

3,4-DABA (3.04 g, 20 mmol) was dissolved in 50 ml methanol while kept in an ice bath. Subsequently, 12N hydrochloric acid (approx. 3.33 ml) was added dropwise into this solution, until the powder was completely dissolved. The pale-pink-colored salt of 3,4-Diaminobenzoic acid dihydrochloride (3,4-DABA·2HCl) was obtained via solvent evaporation (yield: 4.32 g, 96%).

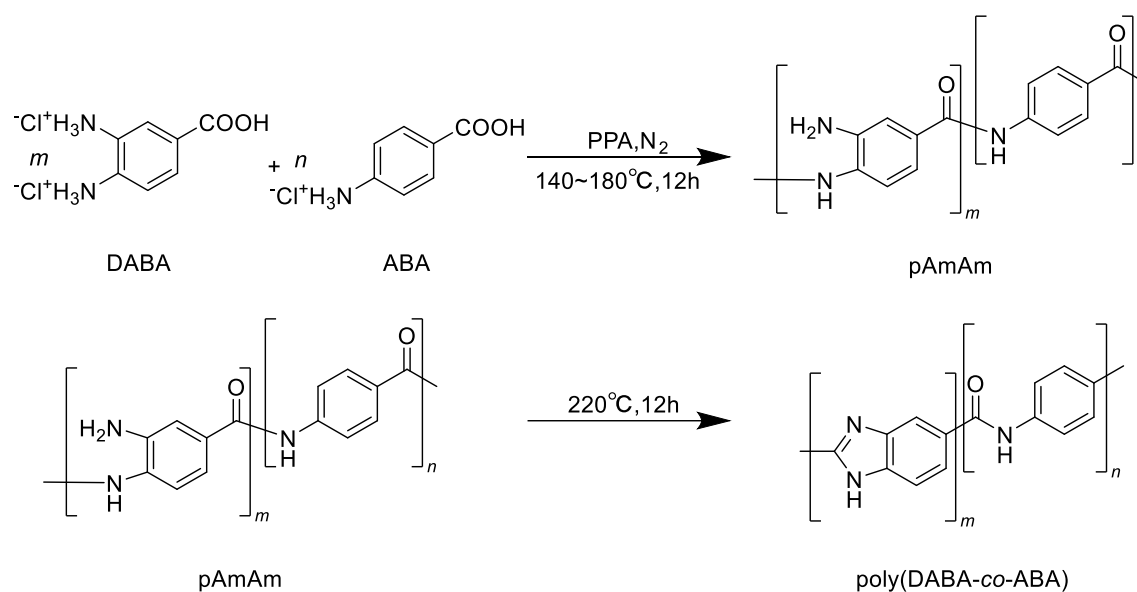
#### Preparation of 4-aminobenzoic acid hydrochloride (ABA·HCl)



**Scheme 3.2** Synthesis of 4-aminobenzoic acid hydrochloride (ABA·HCl).

20 ml acetone was used to dissolve ABA (1.37 g, 10 mmol). Add 12 N hydrochloric acid (approx. 0.83 ml) dropwise until there is no precipitation appears in the solution. The pale-yellow-colored salt of 4-aminobenzoic acid dihydrochloride (ABA·HCl) was obtained via filtration and evaporated under reduced pressure. (yield: 1.60 g, 92%).

## Synthesis of copolymer poly(BI-co-A)



**Scheme 3.3** Synthetic scheme of poly(BI-co-A) from bio-derived monomers 34DABA and ABA.

A typical synthetic procedure for poly(BI-co-A) with a composition of 34DABA and ABA (85:15), which showed ultrahigh thermal resistance as described in the previous research, was given below. 50 g poly (phosphoric acid) (PPA) was added into a three-necked flask equipped with a magnetic stirrer and heated at 120°C for 1 h in a nitrogen atmosphere. Subsequently, 1.91 g of 34DABA·2HCl (8.5 mmol) and 0.26 g of ABA·HCl (1.5 mmol) were added into PPA slowly and stirred for 1h to remove the moisture. After the powder dissolved completely, the solution was heated at 140 °C for 1 h, 160 °C for 1 h, and 180 °C for 8 h, respectively, until the solution became viscous and then maintained

### *Chapter III*

#### *Fabrication of silica composite and porous poly(benzimidazole-aramid) film*

at 220 °C for 12 h. During the process, the viscosity of the solution increased significantly with increasing temperature, and the color of the solution changed from red to dark brown. The resulting viscous solution was precipitated into 500 ml of deionized water and washed 12 h. After filtration, a brown solid was obtained and dried at 150 °C for 12 h. Finally, the solid was crushed into powder and neutralized with an aqueous solution of 5 % NaHCO<sub>3</sub>, followed by repeated washing with deionized water until the PH of the cleaning liquid reached 7 (measured using PH test papers, Macherey-Nagel GmbH & Co. KG, Duren, Germany).

### **3.3 Measurements**

To confirm the chemical structure of monomers and monomers salts, proton nuclear magnetic resonance ( $^1\text{H}$  NMR) spectra with a Bruker AVANCE III NMR spectrometer were obtained at a proton frequency of 400MHz with a solvent of DMSO- $d_6$ . Solid-state  $^{13}\text{C}$  Cross-Polarization with Magic Angle Spinning (CP/MAS) spectra were recorded using zirconia rotors with 4 mm diameter. The samples were packed in a 7 mm diameter zirconia rotor with a Kel-F cap and spun at 10 kHz. A contact time of 2 ms was used, the period between successive accumulation was 5 s, and the total number of scans was 160,000. Fourier transform infrared (FT-IR) spectra of the pristine poly(BI-co-A) film and porous poly(BI-co-A) films were recorded in the wavenumber range of 4000 to 400  $\text{cm}^{-1}$ , using a Perkin-Elmer spectrometer with a diamond-attenuated total reflection (ATR) accessory. The determination of particle size and size distribution of the  $\text{SiO}_2$  was carried out by a HITACHI TM3030 plus tabletop SEM. Energy-dispersive X-ray spectroscopy (EDS) was used to identify residual elements in the prepared films. The film specimens were pre-coated with Au powder under a vacuum for 30 s (thickness: approximately 15 nm). Thermo-gravimetric analysis (TGA) was performed on a HITACHI STA2700 system. The samples (approx. 10 mg) were placed in a platinum crucible heated to a maximum temperature of 800  $^\circ\text{C}$  at a heating rate of 5  $^\circ\text{C min}^{-1}$  under

### *Chapter III*

#### *Fabrication of silica composite and porous poly(benzimidazole-aramid) film*

a nitrogen atmosphere. Wide-angle X-ray diffraction (WAXD) measurement was selected to investigate the crystallization of copolymer films. The film was cut into a length of 30 mm and a width of 1 mm. A high-performance scanning probe microscope (SPM) was evaluated using a SHIMADZU SPM-Nanoa™ under phase observation mode. In addition, the surface shape and adsorption were measured via a nano 3D mapping fast technic, and elastic modulus was further calculated by the Johnson-Kendall-Roberts (JKR) model. The tensile test was carried out at an elongation speed of 1 mm min<sup>-1</sup> using an Instron-3365 mechanical tester instrument at room temperature.

### **3.4 Results and Discussion**

#### **3.4.1 Fabrication of pure poly(BI-co-A) film**

Due to the insolubility in normal organic solvents, a mixture solvent of TFA and MSA was prepared to dissolve fabricated pure poly(BI-co-A) film: poly(BI-co-A) powder (50 mg) and a mixture of TFA (3 ml) with 2 drops of MSA were merged into a screw-capped bottle, equipped with a magnetic stirrer. After stirring at ambient temperature for 24 h until forming a transparent solution, the poly(BI-co-A) solution was cast onto a silicon wafer and further dried to obtain a brown-colored film. Subsequently, the solvent-evaporated poly(BI-co-A) film was immersed in deionized water to remove the residuals. After washing with deionized water repeatedly, the poly(BI-co-A) film was further dried at 200 °C for 12 h under vacuum.

### 3.4.2 Fabrication of silica nanocomposite poly(BI-co-A) films

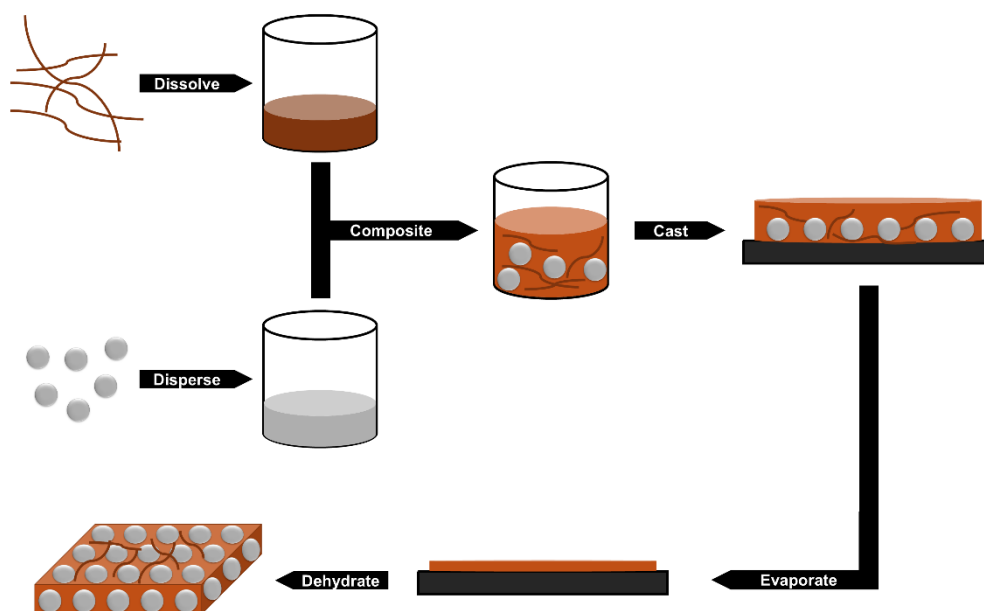


**Figure 3-1.** Schematic illustration of the fabrication process of silica nanocomposite poly(BI-co-A) films. (poly(BI-co-A) = poly(benzimidazole-aramid))

In regard to the fabrication process of silica nanocomposite poly(BI-co-A) films, silica nanospheres with an average size of 300 nm were dispersed in TFA homogeneously by ultrasonication at ambient temperature for 1 h before compositing with polymer solution. After the silica nanospheres dispersion was added into the completely dissolved poly(BI-co-A) solution, the mixing solution was further ultrasonicated for another 1 h

### *Chapter III*

#### *Fabrication of silica composite and porous poly(benzimidazole-aramid) film*

before film casting. Poly(BI-co-A) films with various silica contents were fabricated using the above-mentioned two solutions with different weight percent of the mass of silica nanospheres to the total weight of poly(BI-co-A) and silica nanospheres. (i.e., 10, 20, 30, 40, and 50%). As for the film casting process, the mixture solutions of silica nanocomposite poly(BI-co-A) solution were poured onto a silicon wafer substrate and then evaporated at room temperature. Afterward, the silica nanocomposite poly(BI-co-A) films were peeled off from the silicon substrate washed with deionized water repeatedly, and further dried at 200 °C in a vacuum oven additionally. Eventually, the obtained silica nanocomposite poly(BI-co-A) films were heated at 500 °C in a nitrogen atmosphere by an electric furnace to complete the dehydration treatment (**Figure 3-1**).

## 3.4.3 FT-IR spectra

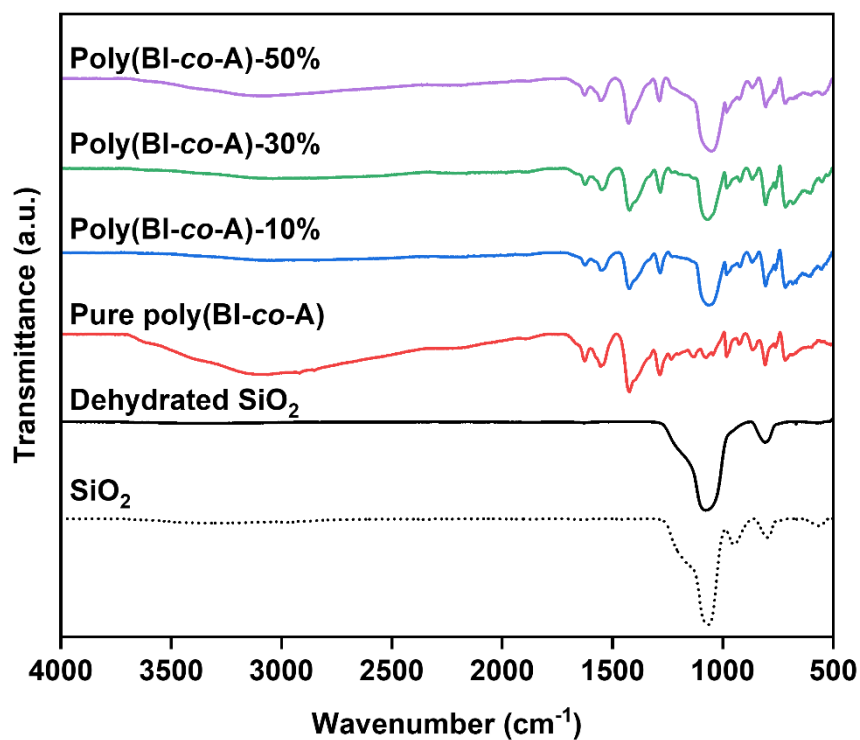


**Figure 3-2.** FT-IR spectra of bare and dehydrated silica nanospheres, and poly(BI-co-A) films with various silica contents. (poly(BI-co-A) = poly(benzimidazole-aramid))

Fourier transform infrared spectroscopy (FT-IR) was employed to identify the chemical structures of silica nanospheres, and pure and composite poly(BI-co-A) films (Figure 3-2). It is obvious that a broad absorption peak at about 1000 – 1270 cm<sup>-1</sup> is assigned to the Si-O-Si asymmetric stretching vibrations, while a weak absorption peak

### *Chapter III*

#### *Fabrication of silica composite and porous poly(benzimidazole-aramid) film*

at  $794\text{ cm}^{-1}$  is assigned to the in-plane Si-O-Si deformation vibration.<sup>17</sup> Moreover, the medium absorption peaks of the -OH group are characterized at about  $3300\text{ cm}^{-1}$ , and the characterized bending and stretching vibration of Si-OH is assigned at  $950\text{ cm}^{-1}$  in the bare silica nanospheres.<sup>18</sup> Conversely, the disappearance of the Si-OH absorption peak in the dehydrated silica spectrum indicates the hydration of silanol functional groups on the surface of the silica nanospheres. Furthermore, a short peak shift of in-plane Si-O-Si deformation vibration from  $794$  to  $804\text{ cm}^{-1}$  was also detected, implying a stronger combination bond, which suggests the successful hydration of silica nanospheres at  $500\text{ }^{\circ}\text{C}$ .<sup>19</sup>

On the other hand, the chemical structure of the synthesized poly(BI-co-A), using high-viscose poly(phosphoric acid) was also confirmed. The characteristic peaks at  $1625$ ,  $1550$ , and  $1285\text{ cm}^{-1}$  were assigned to the stretching vibrations of the C=N, C=C, and C-N groups, respectively, indicating the accomplished polycondensation of poly(BI-co-A). Additionally, a superbly broad absorption peak at the high wavenumber region could be attributed to the numerous -NH and -OH groups from the bonding and free water, implying the high hydrophilicity of pure poly(BI-co-A) film. Regarding the silica nanocomposite poly(BI-co-A) films, a broad absorption peak at about  $1000\text{ cm}^{-1}$  was observed in all the nanocomposite poly(BI-co-A) films spectra, demonstrating the

### *Chapter III*

#### *Fabrication of silica composite and porous poly(benzimidazole-aramid) film*

successful composition of silica nanospheres into the poly(BI-*co*-A) film. Notably, a remarkable weakening of the absorption peak of the -OH group occurred in the poly(BI-*co*-A) film with silica nanospheres of 10 wt% content, indicating the hydrophilicity decreased significantly after the silica nanospheres composition. Although the strength of the absorption peak of the -OH group increased as increasing the silica nanospheres content from 10 to 50 wt%, which comes from the uncompleted dehydration of silanol functional groups on the silica nanospheres, the poly(BI-*co*-A) film with 50 wt% silica nanospheres composition showed improved hydrophobicity than the pure poly(BI-*co*-A) film.

### 3.4.4 SEM morphologies

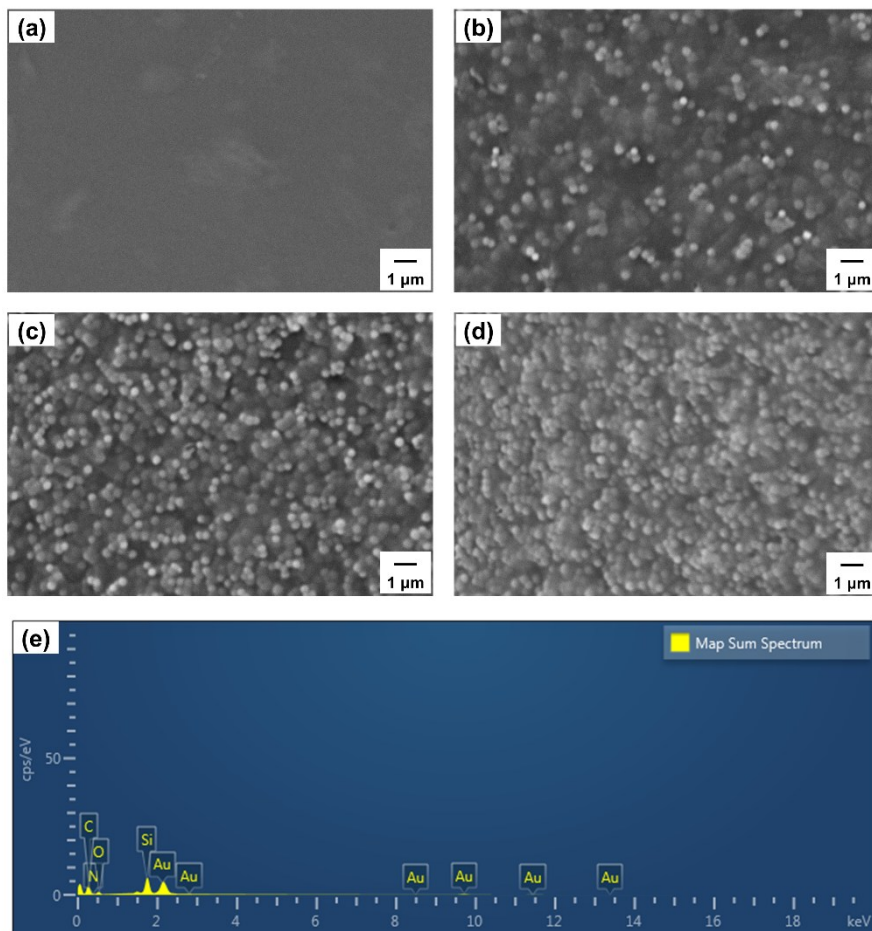


**Figure 3-3.** SEM images of a) pure and silica nanocomposite poly(BI-co-A) films with silica contents of b) 10, c) 30, d) 50 wt%, and e) EDS elemental analysis. (poly(BI-co-A) = poly(benzimidazole-aramid); SEM = scanning electron microscopy; EDS = energy-dispersive X-ray spectroscopy).

**Table 3-1. Elemental analysis results of the fabricated silica nanocomposite poly(BI-co-A) film**

Element	Line Type	Weight %	Atomic %
C	K series	44.24	68.20
N	K series	6.71	8.87
O	K series	11.28	13.05
Si	K series	11.21	7.39
Au	M series	26.56	2.50
Total		100.00	100.00

A scanning electron microscope (SEM) was adopted to investigate the morphologies of the fabricated poly(BI-co-A) films with various silica nanospheres content (**Figure 3-3**). Referring to the surface images, the original poly(BI-co-A) film exhibited a rather uniform surface (**Figure 3-3a**), whereas all the composited films had silica nanospheres on their surfaces, which were revealed to a size of around 300 nm. Moreover, the SEM images confirmed the increased composition caused by increasing the number of silica nanospheres (**Figure 3-3b - d**) and indicated the successful preparation of silica composite poly(BI-co-A) films. The EDS mapping results clarified the existence of silica nanospheres with an atomic percentage ratio of 7.39 at% and 13.05 at% for silicon and

### *Chapter III*

#### *Fabrication of silica composite and porous poly(benzimidazole-aramid) film*

oxygen, respectively. Meanwhile, no elemental sulfur or fluorine was detected, indicating that the used dissolving solvents in the fabrication process were removed completely, which also reveals the skillful silica composite into the poly(BI-co-A) film, supplementally. (**Figure 3-3**).

## 3.4.5 TGA analysis

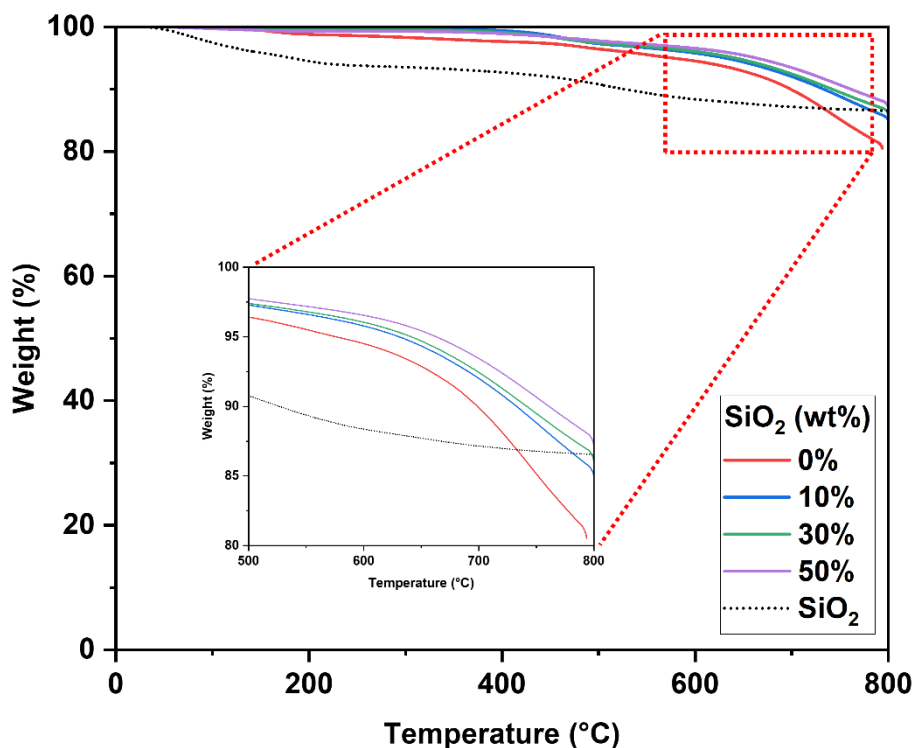


**Figure 3-4.** TGA curves of poly(BI-co-A) films with various silica contents. (TGA = thermogravimetric analysis; poly(BI-co-A) = poly(benzimidazole-aramid)).

Thermogravimetric analysis (TGA) was employed to assess the thermal properties of bare silica nanospheres, pure poly(BI-co-A) films, and their silica nanocomposite films (**Figure 3-4**). Despite the hydration temperature which is affected by the shape and size of silica nanoparticles, the thermal properties of the silica nanospheres used in this work were also investigated. The weight decrease observed before approximately 220 °C could

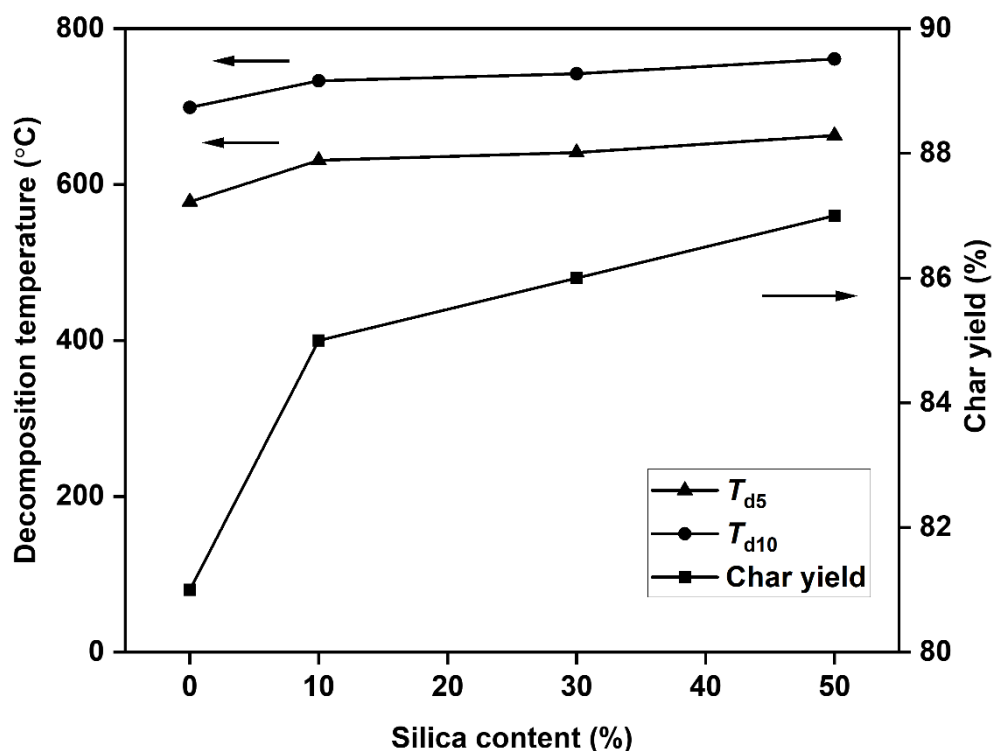


**Figure 3-5.** Thermal properties of poly(BI-co-A) films with various silica contents.

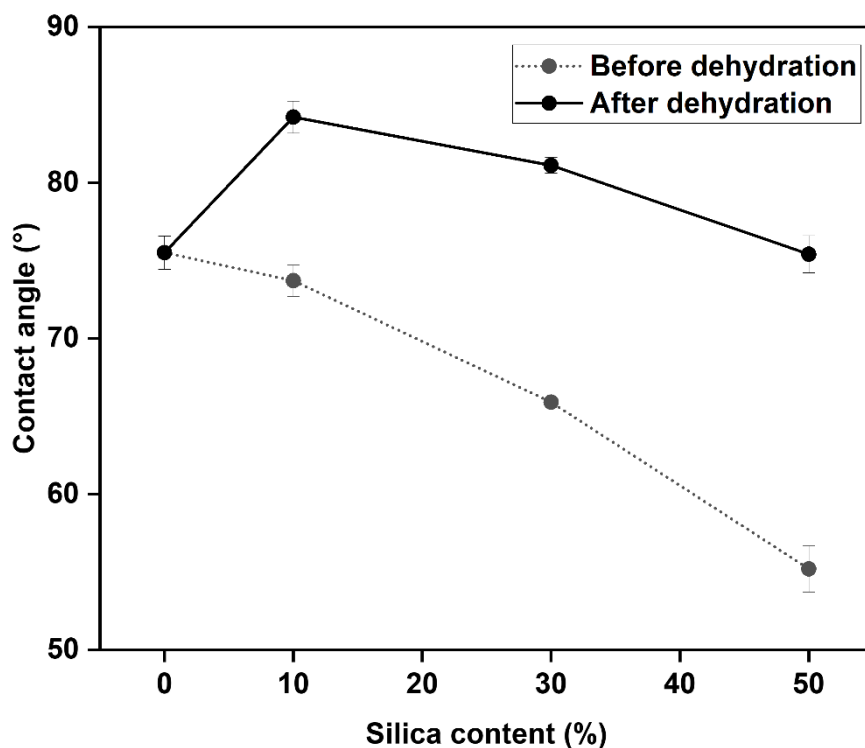
be attributed to the adsorbed free and bound water,<sup>20,21</sup> while the dehydration occurred at approximately 430 °C. Compared to pure poly(BI-co-A) film, poly(BI-co-A) silica nanocomposite films remain stable until approximately 400 °C, suggesting the high thermal stability of the poly(BI-co-A) silica nanocomposite films. Furthermore, 5% weight loss temperature ( $T_{d5}$ ) and 10% weight loss temperature ( $T_{d10}$ ) are taken as indices to evaluate the thermal stability (**Table 3-2**). Poly(BI-co-A) silica nanocomposite films

exhibit significantly higher  $T_{d5}$  and  $T_{d10}$  than pure poly(BI-co-A) film, and the thermal degradation temperatures increase as the amount of silica component.  $T_{d5}$  ranges from 631°C to 663°C, as the silica composition increases from 10 to 50 wt%.  $T_{d10}$  increases from 699 °C to 761 °C, demonstrating the improved thermal stability of silica nano composite.<sup>17,22-24</sup> In addition, the char yield of the composites varies from 81% to 87% (Figure 3-5), which was improved by the addition of silica nanospheres, making them strong precursor resins of the polymer-derived carbon materials.<sup>25,26</sup> These thermal properties outstand this series of composites in all the polymeric materials, implying their potential applications on thermal-retardant and non-flammable materials in extreme environments.

**Table 3-2. Thermal properties of the fabricated poly(BI-co-A) films with various silica contents (poly(BI-co-A) = poly(benzimidazole-aramid))**

films	$T_{d5}$ (°C)	$T_{d10}$ (°C)	Char yield (%)
poly(BI-co-A)-0%	578	699	81
poly(BI-co-A)-10%	631	733	85
poly(BI-co-A)-30%	641	742	86
poly(BI-co-A)-50%	663	761	87

## 3.4.6 Contact angle test



**Figure 3-6.** Surface wettability results of poly(BI-co-A) films with various silica contents.

A contact angle (CA) meter was employed to investigate the surface wettability of fabricated pure poly(BI-co-A) film, and the effect of silica nanospheres composition (**Figure 3-6**). The CA of pure poly(BI-co-A) film displayed slight hydrophilicity with a value of 75.5°, owing to the formed numerous hydrogen bonds from imidazole rings and amide bonds in the poly(BI-co-A) molecular chains. Moreover, the silica nanocomposite

poly(BI-co-A) films showed decreased values of CA from 75.5° to 55.2° with increasing the silica nanospheres content, as a result of the increased hydrogen bonds from the hydroxy functional groups on the surface of silica nanospheres. However, after dehydrating the silica nanocomposite poly(BI-co-A) films, a wettability improvement was accomplished and the CA value improved to 84.2° for the nanocomposite poly(BI-co-A) film with 10% silica nanospheres, which could be attributed to the reduced amount of hydrogen bonds on the surface of silica nanospheres after the dehydration treatment.

**Table 3-3. Contact angle of pure poly(BI-co-A) film, before and after dehydration of silica nanocomposite poly(BI-co-A) films with various silica contents**

films	Contact angle (°)	
poly(BI-co-A)-0%	75.5±1.1	
	Before dehydration	After dehydration
poly(BI-co-A)-10%	73.7±1.0	84.2±1.0
poly(BI-co-A)-30%	65.9±0.3	81.1±0.5
poly(BI-co-A)-50%	55.2±1.5	75.4±1.2

## 3.4.7 Fabrication of porous poly(BI-co-A) films

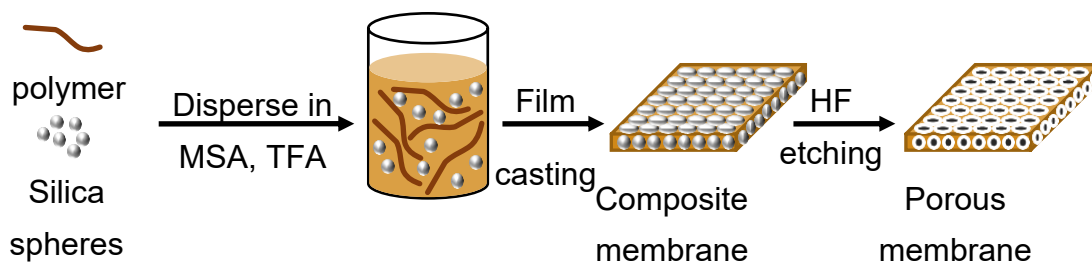


**Figure 3-7.** Illustration of the preparation of porous poly(BI-co-A) films via a hard-templating method.

Poly(BI-co-A) powder was dissolved in a flask in a mixture of TFA and  $\text{CH}_3\text{SO}_3\text{H}$  (2 ~ 3%).  $\text{SiO}_2$  spheres were dispersed in TFA homogeneously by ultrasonication at room temperature for 1 h.  $\text{SiO}_2$  colloid solution was added into the completely dissolved poly(BI-co-A) solution and further ultrasonicated for 1 h before film casting. Poly(BI-co-A) films with various porosities were fabricated using the above-mentioned two solutions with different weight percent of  $\text{SiO}_2$  to the total mass of poly(BI-co-A), (i.e., 10%, 20%, 30%, 40%, and 50%). As for the film casting process, the mixture solutions of poly(BI-co-A)- $\text{SiO}_2$  and pure poly(BI-co-A) solution were coated onto a glass substrate and then evaporated at room temperature for 24 h. The films were peeled off from the glass substrate and immersed in deionized water for 24 h to remove residual acid. The obtained pristine poly(BI-co-A) film and composite films were further dried at 200 °C under

### *Chapter III*

#### *Fabrication of silica composite and porous poly(benzimidazole-aramid) film*

vacuum. Afterward, the obtained composite films were immersed in a 40% HF solution for 24 h to remove SiO<sub>2</sub> from the films. The obtained porous poly(BI-co-A) films were soaked in deionized water for 24 h and further dried at 150 °C for 12 h under vacuum. The films were named poly(BI-co-A)-X%, where X% means the weight percent of SiO<sub>2</sub>. The preparation procedure for porous poly(BI-co-A) films is illustrated in **Figure 3-7**.

### 3.4.8 FT-IR spectra of porous film

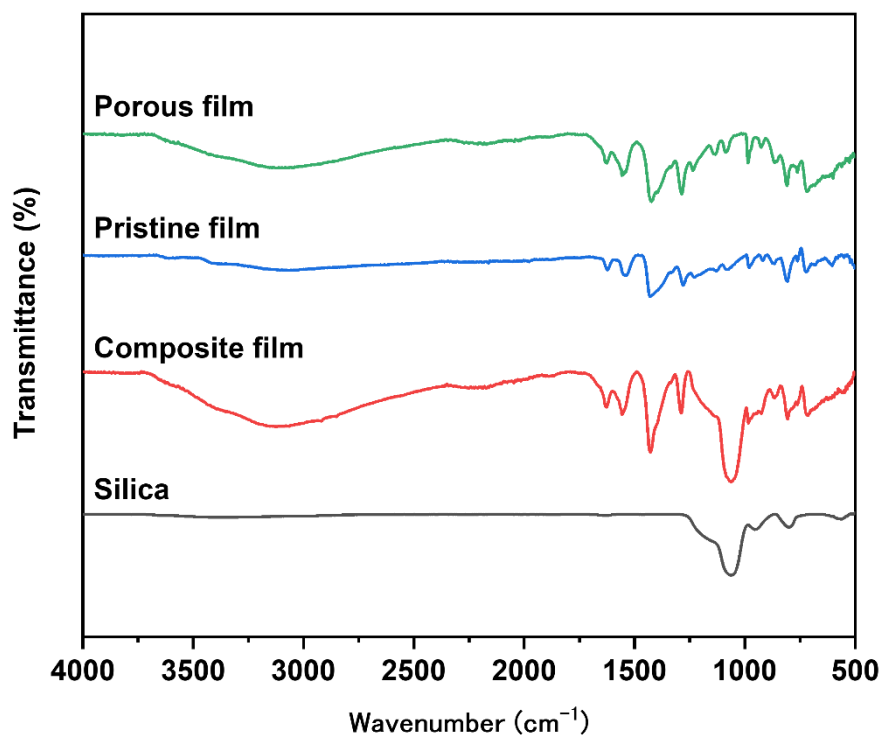


**Figure 3-8.** FT-IR spectra of silica spheres, composite poly(BI-*co*-A), pristine poly(BI-*co*-A), and porous poly(BI-*co*-A) film.

The chemical structures of silica spheres and films were confirmed by FT-IR spectra as displayed in **Figure 3-8**. For the silica spectra, the broad absorption band at 1000-1180 cm<sup>-1</sup> was assigned to the Si-O-Si groups. As for the pristine poly(BI-*co*-A) spectra, the characteristic bands at 1636, 1553, and 1284 cm<sup>-1</sup> were assigned to the stretching vibration of the C=N, C=C, and C-N groups, respectively, the broad absorption band at

### Chapter III

#### Fabrication of silica composite and porous poly(benzimidazole-aramid) film

3250-3450  $\text{cm}^{-1}$  corresponding to N-H groups. There is a medium-strong peak observed at 1000-1180  $\text{cm}^{-1}$  in the composite poly(BI-co-A) spectra, indicating that the silica spheres were templated certainly. After HF etching, the Si-O-Si adsorption peak disappeared in the porous poly(BI-co-A) spectra, indicating that the silica spheres were removed completely and there is no change occurred to the chemical structure since the observed characteristic peaks of poly(BI-co-A). Uniformed pristine poly(BI-co-A) (**Figure 3-9a**) and porous poly(BI-co-A) (**Figure 3-9b**) films with high transparency were obtained via the sol-gel method.

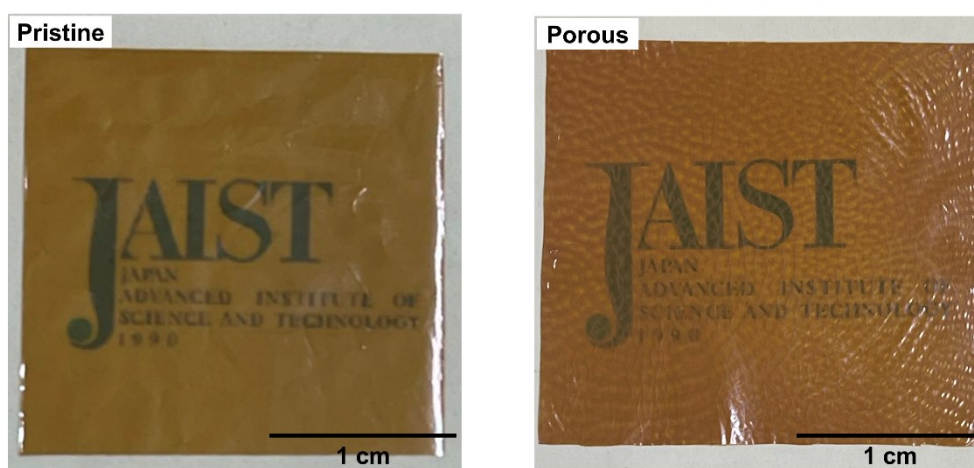


**Figure 3-9.** Photos of fabricated (a) pristine and (b) porous poly(BI-co-A) film.

## 3.4.9 Porosities of the prepared porous films

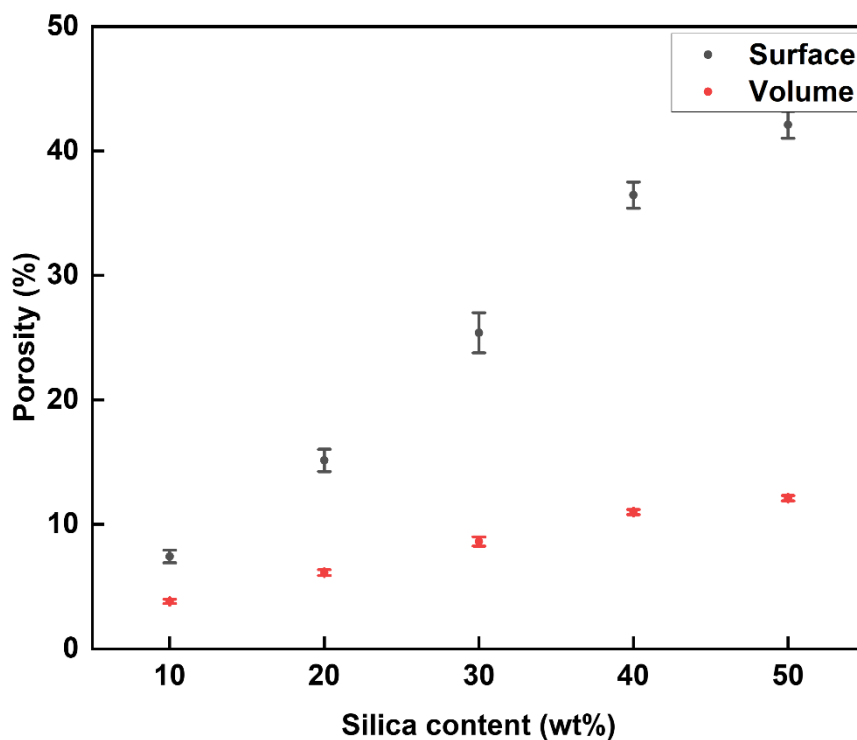


**Figure 3-10.** Porosity of the porous poly(BI-co-A) films with different silica contents.

The porosity of the porous poly(BI-co-A) films with different contents of silica spheres was measured via an image processing method by scanning the surface of the films. The porosity of porous poly(BI-co-A) film was efficiently adjusted, upgrading from 7.4 to 42%, while increasing the content of monodispersed silica spheres, demonstrating that the porosity of thermal resistant polymer film could be well controlled via a hard-templating method (Figure 3-10).

3.4.10 SEM morphology images

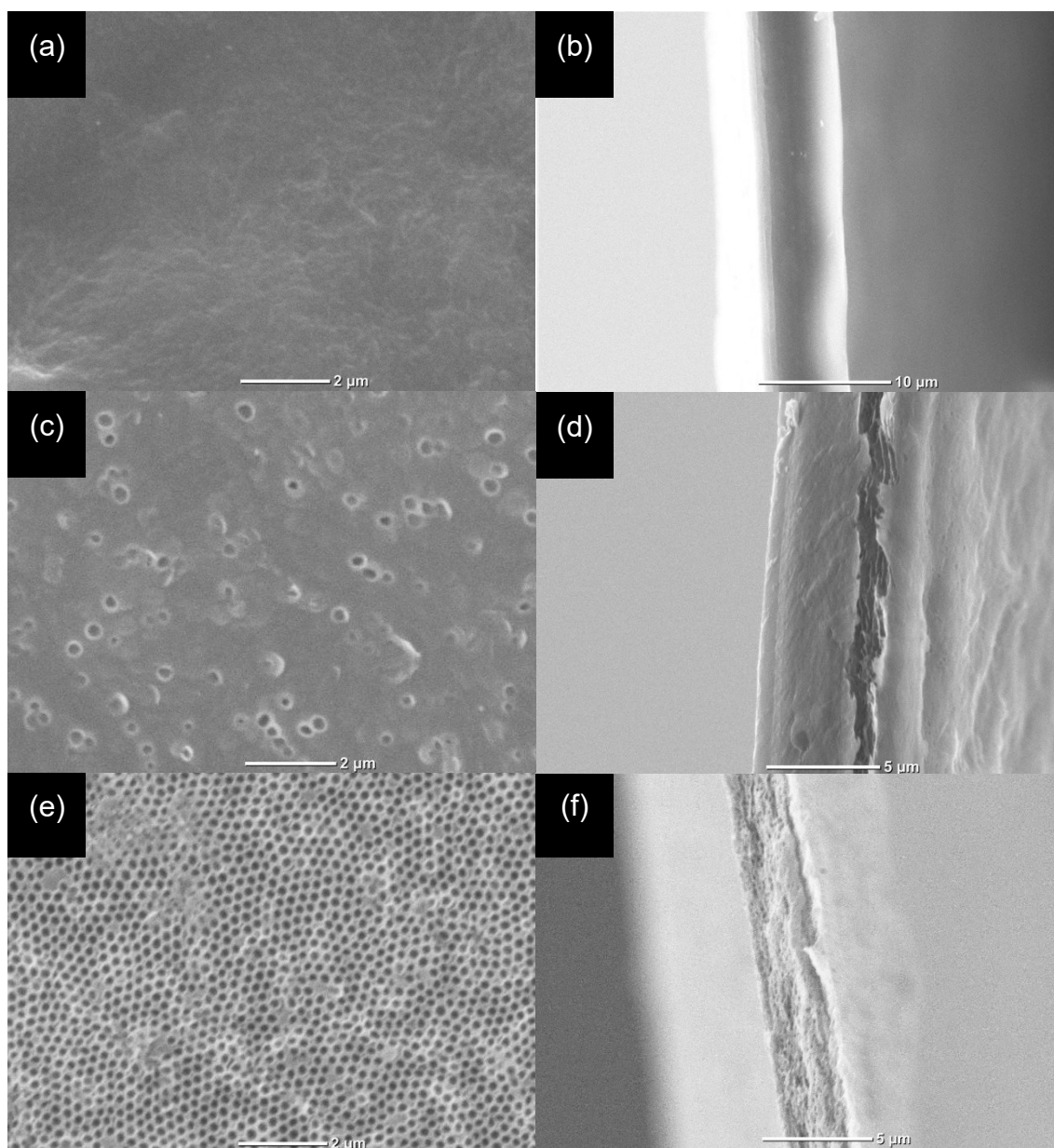


**Figure 3-11.** Scanning electron microscope (SEM) images of (a) surface and (b) cross-section of pristine poly(BI-co-A) film, those of (c) surface and (d) cross-section of porous poly(BI-co-A)-30% film, and those of (e) surface and (f) cross-section of porous poly(BI-co-A)-50% film.

**Figure 3-11** shows SEM images of pristine poly(BI-*co*-A) film and porous poly(BI-*co*-A) film with a macroporous structure. As seen in **Figures 3-11a** and **b**, the pristine poly(BI-*co*-A) film exhibited a dense and homogeneous morphology without any pore on either the surface or edge. The number of pores increased with increasing silica contents (**Figure 3-11c** and **d**). As for the poly(BI-*co*-A)-50% film (**Figure 3-11e**), it is observed that the uniformed macropore structure displayed both on the surface and edge (**Figure 3-11f**) after HF etching with a diameter of  $250 \pm 20$  nm, which corresponded the size of silica spheres.

## 3.4.11 Mechanical properties

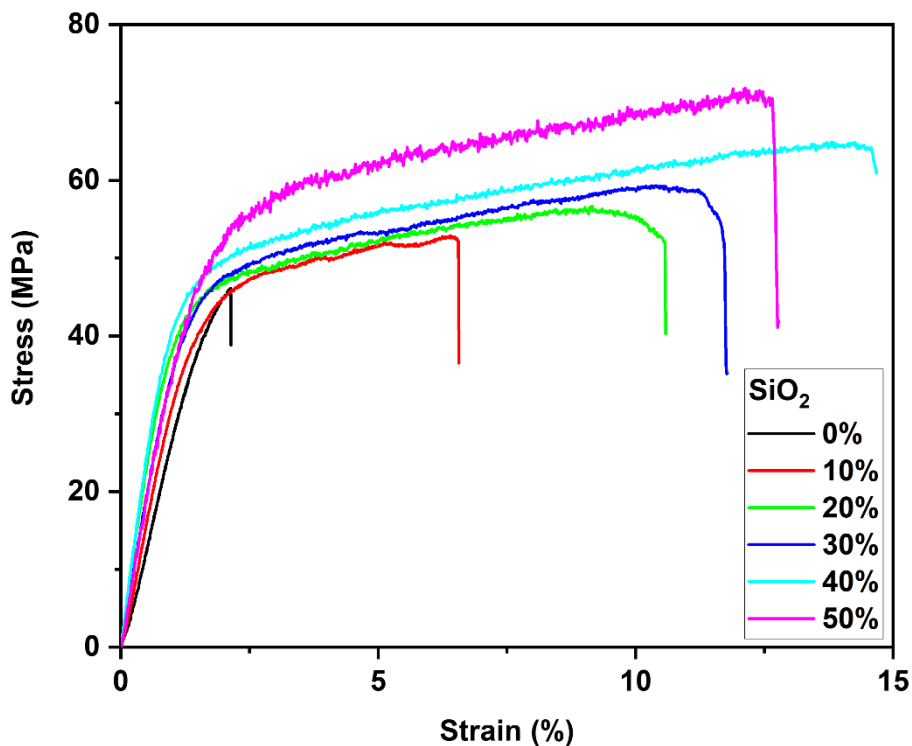


**Figure 3-12.** Stress-strain curves of pristine poly(BI-co-A) film and porous poly(BI-co-A) film with different SiO<sub>2</sub> compositions (0-50%).

It is well-known that PBI has high elastic properties because of its rigid backbone structure, numerous hydrogen bonds, and strong intermolecular interaction. It is well-known that when pores are introduced into polymer films, the elongation ratio is improved, but the strength and hardness are significantly reduced.<sup>27-29</sup> However, after introducing porous structure into poly(BI-co-A) film, Young's modulus increased from

### *Chapter III*

#### *Fabrication of silica composite and porous poly(benzimidazole-aramid) film*

3.2 GPa to 5.8 GPa. Elongation of break increased from 3.4%, which was brittle to 24.5% (Figure 3-12). Compared to the pristine poly(BI-co-A) film, the porous poly(BI-co-A) film showed much higher toughness, at 0.6 MJ/m<sup>3</sup> and 27.1 MJ/m<sup>3</sup>, respectively. Despite the numerous pores in the surface and edge, the fabricated porous poly(BI-co-A) film showed an unusual mechanical property compared to that reported in other literature. Meanwhile, this interesting structure was further investigated by a Scanning Probe Microscope (SPM).

## 3.4.12 WAXD patterns

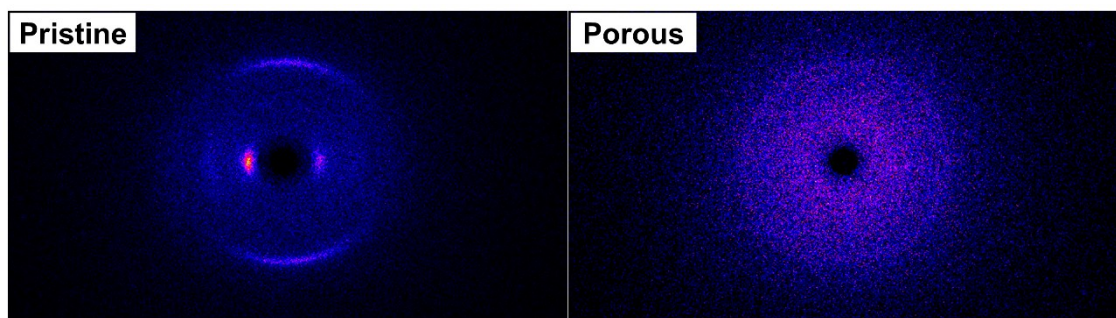


**Figure 3-13.** Wide-angle X-ray diffraction (WAXD) images of pristine and porous poly(BI-co-A) films.

**Table 3-4. Estimated crystallinity of pristine and porous poly(BI-co-A) film**

	Peak position ( $2\theta$ )	d-spacing (nm)	Degree of orientation	Degree of crystallinity (%)
Pristine film	26.3	0.14	0.8	7.8
Porous film	26.3	0.14	0	4.9

The crystallinity of the film was investigated by wide-angle X-ray diffraction. As is shown in **Figure 3-13**, the pristine film shows a relatively high degree of orientation of 0.8 while the orientation is eliminated in the porous film with an orientation degree of 0, illustrating the orientational change after the formation of porous structures. This explains the increase in elongation of poly(BI-co-A) film. The calculation formula for the degree

### *Chapter III*

#### *Fabrication of silica composite and porous poly(benzimidazole-aramid) film*

of orientation is shown below.

$$O(\%) = \frac{360^\circ - \sum W_i}{360^\circ} \times 100 (\%) \quad (1)$$

Where  $O$  is the degree of orientation and  $W_i$  is FWHM of the peak.

## 3.4.13 High-performance SPM

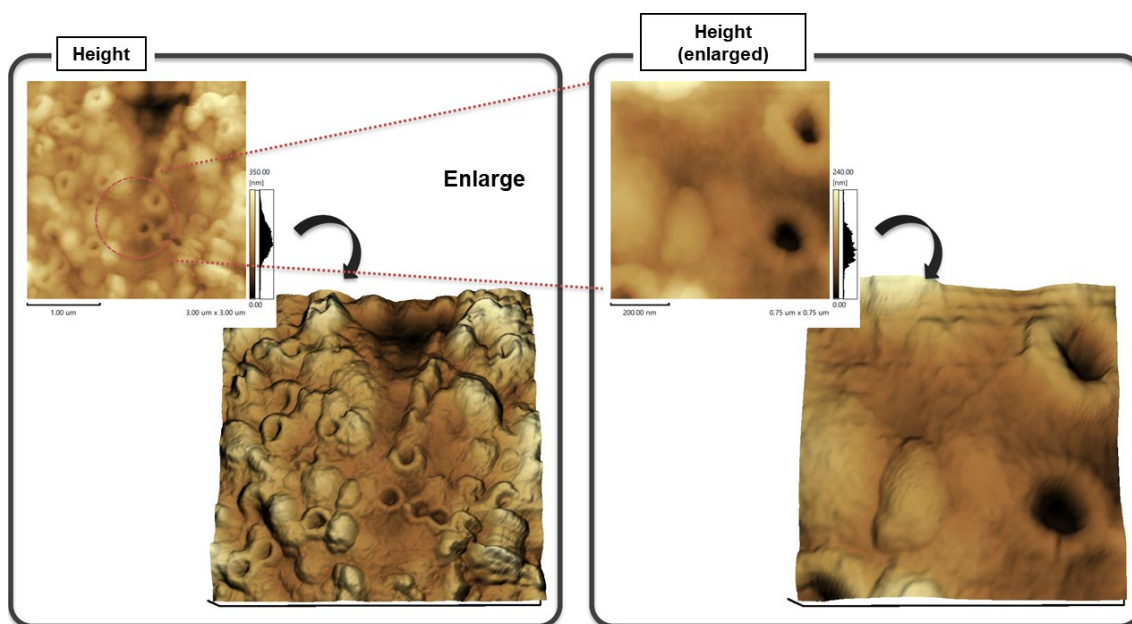


**Figure 3-14.** Atomic force microscope (AFM) images of porous poly(BI-co-A) film.

A high-performance scanning probe microscope (SPM) was adopted to further investigate the morphology of pores in porous poly(BI-co-A) film. As shown in **Figure 3-14**, the areas around the pore were brighter than the areas that are apart from the pore, indicating that the areas around the pore (80.6 nm) were higher than the areas apart from the pore (68.2 nm), which is calculated accurately via a phase observation mode. The outer diameter (319 nm) of the pore was measured, corresponding to the diameter of silica nanospheres. The inner diameter (142 nm) was lower than the outer diameter, which is caused by the expansion of the pores.

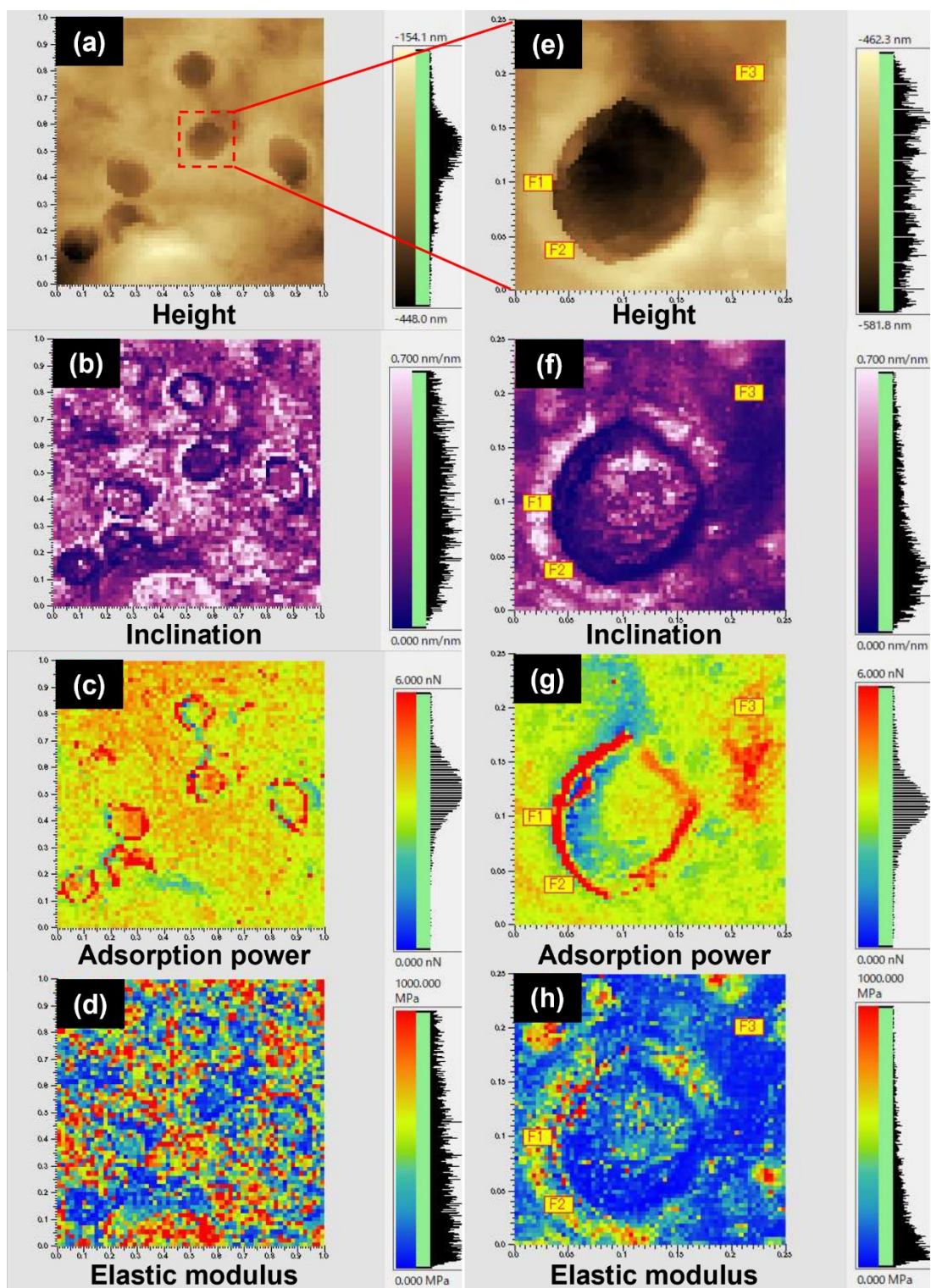


Figure 3-15. High-performance scanning probe microscope (SPM) images of the porous poly(BI-co-A) film.

**Table 3-5. Calculated mechanical results of porous poly(BI-co-A) film**

	Inclination (nm/nm) <sup>b</sup>	Adsorption Power (nN) <sup>b</sup>	Elastic Modulus (MPa) <sup>b</sup>
Around pore F1 <sup>a</sup>	0.817	3.31	708
Around pore F2 <sup>a</sup>	0.697	3.08	636
Apart from pore F3 <sup>a</sup>	0.178	4.51	72.2

<sup>a</sup> F1, F2 (area around pore) F3 (area apart from pore)

<sup>b</sup> Calculated results via the Johnson-Kendall-Roberts (JKR) model.

Nevertheless, the mechanical properties of the pore were investigated under a 3D mapping mode as shown above. Two areas around the pore (F1 and F2 in **Figure 3-15**) and one area apart from the pore (F3 in **Figure 3-15**) were selected to calculate the inclination, adsorption, and elastic modulus. The inclination of the areas around the pore (F1 and F2) and the area apart from pore (F3) was 0.817, 0.697, and 0.178 nm/nm, respectively, also demonstrating the different morphology of the areas of the pore. The adsorption power of F1, F2, and F3 was measured at 3.31, 3.08, and 4.51 nN, respectively. Moreover, the elastic modulus of F1, F2, and F3 was calculated via the Johnson-Kendall-Roberts (JKR) model,<sup>30,31</sup> which is shown below.

$$E = \frac{3(1-\nu^2)}{4} \left( \frac{1+16\sqrt{3}}{3} \right)^{\frac{3}{2}} \frac{-F_1}{\sqrt{R(\delta_0-\delta_1)^3}} \quad (2)$$

Where E is the elastic modulus,  $\nu$  is the poisson's ratio, F is the force at maximum adhesion,

### *Chapter III*

#### *Fabrication of silica composite and porous poly(benzimidazole-aramid) film*

$\delta$  is the deformation of the sample, and  $R$  is the curvature radius of the cantilever, respectively.

The calculated modulus of F1 (708 MPa), F2 (636MPa), and F3 (72.2 MPa) illustrated that the area around the pore is more durable than the area apart from the pore, which can also be observed from the modulus images as shown in **Figures 3-15d** and **h**.

The formation mechanism of the expansion area around the pore could be attributed to the aggregation of copolymer poly(BI-*co*-A) chains around silica spheres during the solvent evaporation process. The different evaporation speeds of the area around the pore and that apart from the pore constructed this volcano-like porous structure.

## 3.4.14 Hypothesis of mechanism

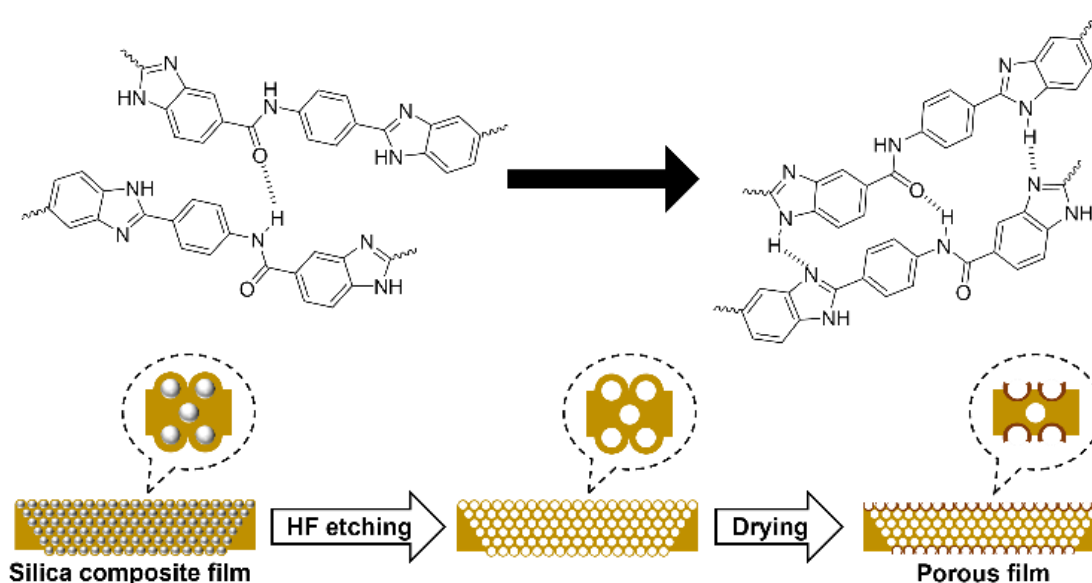


**Figure 3-16.** The mechanism for the formation of hard craters in poly(BI-co-A) film.

The surface energy causes the poly(BI-co-A) film covering the SiO<sub>2</sub> nanoparticles to form a crater-like shape in the holes formed by the SiO<sub>2</sub> nanoparticles removal. This formation may be attributed to the enhancement of intermolecular hydrogen bonds of poly(BI-co-A) chains in the presence of HF aqueous solution plasticizer, as well as the reduction of free energy due to the disappearance of SiO<sub>2</sub> nanoparticles (**Figure 3-16**). In the case of using SiO<sub>2</sub> nanoparticles with a particle diameter of 20 nm, uniform pores were not observed due to aggregation of the SiO<sub>2</sub> nanoparticles. However, even in this case, where the particle size is not uniform, a white region around the pores was also observed as well, indicating the formation of “hard craters”. This result indicated that it

### *Chapter III*

#### *Fabrication of silica composite and porous poly(benzimidazole-aramid) film*

is effective in improving the mechanical properties by SiO<sub>2</sub> addition and HF etching into the polymer.

### **3.5 Conclusion**

In this Chapter, porous poly(BI-*co*-A) films with an uniform porous structure were prepared via a hard-template method successfully. The pores size is in the range of 200 nm to 300 nm were monodisperse and spherical, and the porosity of films was efficiently adjusted by increasing the content of silica spheres.

The prepared porous poly(BI-*co*-A) films showed much higher toughness and mechanical stability. Young's modulus of the poly(BI-*co*-A) film increased from 3.2 GPa to 5.8 GPa of porous poly(BI-*co*-A) film. The obtained porous poly(BI-*co*-A) film showed a high toughness of 27.1 MJ/m<sup>3</sup>, which was elucidated by comparing the degree of orientation and crystallinity of porous poly(BI-*co*-A) to those of the pristine poly(BI-*co*-A) film.

More importantly, the porous poly(BI-*co*-A) films were fabricated from ultrahigh thermoresistant polymer, which has great potential in applications such as catalyst support, gas storage, proton exchange membrane, etc.

## References

- (1) Xia, Q.; Chen, C.; Yao, Y.; Li, J.; He, S.; Zhou, Y.; Li, T.; Pan, X.; Yao, Y.; Hu, L. A Strong, Biodegradable and Recyclable Lignocellulosic Bioplastic. *Nat Sustain* **2021**, *4* (7), 627–635. <https://doi.org/10.1038/s41893-021-00702-w>.
- (2) Rosenboom, J.-G.; Langer, R.; Traverso, G. Bioplastics for a Circular Economy. *Nat Rev Mater* **2022**, *7* (2), 117–137. <https://doi.org/10.1038/s41578-021-00407-8>.
- (3) Tian, X.; Wang, S.; Li, J.; Liu, F.; Wang, X.; Chen, H.; Wang, D.; Ni, H.; Wang, Z. Benzimidazole Grafted Polybenzimidazole Cross-Linked Membranes with Excellent PA Stability for High-Temperature Proton Exchange Membrane Applications. *Appl Surf Sci* **2019**, *465*, 332–339. <https://doi.org/10.1016/j.apsusc.2018.09.170>.
- (4) Wang, X.; Chen, W.; Yan, X.; Li, T.; Wu, X.; Zhang, Y.; Zhang, F.; Pang, B.; He, G. Pre-Removal of Polybenzimidazole Anion to Improve Flexibility of Grafted Quaternized Side Chains for High Performance Anion Exchange Membranes. *J Power Sources* **2020**, *451*, 227813. <https://doi.org/10.1016/j.jpowsour.2020.227813>.
- (5) Wang, Y.; Chen, L.; Yu, J.; Zhu, J.; Shi, Z.; Hu, Z. Strong and Conductive Polybenzimidazole Composites with High Graphene Contents. *RSC Adv* **2013**, *3* (30), 12255. <https://doi.org/10.1039/c3ra40889b>.
- (6) Kim, J.; Kim, K.; Ko, T.; Han, J.; Lee, J.-C. Polybenzimidazole Composite Membranes

### Chapter III

#### *Fabrication of silica composite and porous poly(benzimidazole-aramid) film*

Containing Imidazole Functionalized Graphene Oxide Showing High Proton Conductivity and Improved Physicochemical Properties. *Int J Hydrogen Energy* **2021**, *46* (22), 12254–12262. <https://doi.org/10.1016/j.ijhydene.2020.02.193>.

- (7) Zeng, L.; Zhao, T. S.; An, L.; Zhao, G.; Yan, X. H. A High-Performance Sandwiched-Porous Polybenzimidazole Membrane with Enhanced Alkaline Retention for Anion Exchange Membrane Fuel Cells. *Energy Environ Sci* **2015**, *8* (9), 2768–2774. <https://doi.org/10.1039/C5EE02047F>.
- (8) Geng, K.; Tang, H.; Ju, Q.; Qian, H.; Li, N. Symmetric Sponge-like Porous Polybenzimidazole Membrane for High Temperature Proton Exchange Membrane Fuel Cells. *J Memb Sci* **2021**, *620*, 118981. <https://doi.org/10.1016/j.memsci.2020.118981>.
- (9) Cui, X.; Zhang, C.; Araby, S.; Cai, R.; Kalimuldina, G.; Yang, Z.; Meng, Q. Multifunctional, Flexible and Mechanically Resilient Porous Polyurea/Graphene Composite Film. *Journal of Industrial and Engineering Chemistry* **2022**, *105*, 549–562. <https://doi.org/10.1016/j.jiec.2021.10.017>.
- (10) Pálvölgyi, P. S.; Sebök, D.; Szenti, I.; Bozo, E.; Ervasti, H.; Pitkänen, O.; Hannu, J.; Jantunen, H.; Leinonen, M. E.; Myllymäki, S.; Kukovecz, A.; Kordas, K. Lightweight Porous Silica Foams with Extreme-Low Dielectric Permittivity and Loss for Future 6G Wireless Communication Technologies. *Nano Res* **2021**, *14* (5), 1450–1456.

### Chapter III

#### *Fabrication of silica composite and porous poly(benzimidazole-aramid) film*

<https://doi.org/10.1007/s12274-020-3201-2>.

- (11) Luo, T.; Dreusicke, B.; Wessling, M. Tuning the Ion Selectivity of Porous Poly(2,5-Benzimidazole) Membranes by Phase Separation for All Vanadium Redox Flow Batteries. *J Memb Sci* **2018**, *556*, 164–177. <https://doi.org/10.1016/j.memsci.2018.03.086>.
- (12) Chaudhari, H. D.; Illathvalappil, R.; Kurungot, S.; Kharul, U. K. Preparation and Investigations of ABPBI Membrane for HT-PEMFC by Immersion Precipitation Method. *J Memb Sci* **2018**, *564*, 211–217. <https://doi.org/10.1016/j.memsci.2018.07.026>.
- (13) Jiang, W.; Zhu, Y.; Zhu, G.; Zhang, Z.; Chen, X.; Yao, W. Three-Dimensional Photocatalysts with a Network Structure. *J Mater Chem A Mater* **2017**, *5* (12), 5661–5679. <https://doi.org/10.1039/C7TA00398F>.
- (14) Borai, E. H.; Hamed, M. G.; El-kamash, A. M.; Siyam, T.; El-Sayed, G. O. Template Polymerization Synthesis of Hydrogel and Silica Composite for Sorption of Some Rare Earth Elements. *J Colloid Interface Sci* **2015**, *456*, 228–240. <https://doi.org/10.1016/j.jcis.2015.06.020>.
- (15) Nag, A.; Ali, M. A.; Kawaguchi, H.; Saito, S.; Kawasaki, Y.; Miyazaki, S.; Kawamoto, H.; Adi, D. T. N.; Yoshihara, K.; Masuo, S.; Katsuyama, Y.; Kondo, A.; Ogino, C.; Takaya, N.; Kaneko, T.; Ohnishi, Y. Ultrahigh Thermoresistant Lightweight Bioplastics Developed from Fermentation Products of Cellulosic Feedstock. *Adv Sustain Syst* **2021**,

### Chapter III

#### *Fabrication of silica composite and porous poly(benzimidazole-aramid) film*

5 (1). <https://doi.org/10.1002/adsu.202000193>.

- (16) Zhong, X.; Nag, A.; Zhou, J.; Takada, K.; Amat Yusof, F. A.; Mitsumata, T.; Oqmhula, K.; Hongo, K.; Maezono, R.; Kaneko, T. Stepwise Copolymerization of Polybenzimidazole for a Low Dielectric Constant and Ultrahigh Heat Resistance. *RSC Adv* **2022**, *12* (19), 11885–11895. <https://doi.org/10.1039/D2RA01488B>.
- (17) Yeob, J.; Hong, S. W.; Koh, W.-G.; Park, I. Enhanced Mechanical and Thermal Properties of Polyimide Films Using Hydrophobic Fumed Silica Fillers. *Polymers (Basel)* **2024**, *16* (2), 297. <https://doi.org/10.3390/polym16020297>.
- (18) Liu, H.; Kaya, H.; Lin, Y.; Ogrinc, A.; Kim, S. H. Vibrational Spectroscopy Analysis of Silica and Silicate Glass Networks. *Journal of the American Ceramic Society* **2022**, *105* (4), 2355–2384. <https://doi.org/10.1111/jace.18206>.
- (19) Uchino, T.; Sakka, T.; Lwasaki, M. Interpretation of Hydrated States of Sodium Silicate Glasses by Infrared and Raman Analysis. *J Am Cerarn SOC* **1991**, *74* (2), 306–319.
- (20) Boström, O.; Choi, S.-Y.; Xia, L.; Meital, S.; Lohmann-Richters, F.; Jannasch, P. Alkali-Stable Polybenzimidazole Anion Exchange Membranes Tethered with *N*, *N*-Dimethylpiperidinium Cations for Dilute Aqueous KOH Fed Water Electrolyzers. *J Mater Chem A Mater* **2023**, *11* (39), 21170–21182. <https://doi.org/10.1039/D3TA03216G>.
- (21) Al Munsur, A. Z.; Lee, J.; Chae, J. E.; Kim, H.-J.; Park, C. H.; Nam, S. Y.; Kim, T.-H.

### Chapter III

#### *Fabrication of silica composite and porous poly(benzimidazole-aramid) film*

Hexyl Quaternary Ammonium- and Fluorobenzoyl-Grafted SEBS as Hydrophilic–Hydrophobic Comb-Type Anion Exchange Membranes. *J Memb Sci* **2022**, *643*, 120029. <https://doi.org/10.1016/j.memsci.2021.120029>.

- (22) Katsikis, N.; Zahradnik, F.; Helmschrott, A.; Münstedt, H.; Vital, A. Thermal Stability of Poly(Methyl Methacrylate)/Silica Nano- and Microcomposites as Investigated by Dynamic-Mechanical Experiments. *Polym Degrad Stab* **2007**, *92* (11), 1966–1976. <https://doi.org/10.1016/j.polymdegradstab.2007.08.009>.
- (23) Dong, Q.; Ding, Y.; Wen, B.; Wang, F.; Dong, H.; Zhang, S.; Wang, T.; Yang, M. Improvement of Thermal Stability of Polypropylene Using DOPO-Immobilized Silica Nanoparticles. *Colloid Polym Sci* **2012**, *290* (14), 1371–1380. <https://doi.org/10.1007/s00396-012-2631-0>.
- (24) Khankruea, R.; Pivsa-Art, S.; Hiroyuki, H.; Suttiruengwong, S. Thermal and Mechanical Properties of Biodegradable Polyester/Silica Nanocomposites. *Energy Procedia* **2013**, *34*, 705–713. <https://doi.org/10.1016/j.egypro.2013.06.803>.
- (25) Borrego, E. I.; Athukorale, S.; Gorla, S.; Duckworth, A. K.; Baker, M.; Rosales, J.; Johnson, W. W.; Kundu, S.; Toghiani, H.; Farajidizaji, B.; Pittman, C. U.; Smith, D. W. High Carbon Yielding and Melt Processable Bis-Ortho-Diynylarene (BODA)-Derived Resins for Rapid Processing of Dense Carbon/Carbon Composites. *Compos B Eng* **2022**,

*Chapter III*

*Fabrication of silica composite and porous poly(benzimidazole-aramid) film*

242, 110080. <https://doi.org/10.1016/j.compositesb.2022.110080>.

- (26) Buchmeiser, M. R.; Muks, E.; Schowner, R.; Frank, E.; Hageroth, U.; Henzler, S.; Spörl, J.; Ota, A.; Beyer, R.; Müller, A. Structure Evolution in All-Aromatic, Poly(p-Phenylene-Vinylene)-Derived Carbon Fibers. *Carbon N Y* **2019**, *144*, 659–665. <https://doi.org/10.1016/j.carbon.2018.12.096>.
- (27) Taki, K.; Hosokawa, K.; Takagi, S.; Mabuchi, H.; Ohshima, M. Rapid Production of Ultralow Dielectric Constant Porous Polyimide Films via CO<sub>2</sub> - *Tert* -Amine Zwitterion-Induced Phase Separation and Subsequent Photopolymerization. *Macromolecules* **2013**, *46* (6), 2275–2281. <https://doi.org/10.1021/ma302406m>.
- (28) Jheng, L.-C.; Chang, W. J.-Y.; Hsu, S. L.-C.; Cheng, P.-Y. Durability of Symmetrically and Asymmetrically Porous Polybenzimidazole Membranes for High Temperature Proton Exchange Membrane Fuel Cells. *J Power Sources* **2016**, *323*, 57–66. <https://doi.org/10.1016/j.jpowsour.2016.05.043>.
- (29) Che, X.; Zhao, H.; Ren, X.; Zhang, D.; Wei, H.; Liu, J.; Zhang, X.; Yang, J. Porous Polybenzimidazole Membranes with High Ion Selectivity for the Vanadium Redox Flow Battery. *J Memb Sci* **2020**, *611*, 118359. <https://doi.org/10.1016/j.memsci.2020.118359>.
- (30) Johnson, K. L.; Kendall, K.; Roberts, A. D. Surface Energy and the Contact of Elastic Solids. *Proceedings of the Royal Society of London. A. Mathematical and Physical*

*Chapter III*

*Fabrication of silica composite and porous poly(benzimidazole-aramid) film*

*Sciences* **1971**, 324 (1558), 301–313. <https://doi.org/10.1098/rspa.1971.0141>.

- (31) Li, J. K.; Li, I. T. S.; Walker, G. C.; Sullan, R. M. A.; Zou, S.; Sun, Y. Polymer Nanomechanics. In *Polymer Science: A Comprehensive Reference*; Elsevier, 2012; Vol. 1–10, pp 377–404. <https://doi.org/10.1016/B978-0-444-53349-4.00184-9>.

## *Chapter IV*

### *Conclusions*

## *Chapter IV*

### *Conclusions*

Polybenzimidazole (PBI) is a high-performance polymer known for its excellent thermal stability, mechanical properties, and chemical resistance. In particular, poly(2,5-benzimidazole) (ABPBI) is the simplest chemical structure of PBI, consisting of repeated benzene and imidazole rings, suggesting a high possibility of industrial applications. However, several challenges of ABPBI remain such as low sustainability and poor cost-performance caused by the time-consuming polycondensation process for a commercial product, heterogeneity and low flexibility of processed film due to the rigid backbones of ABPBI, lack of processability with insolubility in common organic solvents, and moisture sensitivity which limited their further application as a super engineering plastic. One of the primary challenges facing the widespread adoption of ABPBI films is the high production cost. The complex synthesis and processing techniques required to produce ABPBI result in its poor cost performance compared to other polymers. Moreover, scaling up the production of ABPBI films while maintaining their unique properties with crucial uniformity is also required in manufacturing technologies.

In chapter II, ABPBI was synthesized successfully by using Eaton's reagent, which is a timesaving polycondensation procedure. Notably, the adopted monomer 34DABA is bio-derivable, which remarkably improves sustainability and reduces the production cost

of ABPBI. The chemical structure of ABPBI was confirmed by FT-IR analysis, indicating successful polycondensation.

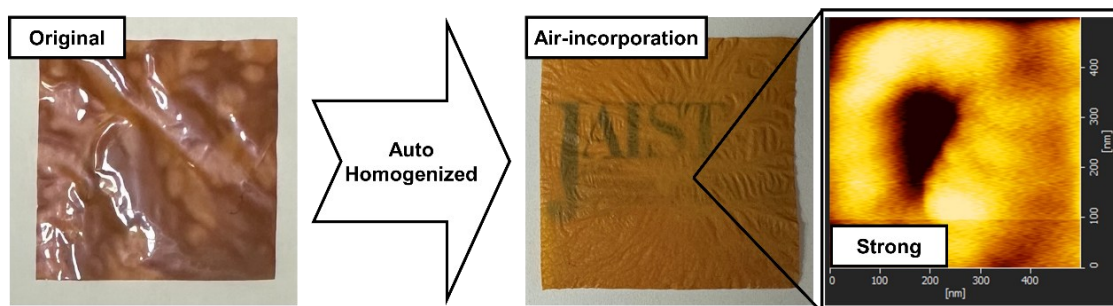


**Figure 4-1.** The illustration of the homogenization of ABPBI film.

On the other hand, the fabricated ABPBI films by solution casting using TFA including a small amount of MSA as a solvent showed heterogeneous and featured branched patterns of thick brown regions (**Figure 4-1**). This may have originated from the surface condensation of ABPBI to form sticky fibrous aggregates. Subsequently, a hard-templating method using silica nanoparticle fillers was employed to homogenize the ABPBI films. The composite ABPBI films had reduced heterogeneity and roughness compared with the original ABPBI films. Herein, a formation mechanism was proposed whereby the ABPBI aggregate stuck to the surfaces of the silica nanoparticles, which were well dispersed all over the film by ultrasonication. The reduced cost of production

and improved uniformity suggest the potential of ABPBI as a material for a broader range of industrial uses, e.g., fuel cell separators, leakproof films, and filtration membranes.

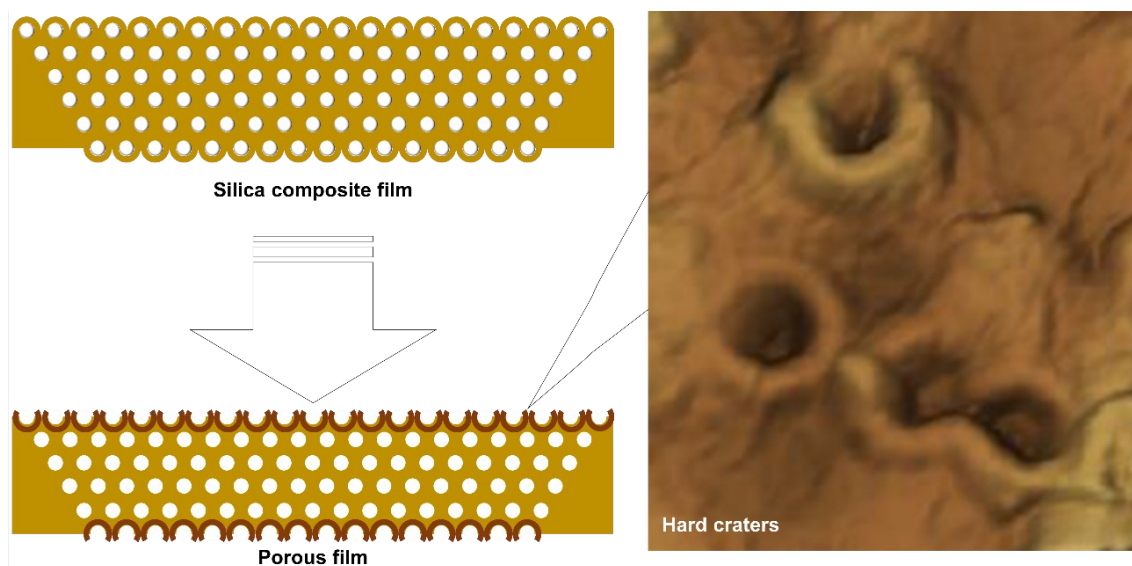


**Figure 4-2.** The illustration of the fabrication of hard craters to the porous film.

Although ABPBI is strong and rigid, it is relatively brittle as well. Its low elongation at break limits its use in applications. Therefore, flexibility or toughness is required. In chapter III, another bio-derivable monomer ABA was incorporated into the ABPBI backbones named poly(BI-co-A) to provide flexibility. Poly(BI-co-A) was synthesized using viscous poly(phosphoric acid) whose chemical structure was confirmed by FT-IR analysis. Moreover, to further enhance the durability, flexibility, and performance of poly(BI-co-A) film, a porous structure was introduced via a silica-etching method (**Figure 4-2**). The pores of a size in the range of 200 - 300 nm and the shape was spherical,

and the porosity of porous poly(BI-co-A) films was efficiently adjusted via the content of added silica nanospheres. The prepared porous poly(BI-co-A) films showed much higher toughness and mechanical stability, which could be expected to play a crucial role in enabling the next generation of durable and resilient electronic devices, including their potential use in high-performance sensors, smart textiles, and flexible batteries.

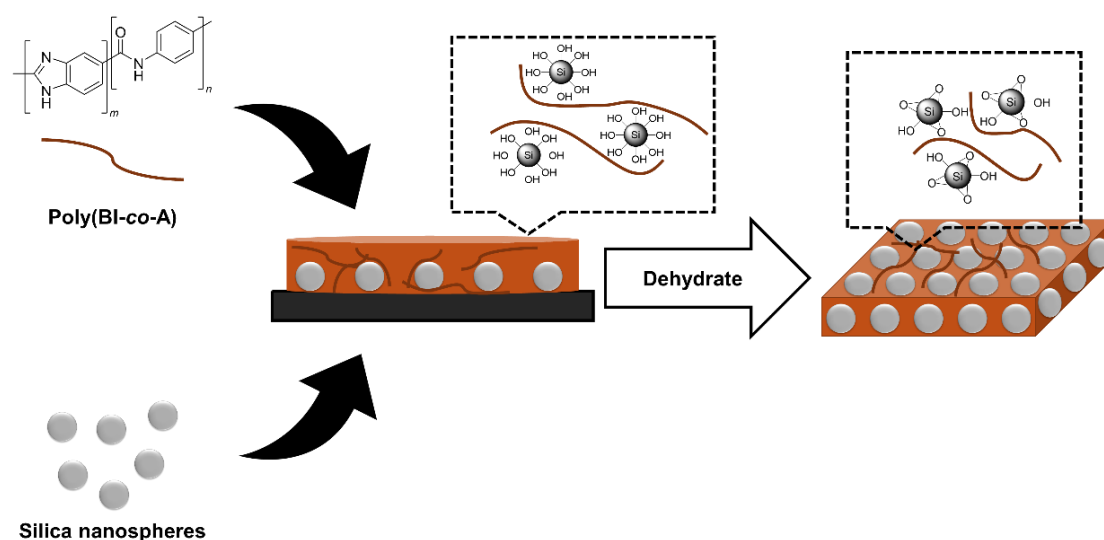


**Figure 4-3.** The schematic illustration of the wettability amelioration by dehydration.

However, poly(BI-co-A) film has some degree of water absorption, which can affect its mechanical properties over time, especially under humid conditions. This could be problematic in applications where dimensional stability or mechanical strength must be maintained in moist environments. Therefore, dehydration treatment of silica

## *Chapter IV*

### *Conclusions*

nanocomposite poly(BI-co-A) films in an electric furnace was employed to improve the surface wettability of the poly(BI-co-A) film by decreasing the hydrogen bonds in the films (**Figure 4-3**). The fabricated silica nanocomposite poly(BI-co-A) films displayed an enhanced thermal resistance, even comparable to some metals, implying their replacement of heavyweight metal or inorganic materials. Nevertheless, the improved wettability of poly(BI-co-A) films further ensures their potential candidate for applications in an extreme environment such as fuel cell membranes, barriers, and anti-foul film, aircraft, and spacecraft.

Regarding the future scope of this work, the successful PBI films with enhanced performance such as low-cost procedure, sustainable resources, high uniformity, improved flexibility, and enhanced toughness, have significant potential in a variety of industries, from energy and aerospace to electronics and environmental protection. Due to their role in improving fuel cell performance, protecting advanced electronic devices, or enabling cleaner industrial processes, PBI films are set to play a key role in the future of materials science and engineering. The ongoing advancements in manufacturing, sustainability, and application development will further expand the use of PBI films, making them critical materials for the 21st century and beyond.

# Research Achievements

## ① Papers

1. **Jiabei Zhou**, Xianzhu Zhong, Kenji Takada, Masayuki Yamaguchi, and Tatsuo Kaneko. Thermal Resistance Enhancement and Wettability Amelioration of Poly(benzimidazole-aramid) Film by Silica Nanocomposites. *Polymers* **2024**, *16*(24), 3563.
2. **Jiabei Zhou**, Xianzhu Zhong, Kenji Takada, Maiko K. Okajima, Masayuki Yamaguchi, and Tatsuo Kaneko. Auto-homogenization of Polybenzimidazole Composites with Enhanced Mechanical Performance by Air Incorporation. *Langmuir* **2024**, *40*, 23780-23787.
3. **Jiabei Zhou**, Xianzhu Zhong, Aniruddha Nag, Yang Liu, Kenji Takada and Tatsuo Kaneko. Reinforcement of Ultrahigh Thermoresistant Polybenzimidazole Films by Hard Craters. *Polym. Chem.* **2022**, *13*, 4086-4089.
4. Kaito Watanabe, Junko Ikeda, Xianzhu Zhong, **Jiabei Zhou**, Tatsuo Kaneko, Mika Kawai, and Tetsu Mitsumata. Electric Conductivity Transitions of Water-Absorbable Polybenzimidazole Films. *Polymers* **2025**, *17*, 167.
5. Xianzhu Zhong, **Jiabei Zhou**, Mohammad Asif Ali, Aniruddha Nag, Kenji Takada, Kaito Watanabe, Mika Kawai, Tetsu Mitsumata, and Tatsuo Kaneko. Antiresonance Stabilization of Wholly Aromatic Bioplastics Using a Heteroelement Booster for Superthermostable Flexible Insulators. *Macromolecules* **2024**, *57* (1), 356-363.
6. Xianzhu Zhong, Aniruddha Nag, **Jiabei Zhou**, Kenji Takada, Motoyuki Kusano and Tatsuo Kaneko, Pin-point Surgery of Proton-deuterium Substitution to Enhance Polybenzimidazole Thermoresistances. *Chemistry Letters* **2023**, *52*, 819-822.
7. Xianzhu Zhong, Aniruddha Nag, **Jiabei Zhou**, Kenji Takada, Fitri Adila Amat Yusof, Tetsu Mitsumata, Kenji Oqmhula, Kenta Hongo, Ryo Maezono and Tatsuo Kaneko, Stepwise Copolymerization of Polybenzimidazole for Exhibiting Low Dielectric Constant and Ultrahigh Heat Resistance, *RSC Adv.* **2022**, *12*, 11885-11895.
8. Aniruddha Nag, Mohammad Asif Ali, **Jiabei Zhou**, Makoto Ogawa and Tatsuo Kaneko. Synergistic Effects of Polybenzimidazole and Aramide on Enhancing Flame Retardancy and Solubility. *Macromol. Mater. Eng.* **2021**, *306*, 2100459.

## ② Books

1. **Jiabei Zhou** and Tatsuo Kaneko. Bio-derived Polybenzimidazole Films with Enhanced Thermal and Mechanical Properties. *Sustainable Green Chemistry in Polymer Research*, Vol. 2, Sustainable Polymers and Applications, Chap. 4, pp. 85-98, 2023.

2. **Jiabei Zhou**, Xianzhu Zhong, Aniruddha Nag, 金子 達雄. 「植物原料を用いた史上最高耐熱プラスチックの開発」 環境配慮型材料 第4号 第2章 第2節 51-64頁 Andtech 出版 9月2022年

③ Awards

1. International Conference on Advanced Materials and Technology (ICAMT 2024), Best poster award
2. 第29回日本ポリイミド・芳香族系高分子会議 優秀ポスター賞 受賞

④ International conferences

1. **Jiabei Zhou**, Kenji Takada, Tatsuo Kaneko and Masayuki Yamaguchi. Enhanced Mechanical Performance of High Thermoresistance Polybenzimidazole Film by Pore-construction. International Conference on Advanced Materials and Technology (ICAMT 2024), Hanoi University of Science and Technology, Hanoi, Vietnam (Poster), October 2024. (査読あり)
2. **Jiabei Zhou**, Aniruddha Nag, Xianzhu Zhong, Kenji Takada, Tatsuo Kaneko. Reinforcement Effects of Silica-etching on Polybenzimidazole Films. The 13th SPSJ International Polymer Conference (IPC 2023), Sapporo Convention Center, Hokkaido, Japan (Oral), July 2023. (査読なし)
3. **Jiabei Zhou**, Aniruddha Nag, Xianzhu Zhong, Kenji Takada, Tatsuo Kaneko. Reinforcement Effects of Nano-etching on Bio-polybenzimidazole Film. The 5th International Union of Materials Research Societies International Conference of Young Researchers on Advanced Materials. IUMRS-ICYAM 2022, Centennial Hall, Kyushu University, Fukuoka, Japan (Hybrid Meeting) (Poster) August 2022. (査読あり)
4. **Jiabei Zhou**, Aniruddha Nag, Xianzhu Zhong, Kenji Takada, Tatsuo Kaneko. Syntheses of Ultrahigh Thermoresistant Bio-polybenzimidazoles from Aromatic Diamino Acids. The 48th World Polymer Congress IUPAC-MACRO2020+, SS8-07, International Convention Center Jeju, Korea (Online short talk) May 2021. (査読あり)

⑤ Domestic conferences (すべて査読なし)

1. **Jiabei Zhou**, Aniruddha Nag, Xianzhu Zhong, Kenji Takada, Tatsuo Kaneko. クレーター構造の構築によりポリベンズイミダゾールフィルムの高靱化 第30回日本ポリイミド・芳香族系高分子会議 東邦大学 習志野キャンパス 千葉県船橋市 ポスター発表 12月2022年
2. **Jiabei Zhou**, Aniruddha Nag, Xianzhu Zhong, Kenji Takada, Tatsuo Kaneko. Toughness Reinforcement of Polybenzimidazole by Forming Hard Craters. 日本化学会秋季事業 第12回CSJ化学フェスタ2022 タワーホール船堀 ポスター発表 10月2022年

3. **Jiabei Zhou**, Aniruddha Nag, Xianzhu Zhong, Kenji Takada, Tatsuo Kaneko. Enhanced Toughness for Polybenzimidazole Copolymer Thin-films by Forming Hard Craters on Surface. 第 71 回高分子討論会 北海道大学 札幌キャンパス 口頭発表 9 月 2022 年
4. **Jiabei Zhou**, Aniruddha Nag, Xianzhu Zhong, 高田 健司、金子 達雄 シリカ粒子エッチング法によるバイオポリベンズイミダゾールの機械物性の向上 第 71 回高分子学会年次大会 オンライン開催 ポスター発表 5 月 2022 年
5. **Jiabei Zhou**, Aniruddha Nag, Xianzhu Zhong, Kenji Takada, Tatsuo Kaneko. Toughening of Ultrahigh Thermoresistant Biopolybenzimidazoles by Forming Porous Structure. 第 29 回日本ポリイミド・芳香族系高分子会議 多賀市民会館 茨城県日立市 ポスター発表 2021 年 12 月
6. **Jiabei Zhou**, Aniruddha Nag, Xianzhu Zhong, Kenji Takada, Tatsuo Kaneko. Toughening of Ultrahigh Thermoresistant Biopolybenzimidazoles by Forming Porous Structure. 第 70 回高分子討論会 オンライン開催 ポスター発表 2021 年 9 月

⑥ Funds

1. 令和 4 年度 J S T 次世代研究者挑戦的研究プログラム 研究員  
「多孔質構造の精密制御による軽量高機能プラスチックの開発」  
代表：ZHOU Jiabei (直接経費 40 + 70 + 40 = 150 万円)
2. 令和 4 年度 公益財団法人 令和環境財団学術研究助成金  
「ナノ孔樹脂の精密構造制御による高性能カーボン・エアコンポジットの開発」  
代表：ZHOU Jiabei (直接経費 50 万円)